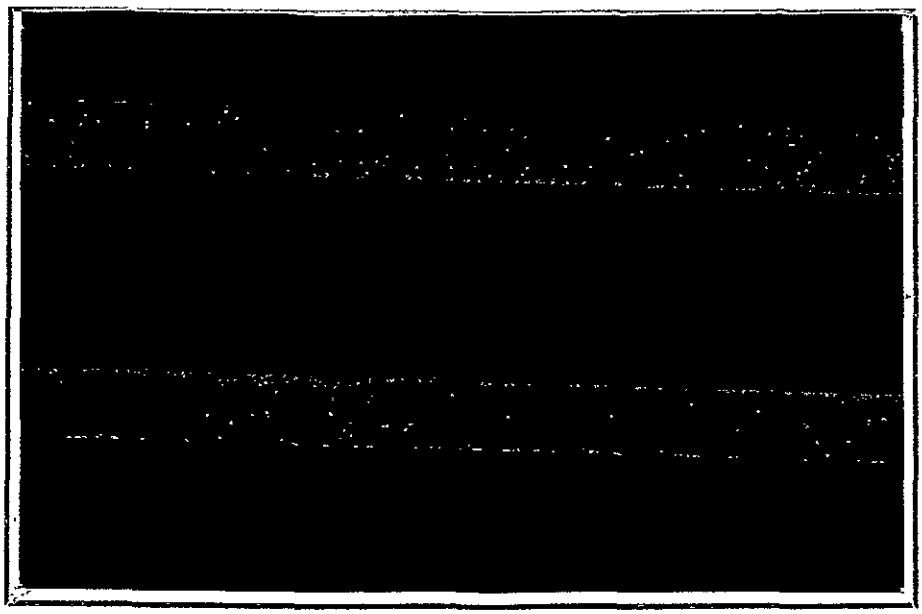

Virginia Polytechnic Institute
and State University

Chemistry Department

Blacksburg, Virginia 24061

FINAL REPORT

EFFECT OF POLYMER PROPERTIES AND ADHEREND SURFACES ON ADHESION

BY

David W. Dwight, Mary Ellen Counts
and James P. Wightman

Prepared for

National Aeronautics
and
Space Administration
December, 1975
NASA GRANT NSG-1124

NASA Langley Research Center
Hampton, Virginia 23365
Materials Division
Donald J. Progar

Chemistry Department
Virginia Polytechnic Institute and State University
Blacksburg, Virginia 24061

TABLE OF CONTENTS

ACKNOWLEDGMENT

Most of the work described in this report was performed on samples supplied by Norm Johnston's Polymer Group at NASA-LaRC. Our studies would not have been possible without their efforts, especially Terry St. Clair in polymer synthesis and Don Progar in strength testing. Also gratefully acknowledged is the expert SEM operation of Frank Mitsianis.

LIST OF TABLES

LIST OF FIGURES

Page

GLOSSARY

TECHNIQUES

SEM - Scanning Electron Microscopy
EDAX - Energy Dispersive Analysis of X-ray Fluorescence
ESCA - Electron Spectroscopy for Chemical Analysis (X-ray photoelectron spectroscopy)
SRIRS - Specular Reflectance Infra-Red Spectroscopy

MATHEMATICAL SYMBOLS

E - elastic modulus
G - energy dissipated per area during fracture (fracture toughness)
ℓ - length of initial crack
δ - thickness of zone of fracture
σ_f - stress at which fracture occurs
γ_s - surface energy created during fracture
ψ - all other components of G, except γ_s, including work of plastic deformation, sound, light, etc.
F - force of peeling tape
θ - adhesive failure energy
θ_o - work of bond fracture after rheological losses have been taken into account
W_a - thermodynamic work of adhesion
τ_o - intrinsic adhesive failure energy
F_o - intrinsic adherend failure energy
i_o - fraction of interfacial failure
r - fraction of adhesive failure
s - fraction of adherend failure
Tg - glass transition temperature
$\dot{c}$ - rate of crack propagation
a_T - WLF shift factor
γ_c - critical surface tension

CHEMICALS, SOLVENTS, ETC.

BTDA - Benzophenone Tetracarboxylic Acid Dianhydride
DABP - Diaminobenzophenone
PMDA - Pyromellitic Dianhydride
ODPA - Oxydiphthalic Anhydride
EAH-13 - m,m"-Diamino Terbenzylone
DG - Diglyme
DMAC - Dimethylacetamide
DMF - Dimethylformamide
HT-S/P13N - Hercules Graphite fiber/Ciba-Giegy Addition Polyimide
LSS - Lap Shear Strength

I. INTRODUCTION

Adhesive bonding of aerospace systems and components is increasing at a rapid pace. Substantial cost savings can be obtained primarily because of reduction in weight and in manufacturing costs. Other advantages over riveted or bolted structures are facile joining of thin and contoured sheets, reduced stress concentration and galvanic corrosion, etc. Adhesives are the only practicable way to join fiber-reinforced composites and honeycomb structures.

However, the service requirements become ever more rigorous, exceeding the propery limits of most synthetic organic polymers. For example, the current goal is an adhesively bonded structure exhibiting usable strength for 10,000 hours at 600^{o}F (316^{o}C). The total system also must be able to withstand exposure to high humidity and severe temperature cycles. Furthermore, restrictions are placed upon polymer synthesis by the need for good processability with very low volatiles under stringent autoclave conditions.

Obviously an interdisciplinary research program is necessary to solve the many problems involved in the application of adhesive bonding in aerospace technology. Such a program was initiated in October 1972 at VPI & SU under Contract NAS1-10646-14, with the initial objective of evaluating surface characteristics associated with good adhesive joints. NASA Langley Research Center provided the aerospace engineering, polymer synthesis and testing aspects of this collaborative approach to improved, high-performance adhesive technology. This report is the third of a

series (1,2) demonstrating that the techniques available at VPI & SU are useful to characterize adherend and fracture surfaces of particular interest to NASA. The results of the first two years of surface studies have been published (3) and appended to this report. Recently LaRC personnel have published some of their work on this program (4-6).

During the current grant period, our earlier studies at VPI & SU were continued, using SEM, EDAX, and ESCA to elucidate the physical and chemical nature of (1) Ti and Al adherend surfaces after various surface treatments, and (2) the effects on fracture surfaces of high temperature aging, and variations in amide, anhydride and solvent during polymer synthesis. New studies were carried out to characterize the effects of (1) high-temperature during shear strength testing, (2) fiber-reinforced composites as adherends, (3) acid/base nature of adherends, (4) aluminum powder adhesive filler, and (5) bonding pressure. The new EDAX capability on the SEM stood out as an exceptionally powerful tool for the study of NASA-LaRC problems.

Expertise increased at both locations during the latter half of the grant period, with the addition of two Research Associates with considerable experience. Therefore, this report will attempt to bring together the related details of the first three years of work, and indicate the most promising directions for future research. Comprehensive and unifying theories of adhesion have appeared recently and it is within the framework of these theoretical ideas that all of the results to date cohere, and the next experimental steps are clarified.

The Physical Basis of Adhesion

Kaelble (7) identifies each of the factors involved in adhesive bond performance, and thoroughly reviews the experimental and theoretical details of each factor separately. However, the overall picture is so complex that he leaves the reader with, "The challenge is to apply and intelligently combine these separate theories in order to describe adequately the true physical chemistry of adhesion..." More recently, Good (8) (collaborating with M. L. Williams, et al.) and Andrews and Kinloch (9) (following the lead of A. N. Gent) have proposed different forms of unified adhesion theories. Also very useful in understanding the main factors that determine the strength of adhesive joints, and especially the micro-mechnics of brittle adhesive failure, is a brilliant, but obscure review due to Orowan (10). The following overview of adhesion theory borrows liberally from these four primary references.

The various factors influencing adhesive joint strength are most logically organized by first analyzing the phenomenon into three component parts: (1) the materials from which the joint is constructed (2) the process of forming the joint (and aging), and (3) the fracture of the joint. Now the most efficient approach to arrive at a quantitative theory is to ignore the first two parts above at first, and study part (3), considering the formed joint as one piece of material. The analysis proceeds according to the classical Griffith-Irwin crack theory of fracture mechanics. The results show that the important parameters are: (1) the

elastic modulus, (2) the energy dissipation per unit crack extension, and (3) the thickness of the zone in which the fracture occurs.

As the name of the theory anticipates, a basic assumption is necessary about the distribution of the size of initial cracks and their location in the matrix. Since there is little data available from which to construct a model for the initial distribution of crack-initiation sites, theoretical analyses assume the initiation sites to be constant length and randomly distributed in the matrix (8). More accurate and quantitative accounting of the initial distribution of cracks brings part (2) above into the theory, i.e., in NASA-LaRC adhesive joints, it is the process of forming the joint that determines the initial crack distribution (1-3).

Let us analyze a model of a NASA-LaRC adhesive joint, treating only one interface (Figure 1).

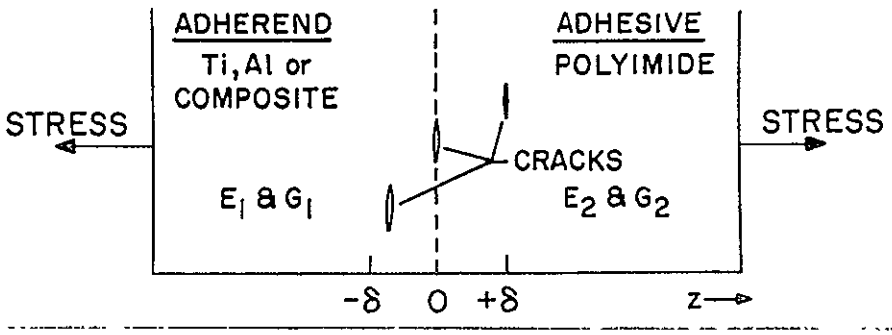

FIGURE 1. Simple model of one interface of a NASA-LaRC adhesive joint under tension.

The Griffith-Irwin theory shows that for a solid of elastic modulus E, containing a crack of length ℓ, the stress σ_f at which fracture will occur is given by

$$\sigma_f = K\sqrt{EG/\ell} \qquad (1)$$

where $K \cong 1$ is a constant, and

$$G = 2\gamma_s + \psi \qquad (2)$$

is the total work dissipated per unit crack extension (fracture toughness). Some work is stored in new surface energy, γ_s. Note that γ_s is <u>not</u> related to the surface energy of the adherend unless the fracture proceeds exactly at the interface. In fact, interfacial failure is rare, and usually $\psi >> \gamma_s$. ψ includes all other dissipative processes, primarily the energy lost in the elastic and plastic deformation of the two phases. The dissipative work G must be done in a layer of thickness 2δ, which increases with increasing G. δ has been estimated to be on the order of 10^{-5}cm.

Based on the earlier results (1-3) it is reasonable to assume that the fracture zone in NASA-LaRC systems is within an order of magnitude of this distance from the adherend interface.

Returning to the model in Figure 1, let the values of G be G_1 in the adherend and G_2 in the adhesive, and similarly designate the elastic moduli E_1 and E_2. Now we shall proceed qualitatively by replotting Figure 1 to reflect reasonable assumptions about the trends in E(z) and G(z). Then we shall apply the Griffith-Irwin equation by holding ℓ constant and inspecting our new plot for minima in the product E x G (see equation 1). Thus the location of the "critical crack" that will initiate failure at the lowest value of stress σ_f will be determined.

Clearly G and E will be greater in the metal adherend than in the polymeric adhesive; the simplest case is shown by the solid lines in Figure 2, which represent strong bonds across the interface and continuous variation of properties from one phase to the other. From inspection of Figure 2, the minimum in

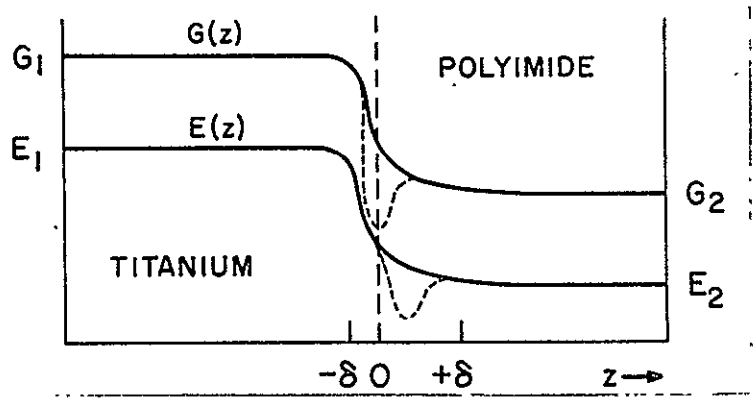

FIGURE 2. Model joint showing qualitative estimates of the elastic modulus (E) and fracture toughness (G). Solid lines-uniform variation of properties and strong interfacial forces. Dashed lines-weak interface (G) and weak polymer surface (E).

the product E x G occurs in the adhesive, and thus for equal-sized initial cracks, fracture will occur at some distance from the interface. The dotted lines in this figure represent the case of weak interfacial bonds (G) or a decrease in polymer modulus (E_2) near the interface. In this situation $\sigma_f = f(E \times G)$ will be minimal very close to, or actually at the interface, depending upon the exact gradients of E(z) and G(z). If the adherend is a polymer/fiber composite, then the modulus and fracture toughness may be equal to, or even less than the adhesive, and the theory would predict failure in the composite.

It is useful to summarize the theoretical picture at this point. First we analyzed an adhesively-bonded joint from the point of view of the strength of materials (fracture mechanics)

and discovered four important factors, (1) the elastic moduli, (2) the fracture toughness, (3) the thickness of the region of failure, and (4) the size and location of cracks "built into" the joint. Then we neglected (4) and qualitatively determined the effects of (1) and (2). Basically the result is that failure will occur in the phase where the product of the elastic modulus and fracture toughness is minimal. Interfacial failure will occur only if the forces across the interface are very weak, and if this is the case, the overall strength of the joint will be very low, too.

Simple consideration (10) will emphasize the fact that the strength of useful joints derives primarily from the physical response of the adhesive (or adherend), either through viscoelastic deformation or by a self-arresting crack mechanism as in the case of brittle adhesives. Consider that in the peeling experiment shown in Figure 3, the work of peeling is dissipated only by the new surface created. The force required to peel the joint is

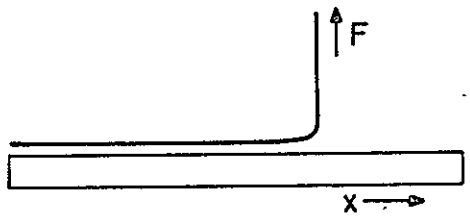

FIGURE 3. Schematic diagram illustrating the peeling of a flexible adhesive tape from an adherend.

simply equal to the total surface energy created in reversible, isothermal peeling, $2\gamma_s$. Now the highest accurately measured value of γ_s is that of mica, found to be 4500 erg/cm^2 in high vacuum,

corresponding to strong ionic bonding (11). With this value,

$$F = 2\gamma_s = 9000 \text{ dyne/cm}$$
$$\cong 1 \text{ ounce per inch width.}$$

For van der Waals bonding usually though to be operative in polymeric adhesives, the peeling force would be some two orders of magnitude less.

The point is that simple atomic or molecular bonds cannot give useful adhesion because the range of action is much too short. A comparison of the tensile stress versus separation distance during the peeling of mica and adhesive tape is semi-quantitatively sketched in Figure 4. In the case of mica, the

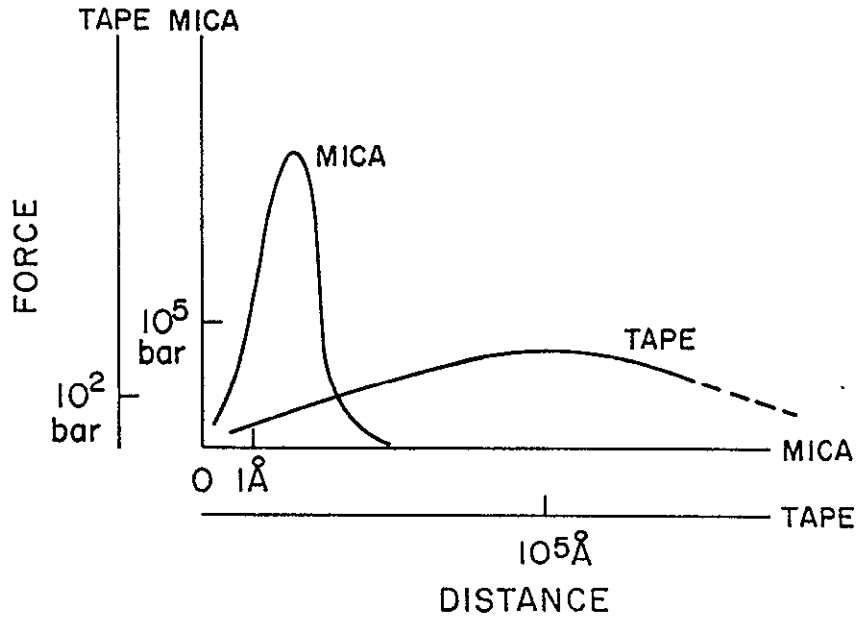

FIGURE 4. Semi-quantitative sketch of the tensile force vs separation distance during the peeling of mica and adhesive tape. Note the different scales of the axes.

critical separation beyond which the force drops rapidly is <5Å; the maximum stress is about 4×10^6 psi, and the area under the

curve is approximately 5,000 erg/cm^2. On the other hand, the maximum tensile stress developed by the adhesive tape is probably several thousand times lower than mica, say 2,000 psi. The range of separation over which this stress develops, however, is of the order of 10^{-3}cm, and the area under the curve is 10^5 erg/cm^2. Thus the work of separation of the mica is less by two or three orders of magnitude: a thin lamella can be blown from a sheet of mica by mouth.

To explicitly and quantitatively account for the separate contributions of interfacial properties and bulk rheology, we use the model of Andrews and Kinloch (9). They show that the adhesive failure energy,

$$\Theta = \Theta_o \cdot f(R) \qquad (3)$$

where Θ_o depends only on the physical and chemical nature of the fracture surface, and f is a function of R, the "reduced" rate of failure propagation obtained from rate and temperature data using the WLF equation. Θ_o is the work of bond fracture and can be expressed generally by

$$\Theta_o = i\, W_a + r\tau_o + s\, F_o \qquad (4)$$

where i, r, and s are respectively the area fractions of interfacial, adhesive and adherend failure, and W_a, τ_o and F_o are the respective intrinsic failure energies. For pure interfacial failure $\Theta_o = W_a$, the thermodynamic work of adhesion.

Experimental data required by this theory are (1) quantitative surface analysis to determine the fractions of interfacial

and bulk failure, i.e. i, r, and s in equation 4, (2) the intrinsic failure energies, W_a, τ_o, and F_o, and (3) the overall joint failure energy Θ measured as a function of temperature and rate of crack propagation. Our previous reports (1-3) have shown that techniques available at VPI & SU, particularly SEM, ESCA and contact angle measurements provide qualitative surface analysis; with some further effort, sufficiently quantitative data to use in part (1) above should be obtainable. The work of adhesion, W_a can be approximated by $W_a = 2\gamma_c$, where γ_c is the "critical surface tension" of the solid, measured by the contact angle method of Zisman (12). The bulk intrinsic failure energies of the adherend and adhesive are the minimum tearing energies, below which no failure can occur regardless of rate or temperature; fatigue studies provide the necessary data. To test whether the overall failure energy is viscoelastically determined, the standard WLF procedure of polymer rheology is employed: the failure energy is multiplied by the factor T_g/T, where T_g is the glass transition temperature, and the rate of crack propagation, $\dot{c}$, is multiplied by a_T, the WLF shift factor that accounts for the change in free volume with temperature. The viscoelastic basis of the failure energy is proved by the superposition of data at different rates and temperatures on one master curve when log $(\Theta\ T_g/T)$ is plotted against log $(\dot{c}\ a_T)$.

Andrews and Kinloch prepared joints with different surface-energy substrates bonded to a single SBR rubber, crosslinked in situ with one initial crack located at the interface at the edge

of the test specimen. They found unique WLF curves for each SBR-substrate pair, independent of the size of the initial crack and also the geometry of the test piece (tensile, peel or shear). The curves for different substrates were parallel, confirming the validity of equation 3, and evaluation of the energy available per area for the actual process of bond cleavage at the interface after rheological losses have been taken into account (θ_o) gave values close to the thermodynamic work of adhesion, if failure was 100% interfacial. Where failure was partly cohesive, about 80% of the value of θ_o was accounted for by the intrinsic failure energy of the adhesive ($r \tau_o$ in Equation (4)), even though $0 < r < 0.2$.

The purpose of this section on adhesion theory is twofold: (1) Provide a general framework in which all the experimental results to data can be discussed and interpreted, and (2) Identify the most important factors to study in order to guide research toward improved high-performance adhesive systems. All the recent theoretical work on adhesive bonding points to the utility of detailed analysis of the fracture surfaces as the first step in elucidating any adhesion phenomena. Thus having determined whether the failure is interfacial or in the adhesive or adherend, and also whether the joint was made without flaws, then one can confidently decide whether to seek improved adhesive-strength performance via improvements at the interface, in polymer (or other materials of construction) properties, or in the technique of making the joint.

II. EXPERIMENTAL

A. Apparatus and Procedures

1. Scanning Electron Microscopy (SEM)

Photomicrographs were obtained (survey at 20X or 50X, high magnification at 200X or 500X, and highest magnification at 1000X to 5000X) using the Advanced Metals Research Corporation Model 900 scanning electron microscope operating at 20 kV. The specimens were cut to approximately 1 x 1 cm with a high pressure cutting bar and fastened to SEM mounting pegs with adhesive-coated, conductive copper tape. To enhance conductivity of insulating samples, a thin ($\sim$200Å) film of Au/Pd alloy was vacuum evaporated onto the samples. Most photomicrographs were taken with the sample inclined at 20° from incident electron beam.

2. Energy-Dispersive X-Ray Fluorescence (EDAX)

Recent improvements in energy-dispersive x-ray analyzers allows rapid elemental analysis to be carried out in the scanning electron microscope (13). The EDAX International Model 707A unit is attached to the AMR-900 SEM, and was first used during the current grant period.

3. Electron Spectroscopy for Chemical Analysis (ESCA)

ESCA data were collected with an AEI ES-100 x-ray photoelectron spectrometer using Al Kα radiation (1486.6 eV). Data were punched onto paper tape by the AEI DS-100 Data System and plotted with a Digital PDP-8/e computer. Samples were cut to approximately 5 x 20 mm and secured to the gold-plated ESCA

probe with double-sided tape. Care was taken to cut samples with features characteristic of the sample as a whole.

4. Specular Reflectance Infrared Spectroscopy (SRIRS)

A Unicam reflectance attachment was used with a Beckman IR-20A infrared spectrophotometer in the specular reflection studies. The study of the acid/base character of adherend surfaces was done by equilibrating adherend samples with dilute solutions of lauric acid and undecyl amine in cyclohexane. Then the adherends were analyzed by SRIRS, before and after rinses with cyclohexane.

B. Materials

The Polymer Group at NASA-LaRC supplied the adherend and fracture-surface samples. They synthesized and formulated unique, new polymer adhesives (4-6), prepared the bonded joints and conducted the lap shear strength measurements according to ASTM D1002-64. Sample designations and descriptions, test conditions and strength results are listed in Table I, along with the techniques used for their study at VPI & SU.

TABLE I

NASA-LaRC #	POLYMER	SOLVENT	LSS	T_{aging} @ 800 hrs.	T_{test}	P_{bond}	COMMENTS	SEM	ESCA
546D3	LARC-III	DG	3775	none	R.T.	40	50% Al	EDAX	
546D4	"	"	1210	"	250°C	"	"	EDAX	
548D3	"	"	3550	"	R.T.	40	63% Al		
548D4	"	"	1600	"	250	"	"		
547D3	"	"	3000	"	R.T.	40	70% Al	X	
547D4	"	"	1875	"	250	"	"		
554D3	"	"	3715	"	R.T.	100	70% Al	EDAX	
554D4	"	"	2335	"	250	"	"	EDAX	
555D3	"	"	3985	"	R.T.	200	"		
555D4	"	"	2335	"	250	"	"		
745D1	BTDA+mm'DABP	"	2960	"	R.T.	50psi	notched	X	
745D2	"	"	2600	"	"	"	"		
745D3	"	"	2560	"	"	"	opp. faces	X(pull directn)	
745D4	"	"	2200	"	"	"	$\overline{LSS}$=2580±15%		
720D2	BTDA+mm'DABP	"	670	295°C	270	"			X
721D4	"	"	850	"	"	"		X(opp.faces)	
731D2	"	"	850	"	"	"	$\overline{LSS}$=760±12%		X

TABLE I (cont'd)

NASA-LaRC #	POLYMER	SOLVENT	LSS	T_{aging} @ 800 hrs.	T_{test}	P_{bond}	COMMENTS	SEM	ESCA
720D1	BTDA+mm'DABP	DG	1200	295	250	50psi			
721D2	"	"	1720	"	"	"		EDAX	
731D3	"	"	1730	"	"	"	$\overline{LSS}$=1465±18%		
720D3	BTDA+mm'DABP	DG	1400	295	225	"			
721D1	"	"	2060	"	"	"		EDAX	
731D4	"	"	2730	"	"	"	$\overline{LSS}$=2065±32%		
720D4	BTDA+mm'DABP	DG	2825	295	R.T.	"			X
721D3	"	"	3000	"	"	"			
731D1	"	"	4315	"	"	"	$\overline{LSS}$=3570±15%	X	X
848D1	BTDA+mm'DABP	DMF	3680	None	"	"			
848D2	"	"	3700	"	"	"		X	
848D3	"	"	4000	"	"	"			
848D4	"	"	4040	"	"	"	$\overline{LSS}$=3860±5%		
878D1	ODPA+mm'DABP	DG	2000	"	"	"			
878D2	"	"	2850	"	"	"			
878D3	"	"	4500	"	"	"		EDAX	X
878D4	"	"	3840	"	"	"	$\overline{LSS}$=3250±38%		
880D1	BTDA+pp'DABP	DG	1500	"	"	"			
880D2	"	"	1400	"	"	"		X(opp. faces)	
880D3	"	"	1500	"	"	"		EDAX	X

TABLE I (cont'd)

NASA-LaRC #	POLYMER	SOLVENT	LSS	T_{aging} @ 800 hrs.	T_{test}	P_{bond}	COMMENTS	SEM	ESCA
880D4	BTDA+pp'DABP	DG	3220	None	R.T.	50psi	$\overline{LSS}$=2310±40%		
881D1	BTDA:PMDA+mm'DABP	"	4480	"	"	"	2 moles BTDA 1 mole PMDA 3 moles mm'-DABP		
881D3	"	"	4920	"	"	"		X	X
881D4	"	"	5140	"	"	"	$\overline{LSS}$=3890±32%	EDAX	
891D1	BTDA+EAH-13	DMAc	3500	"	"	200psi	imidized flow bonding of a film	EDAX	
891D2	"	"	2350	"	"	"			
891D3	"	"	2000	"	"	"			
891D4	"	"	2550	"	"	"	$\overline{LSS}$=2750±27%		X
946D1	BTDA:PMDA+mm'DABP	DG	3360	"	"	100	C/C ... HT-S/P13N molded at 400 psi	X(opp. faces)	
947D1	"	"	3690	"	"	"	C/C ... HT-S/P13N molded at 1000 psi	X(opp. faces)	
948D1	"	"	3750	"	"	"	C/Ti... HT-S/P13N molded at 400 psi	EDAX(opp. faces	
948D3	"	"	3880	"	"	"	C/Ti... HT-S/P13N molded at 1000 psi		

III. RESULTS AND DISCUSSION

A. FRACTURE SURFACES

The major proportion of work done during the current grant period concerned the study of fracture surfaces. Four new sets of samples were supplied by NASA LaRC from their 500-, 700-, 800- and 900-Series. The sample designations and descriptions are listed in Table I along with a notation on which techniques were employed for their study. Using the broad distribution of samples tabulated plus reference to the previous work (1-3), several conclusions can be drawn about the micro-mechanics of joint failure and the effects of variations in adherends, surface treatments, adhesive formulation and strength-testing parameters.

1. Aging and Testing at Elevated Temperatures

Samples 731D1, 721D1, 721D2 and 721D4 represent a series prepared with a standard BTDA+mm'-DABP/DG adhesive and exposed to 295°C for 30 days in air, and then shear tested at 25°, 225°, 250° and 270°C, respectively. The strength of the room temperature test (about 3600 psi) shows that very little thermal- or oxidative-degradation occurred during the severe exposure (N.B. joints were <u>not</u> stressed during aging). Strength drops rapidly at the higher testing temperatures.

SEM examination of this series of samples (Figures 5-9) indicates that two processes occur as the testing temperature increases: (1) the percentage of interfacial failure increases

dramatically, and (2) the amount of plastic deformation and brittle-fracture surface decreases. Apparently the increased temperature weakens the forces across the polymer-metal interface, and the polymer experiences less stress. Recall that theory predicted that joint strength would decrease as the fraction of interfacial failure increased.

The same general features characterize the fracture surface of the sample tested at room temperature (Figure 5) as have been seen in previous (unaged) high strength samples (1-3). At lower magnification there is a fairly uniform distribution of raised material that forms a filigree pattern (A) superimposed upon lower, smooth, oblong areas (B) that have dimensions ranging from 0.02 to 0.5 mm, approximately. The low areas are the bottoms of voids that were probably created during the formation of the joint and expanded during fracture. The filigree is composed of the void-cell walls that have undergone plastic deformation and finally fractured, primarily by a brittle cleavage-crack propagation mechanism. Some of these cracks are smooth and quite parallel to the substrate such as in area C on the higher magnification photomicrograph, but also fine louvers, tilted at an angle to the adherend, appear along the curved line that comes down the center (D). No doubt the fracture process is practically adiabatic, creating locallized "hot spots" that could promote ductility indicated at E. Note that only a very small amount of interfacial failure appears and many very thin walls result from plastic deformation.

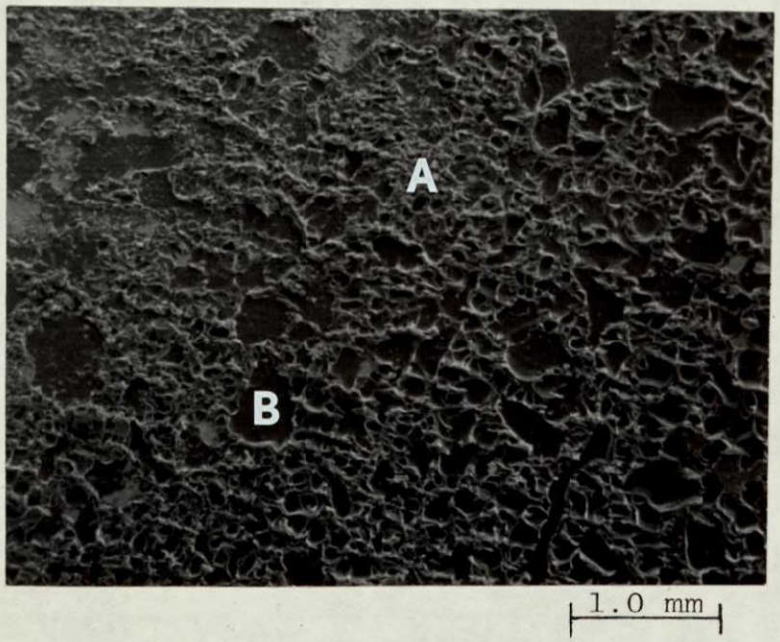

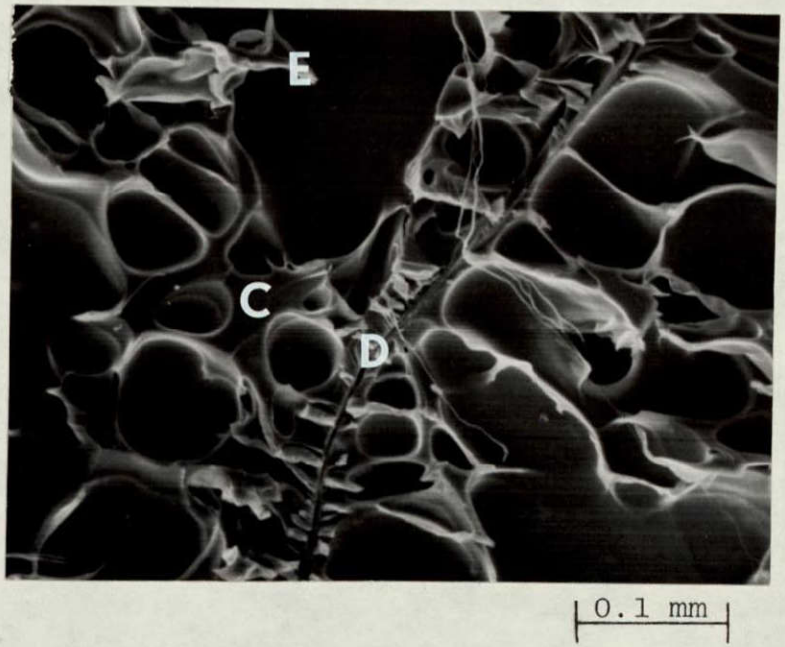

FIGURE 5. Two magnifications of sample #731D1 that gave 3570 psi shear strength at room temperature after aging 30 days at 295°C. Features similar to previous (1-3) high-strength samples.

Generally similar features are seen in the first high temperature sample (Figure 6), but the proportion of interfacial failure (A) and void area (B) has increased. Areas of adhesive that have detached from the opposite adherend show that original interfacial contact was good, because the polymer faithfully replicates the detailed surface features of the titanium in area C. Comparing Figures 5 and 6, it is tempting to say that the voids have coalesced in the latter, sometimes reaching dimensions over 1 mm. Correspondingly, void-cell walls are thicker; area D (higher magnification) provides a striking example of a plastically drawn void-cell wall circumscribed by brittle cleavage cracks.

Figure 7 shows that the fraction of interfacial failure and void area continues to advance with temperature. Large void spaces are almost completely interconnected across the sample. At higher magnification, some strength across the interface is indicated at the place where the louvers between brittle cleavage cracks meet the exposed substrate.

Interfacial failure predominates at the highest test temperature. The opposite sides of mating fracture surfaces are shown in Figure 8; it is quite simple and instructive to locate the matching features. There is very little plastic deformation, hence little strength.

Brittle cleavage cracks without much louvering account for the failure that is not interfacial. The circled area of Side 1 is shown at higher magnification in Figure 9, illustrating a few brittle cleavage crack louvers and also low forces across the polymer/metal interface.

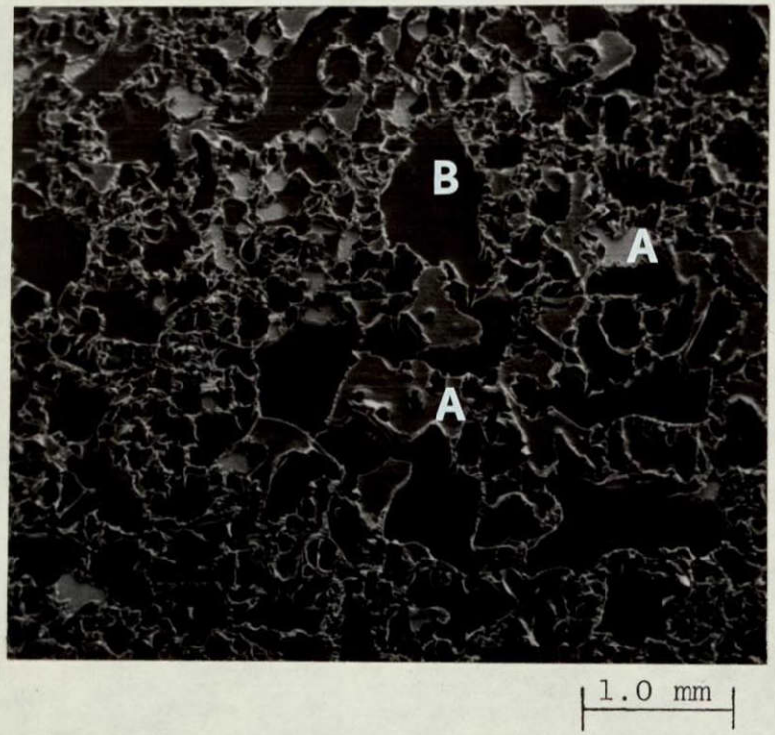

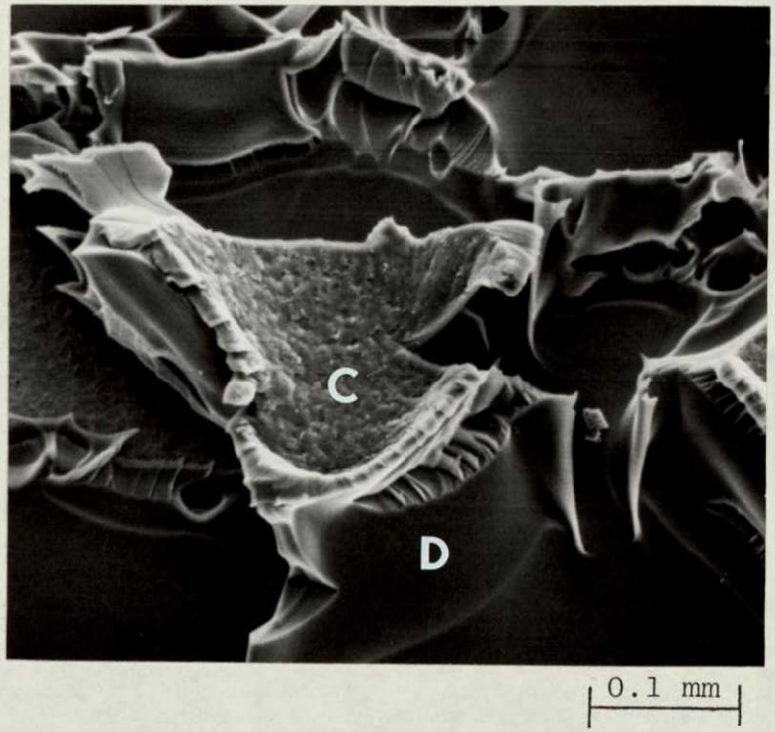

FIGURE 6. Two magnifications of sample #721D1 that gave 2065 psi shear strength at 225°C after aging for 30 days at 295°C. More interfacial failure and void area, and plastic deformations have thicker walls.

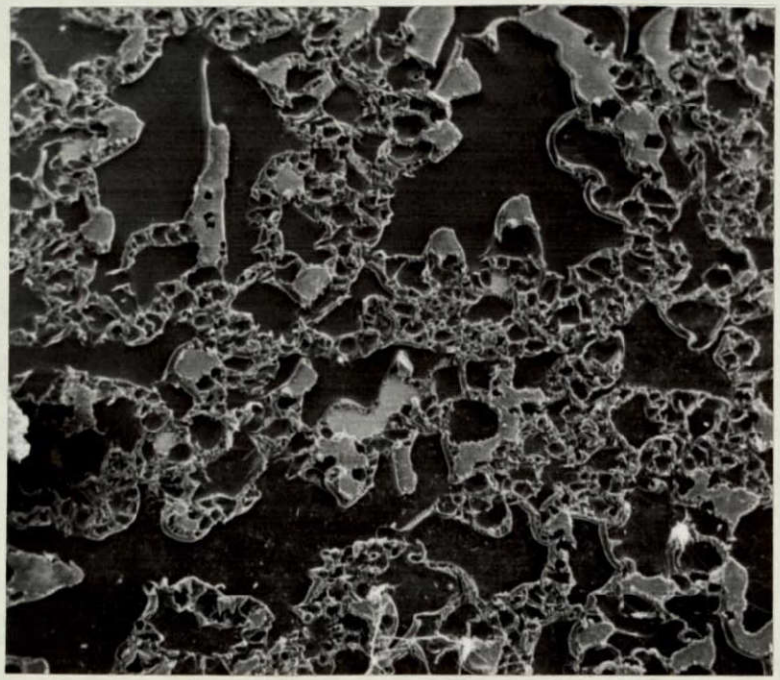

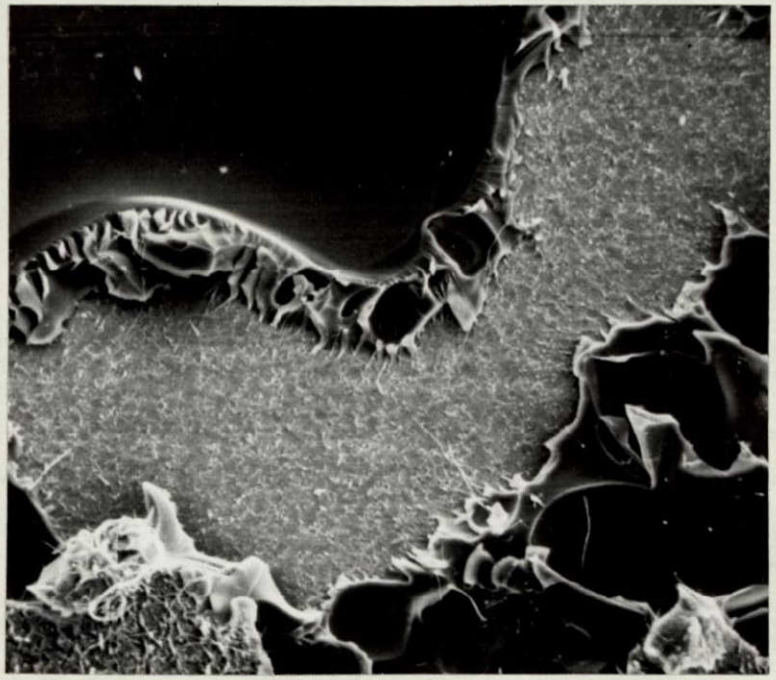

FIGURE 7. Two magnifications of sample #721D2 that gave 1465 psi shear strength at 250°C after aging for 30 days at 295°C. Even more interfacial failure and void area.

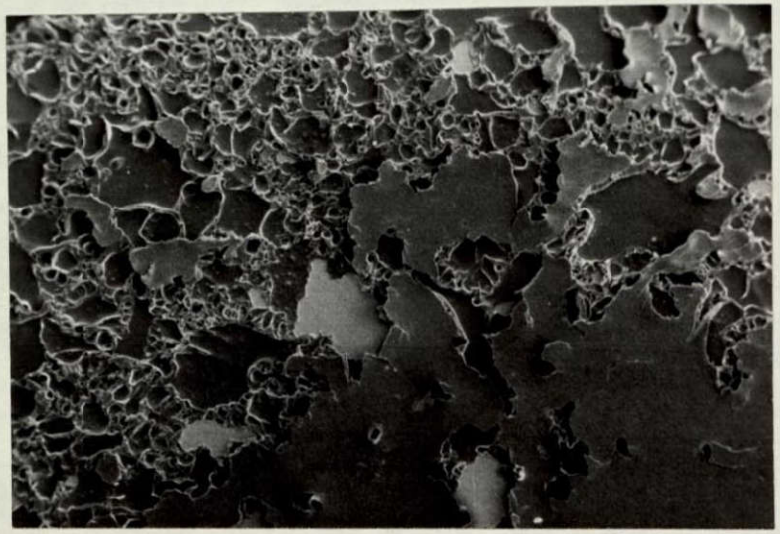

Side 1

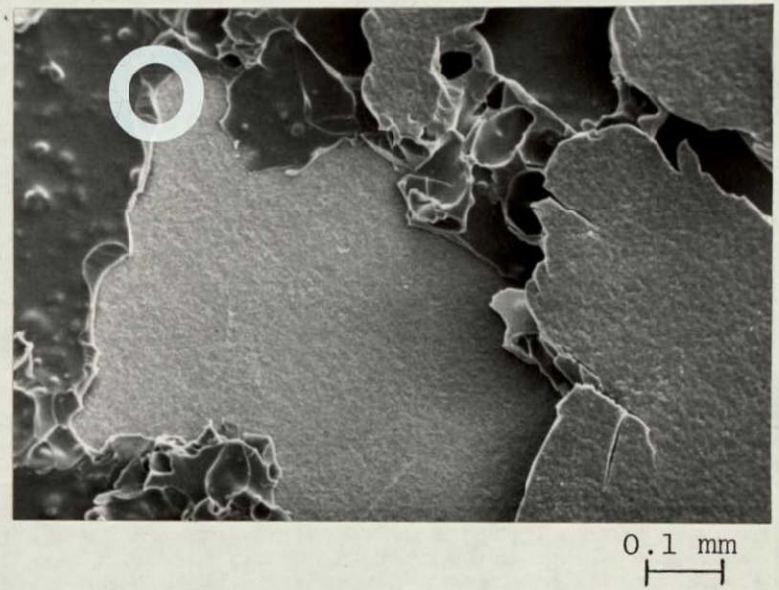

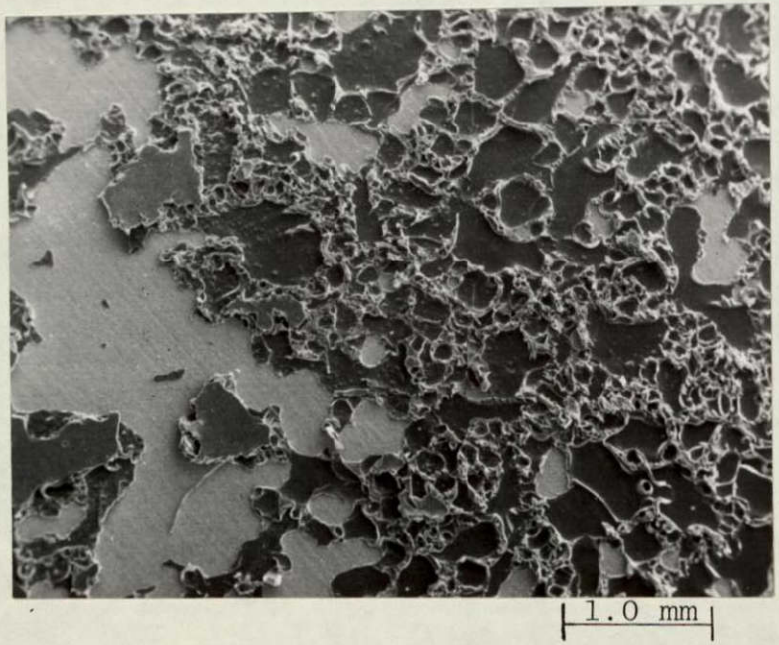

Side 2

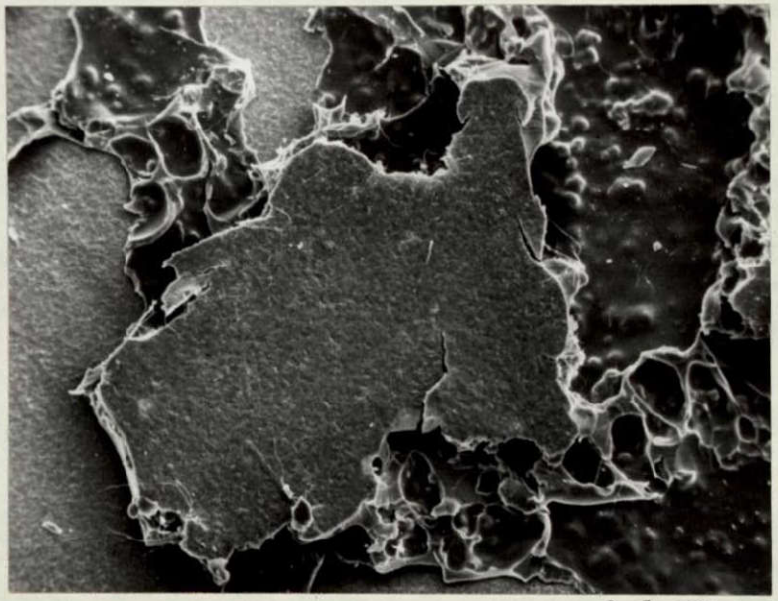

FIGURE 8. Two magnifications of the opposite mating fracture surfaces of sample #721D4 that gave 760 psi shear strength at 270°C after aging for 30 days at 295°C. Extensive interfacial failure, and small amount of plastic deformation and cleavage cracks.

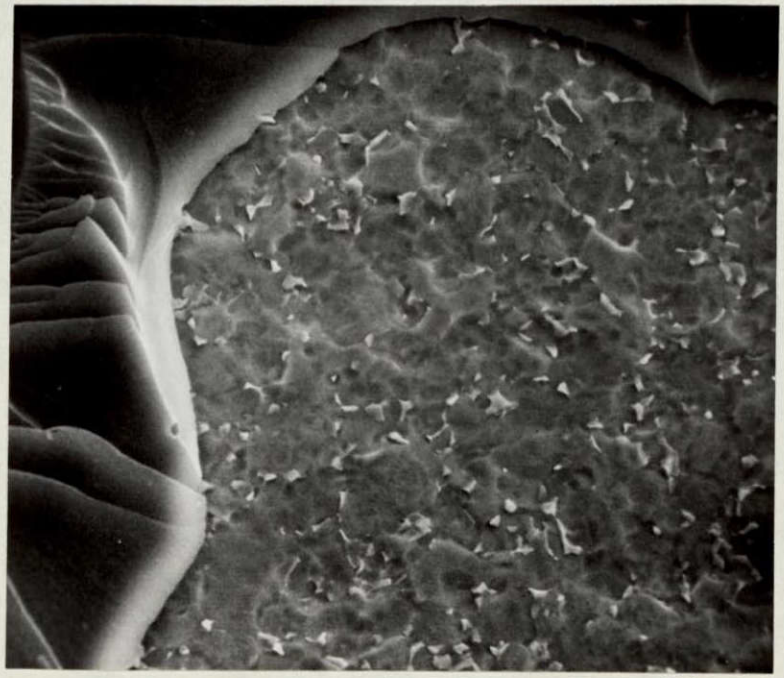

FIGURE 9. High magnification view of area circled on Side 1, Figure 8. No bonding apparent at junction of polyimide and titanium. Good illustration of brittle cleavage cracks at left.

It appears that the polymer/metal interfacial forces are weakened by the high test temperatures, probably due to differential thermal expansion. Filling the adhesive with metal powder has been suggested to alleviate this kind of problem, and a later section reports some success with this approach.

2. Anhydride, Amine and Solvent

Several adhesive formulation parameters were varied in the 800-series. Good shear strengths were obtained in spite of changes in comonomers and solvent, except for the use of p,p'-DABP, which gave 1400 psi. Figures 10-14 display the micro-mechanics of fracture for these samples. The shear strength results can be explained in terms of proportion of voids, interfacial and brittle failure, and plastic deformation.

The use of dimethylformamide (DMF) as solvent for standard polyimide gives little interfacial failure, but a large proportion of connected void area compared to fracture area, shown in Figure 10. Apparently the 3700 psi strength is developed by the initiation and annihilation of a large number of brittle cleavage cracks illustrated by all the louvers in the higher magnification photomicrographs.

Figure 11 shows a large proportion of drawn and fractured polymer in a high-strength sample prepared with anhydride comonomer, ODPA. At higher magnification, a balance between moderate plastic deformation and brittle fracture is apparent.

Mating sections from both sides of the 1400 psi joint are shown in Figure 12. It is difficult to compare this sample with

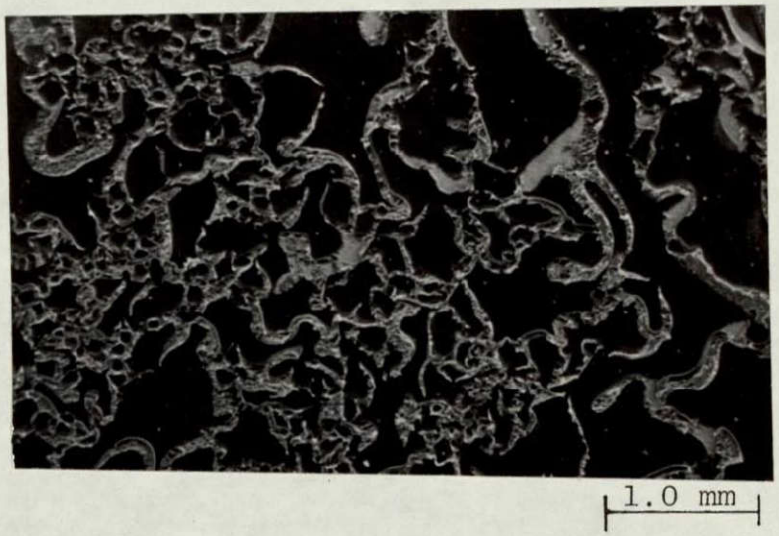

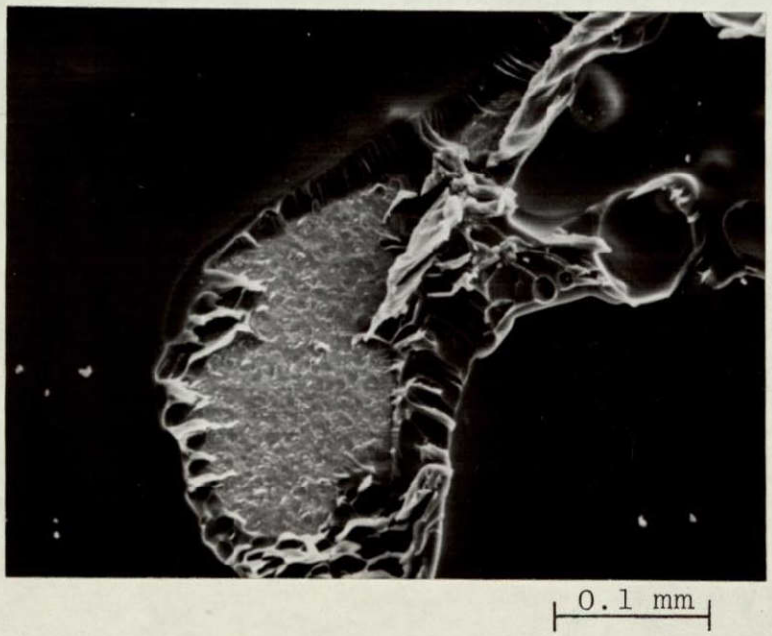

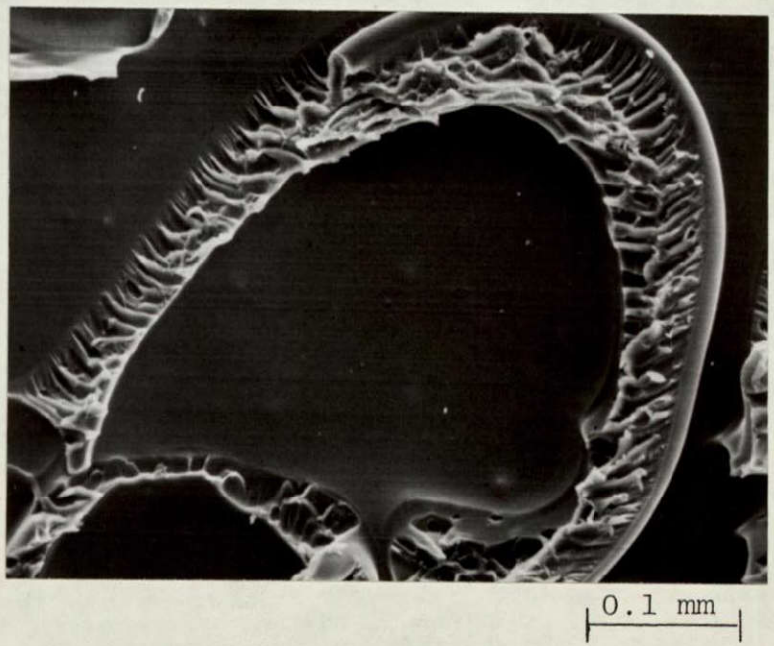

FIGURE 10. Sample #848D2: Standard BTDA/mm'-DABP polyimide in DMF solvent; shear strength 3700 psi.

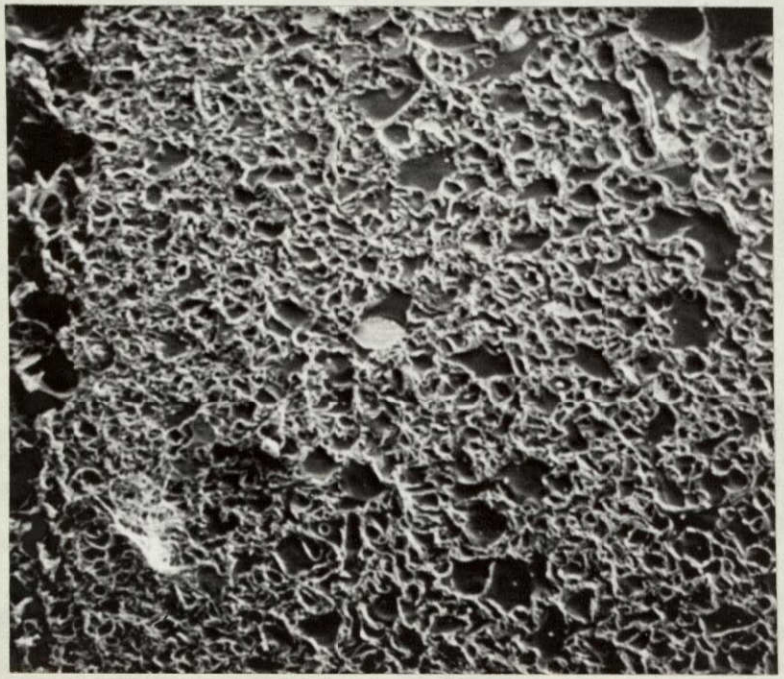

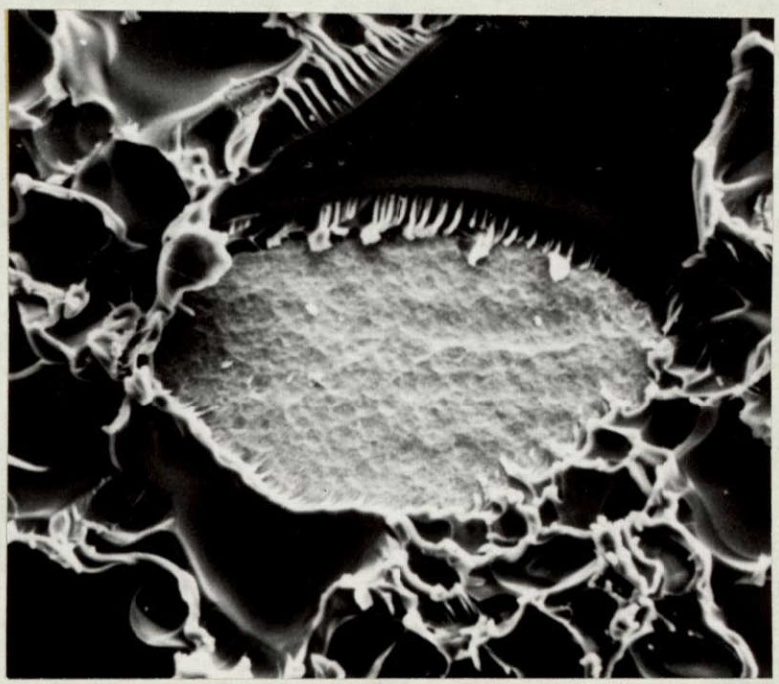

FIGURE 11. Sample #878D3: OPDA/mm'-DABP/DG; shear strength 4500 psi.

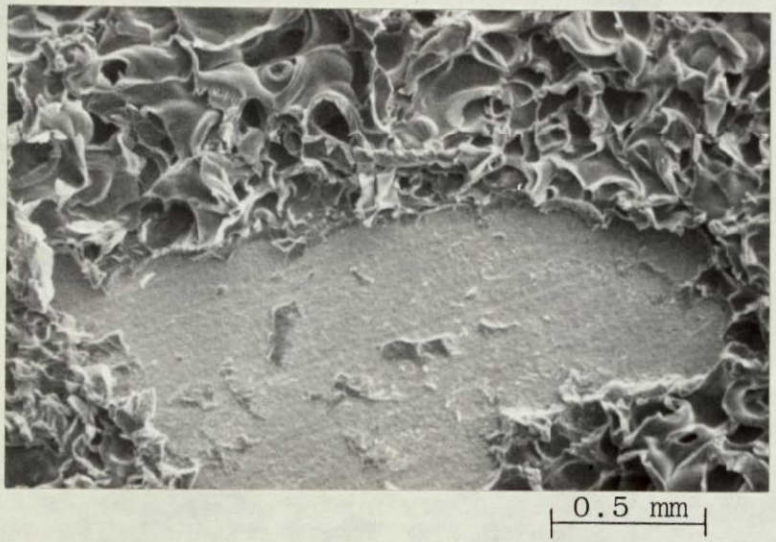

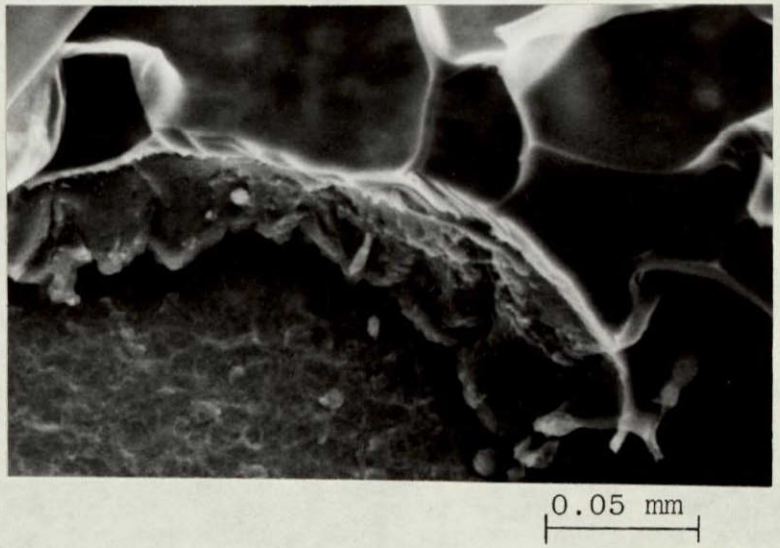

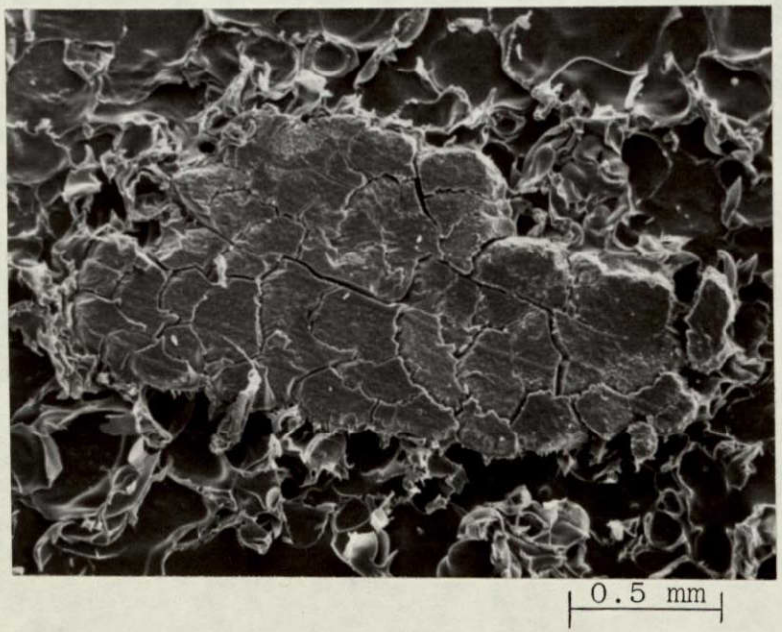

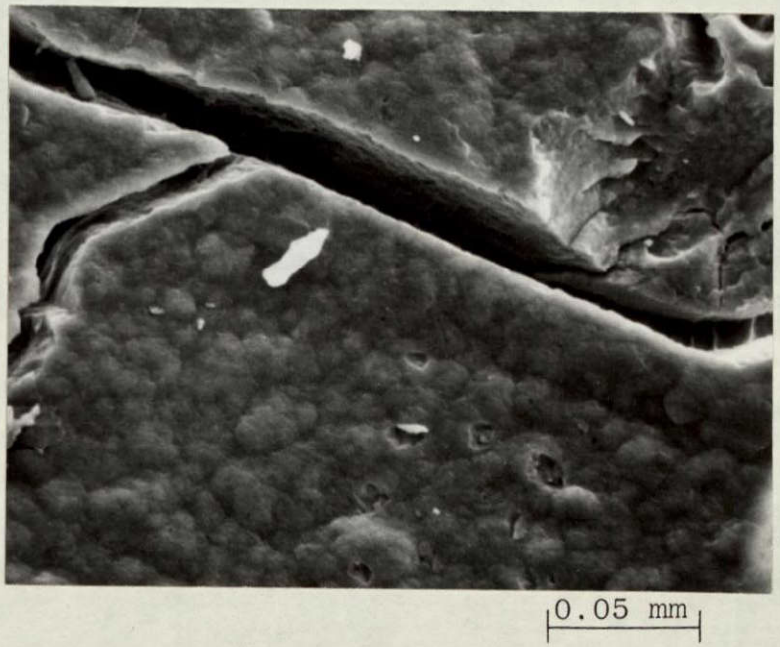

FIGURE 12. Sample #880D2: BTDA/pp'-DABP/DG; shear strength 1400 psi.

the others because the magnifications are different. However, if the lower magnification photomicrograph is representative of the entire fracture surface, then the proportion of interfacial failure is large, again correlating with the low strength. There appears to be quite a bit of plastically deformed polymer surrounding the area of interfacial failure, but no louvers occur, even where the "plug" of adhesive is fragmented by brittle cleavage cracks.

A vexing problem in adhesive evaluation is the scatter of strength-testing data. For example, NASA LaRC prepared an adhesive formulation using one mole of PMDA and two moles of BTDA with three moles of mm'-DABP in diglyme (DG), representing a compromise between strength and durability. The average value of four lap shear strength samples was 3890 psi, but the range was from 2640 psi to 5140 psi. Photomicrographs of the two extreme samples in Figure 13 show more area of plastic deformation and brittle fracture (filigree at low magnification) in the higher strength sample. The balance of drawing and louvering that is clear at higher magnification indicates a large absorption of energy.

The most facinating result was obtained using a totally imidized, film adhesive. EAH-13 comonomer was used to provide enough flow at high temperature so that good interfacial contact occurs during pressing at 200 psi and 300^{o}C for an hour. The photomicrographs in Figure 14 show that the polymer has formed a detailed replica of the titanium surface. Failure is totally interfacial on one side of the joint. It is amazing that 3500 psi shear strength can be obtained without contributions from plastic and brittle mechanisms. Perhaps elastic deformation occurred. Otherwise, the

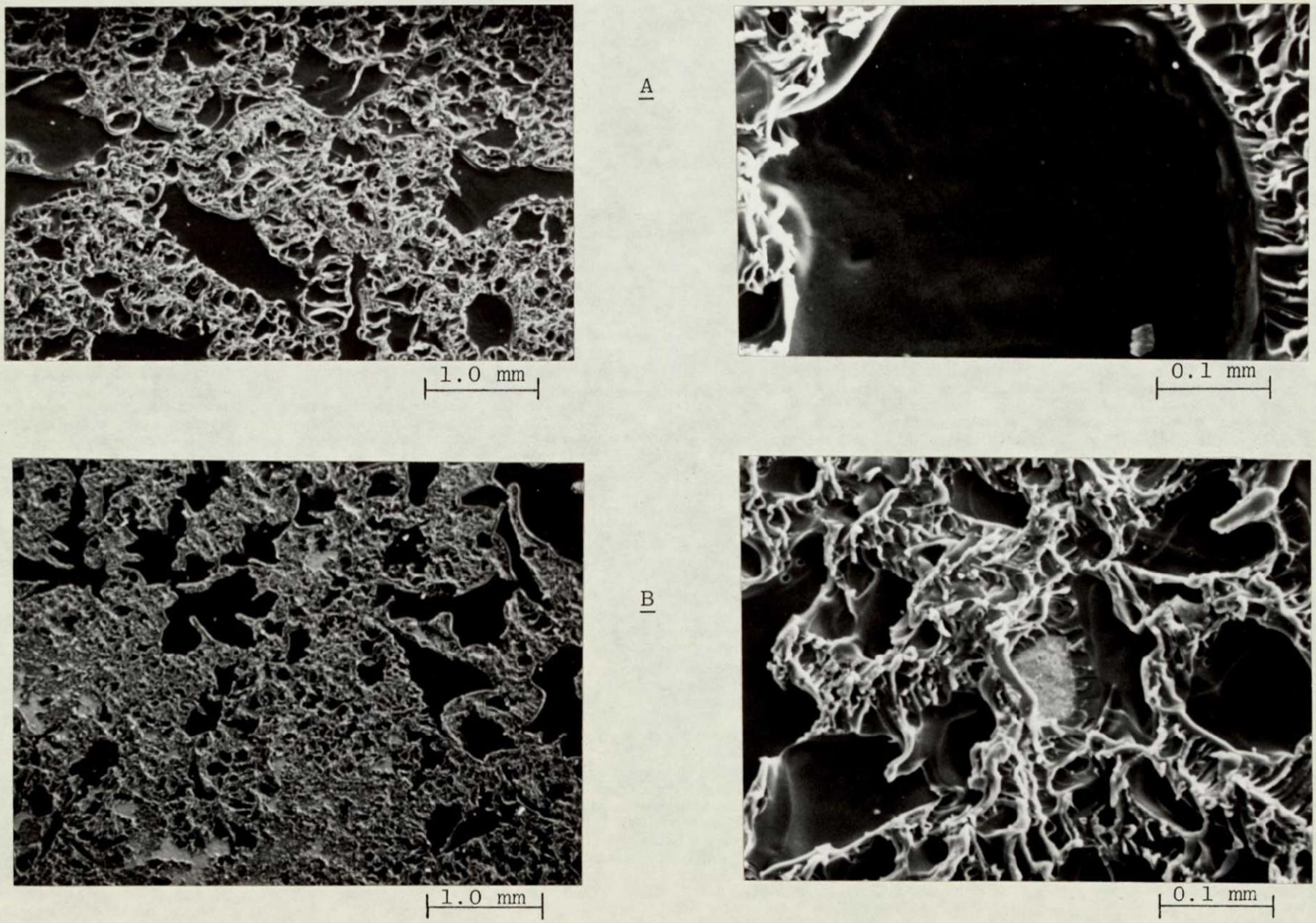

FIGURE 13. 2BTDA+1 PMDA/mm'-DABP/DG, A. Sample #881D1: shear strength 2640 psi; B. Sample #881D4: shear strength 5140 psi. Note correlation between amount of filigree and bond strength.

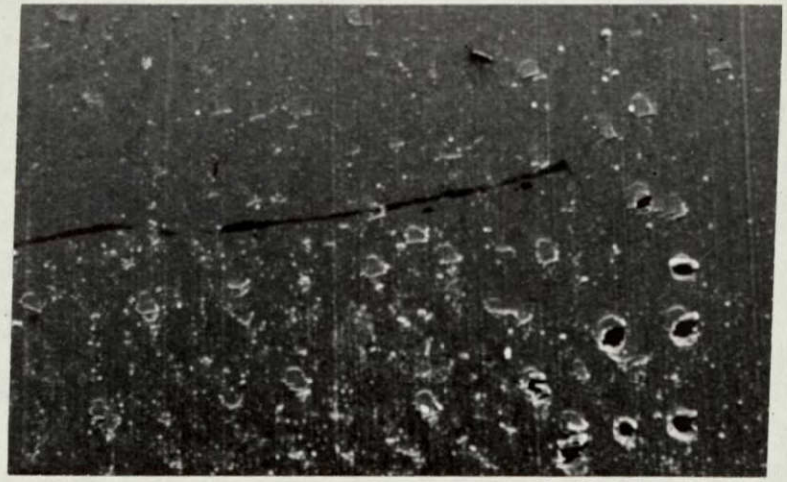

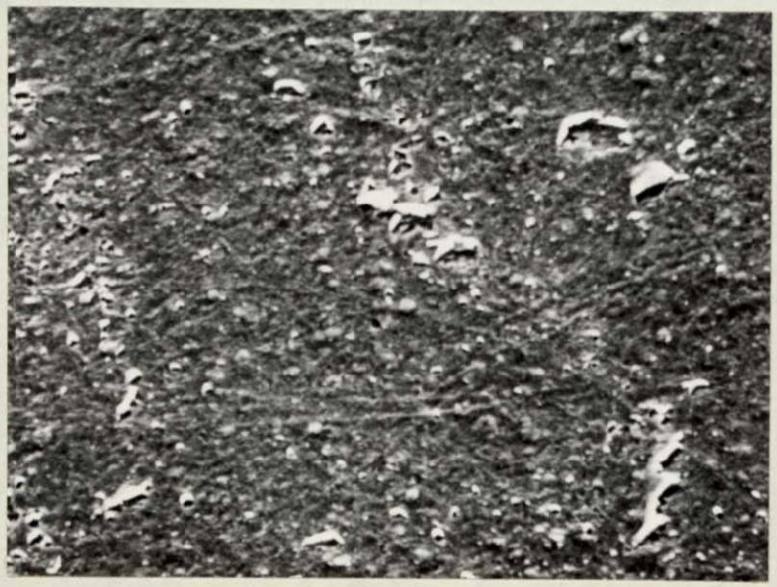

FIGURE 14. Sample #891D1:BTDA/EAA-13/DMAc; shear strength 3500 psi. Note that virtually no void present; completely different appearance when no water of imidization released in the joint.

true area over which polymer/metal polar and dispersion forces interact must be many times the geometrical joint area, due to the adherend roughness.

Of prime importance is the absence of the typical void structures so characteristic of joints prepared by imidization during bonding. Figure 14 makes it clear that not only does the water released during imidization create voids in the joint, but the voids are the weakest aspect of many of these joints. The scatter in joint strength values probably derives from the random way in which the void size and distribution is generated as the polymers cure. The need is clear to develop either new adhesive formulations or bonding techniques to avoid joints with so many inherent flaws.

3. PI/HT-S Fiber Composite Adherends

New types of fracture surfaces occur when composites are used as one or both adherends (Figures 15-18). Shear strengths fall within 10% of 3500 psi and failure occurs by a catastrophic, brittle mechanism, partly in the adhesive and partly in the surface region of the composite.

Failure in the adhesive layer is initiated at inherent voids that are much smaller than the voids seen in Figures 5-14 where titanium adherends were used. Probably the composite matrix absorbs some of the water of imidization. These features are illustrated (Figure 15) in Sample 946D1 that had two composite adherends molded at 400 psi. Only a small wedge of one adherend surface was plucked out; failure was by a brittle mechamism in the myriad of small

void-cell walls in the adhesive. There was little plastic deformation, but a great deal of fine debris, as though the joint had exploded.

When a pressure of 1000 psi was used to mold the composite adherends, more than 50% of the failure took place in the composite surface - with a small increase in strength (Figure 16). More detail of the fracture surface within the composite is shown in Figure 17 at higher magnification. Polymer fracture seems to have no plastic component, the brittle failure area is small and has no louvering. The forces across the fiber-polymer interface appear to be weak.

The result of using composite as one adherend and titanium as the other are shown in Figure 18. Failure is almost entirely in the composite, but it is interesting to note that the voids are larger where failure is in the adhesive layer. Evidently the titanium retarded the diffusion of the water of imidization. A titanium signal was obtained by EDAX examination of area A; therefore the adhesive layer at the bottom of the void must be less than 1 μm thick.

In all three examples in this section a considerable amount of work must have been required to create all the surface area of the fine debris. Also high surface temperatures must have been created because the debris would not be removed by vigorous brushing in the presence of ionizing radiation (to eliminate static electricity). The particles apparently were "welded" to the fracture surface right after failure.

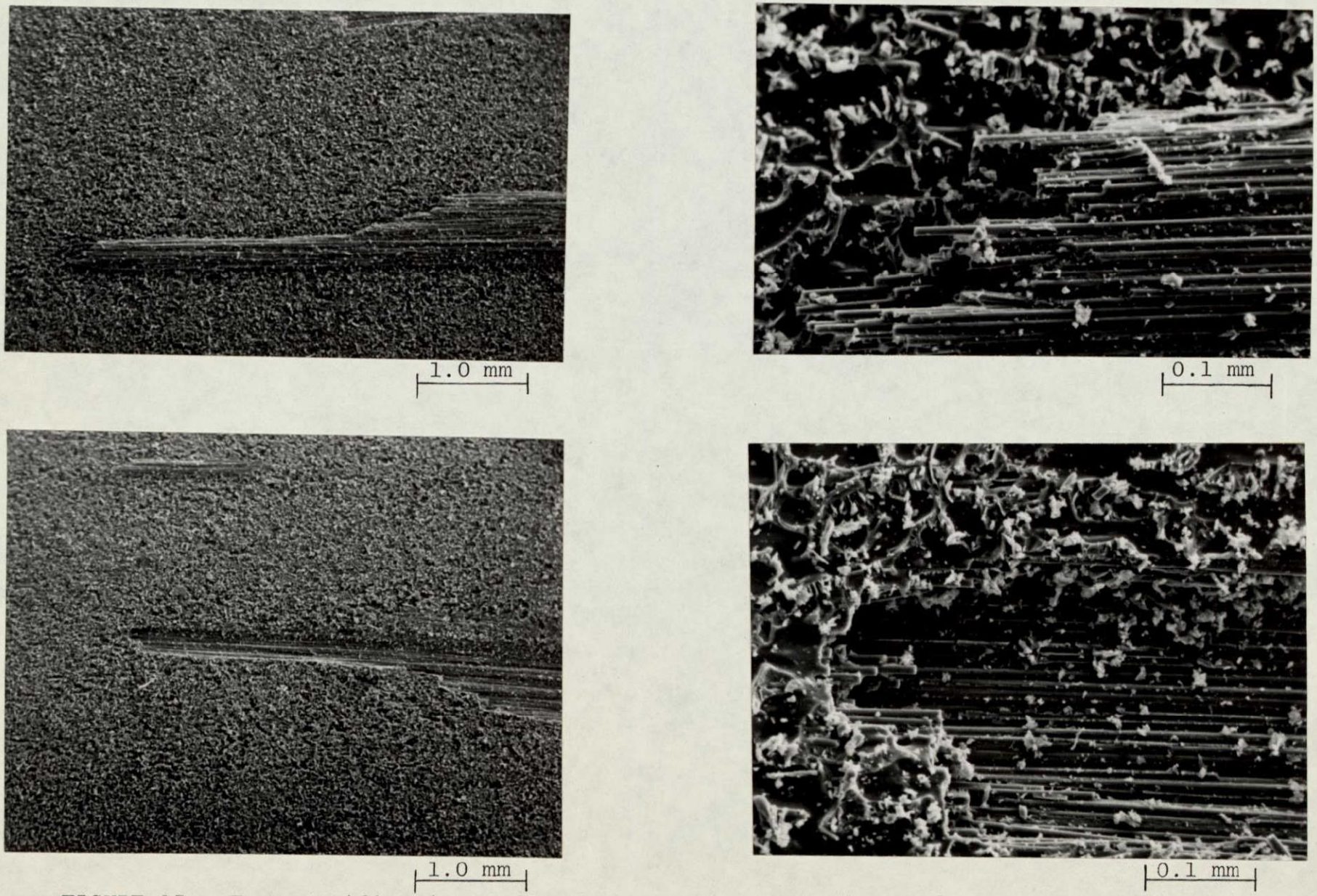

FIGURE 15. Two magnifications of opposite mating fracture surfaces from Sample #946D1; both adherends were HT-S/P13N composites molded at 400 psi. Shear strength was 3360 psi, and failure was mostly in the void-filled adhesive layer.

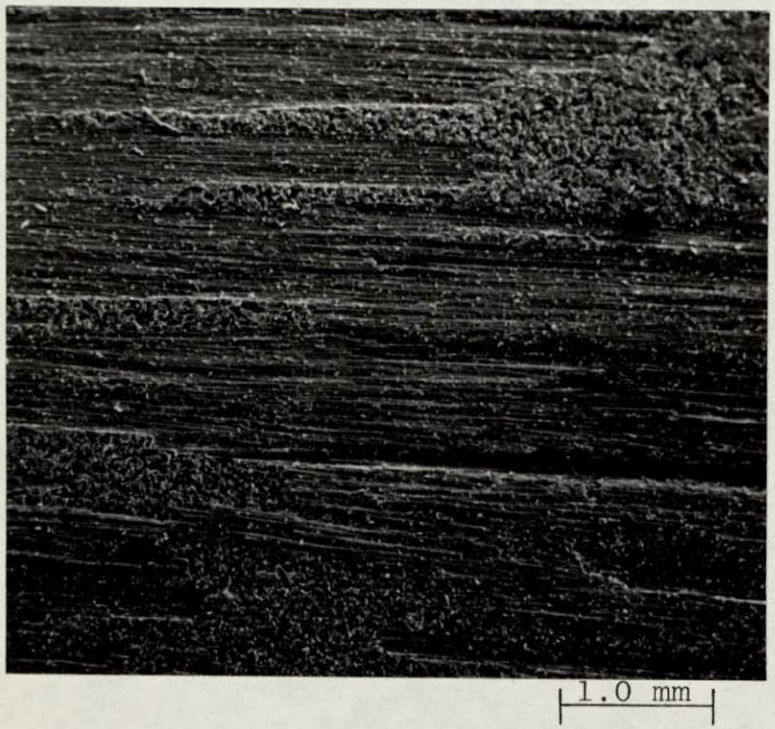

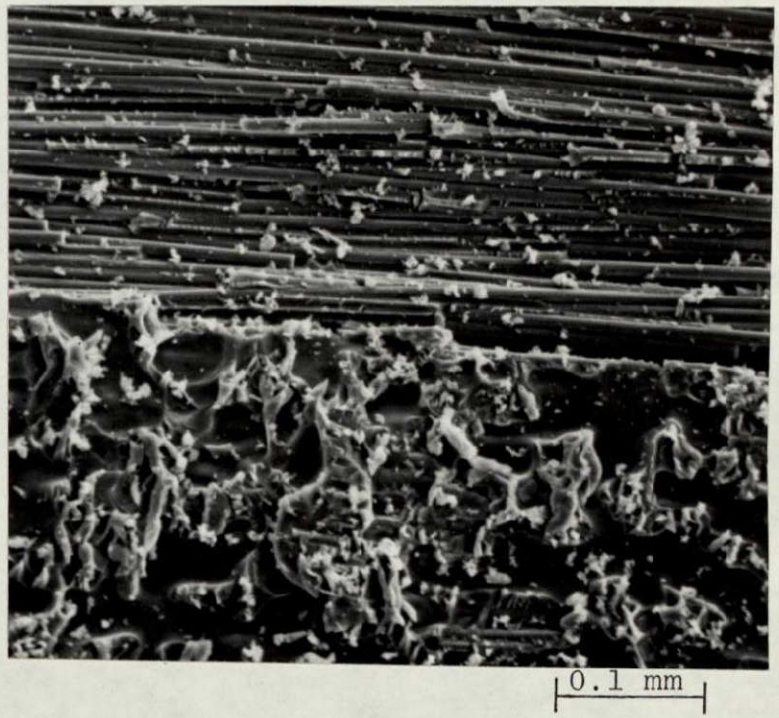

FIGURE 16. Two magnifications of Sample #947D1; adherends were HT-S/P13N composites molded at 1000 psi. Shear strength was 3690 psi and failure was about 2/3 in the composite.

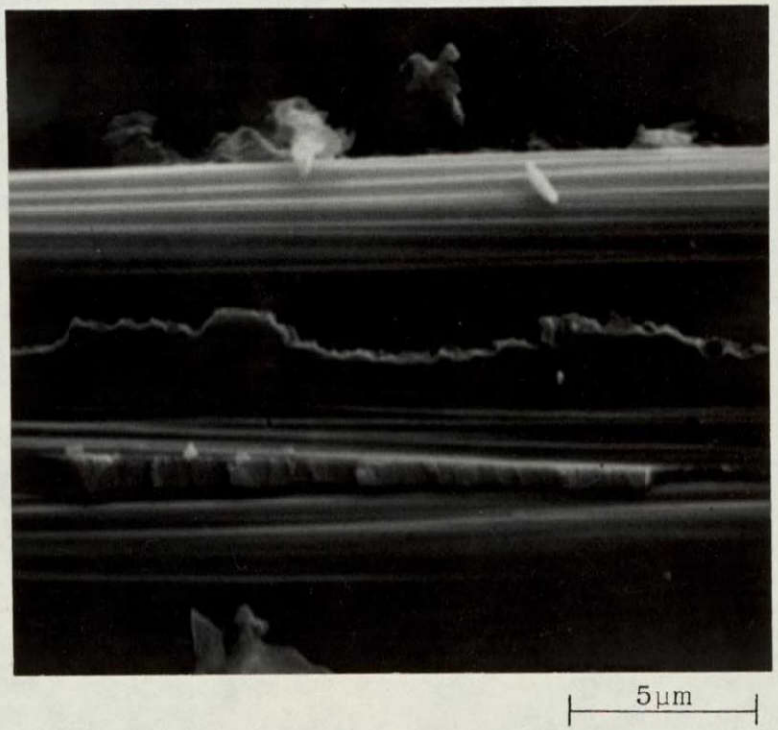

FIGURE 17. High magnification view of composite failure in Sample #947D1. Polymer/fiber interfacial failure is obvious. There is no plastic deformation and brittle fracture surface area is small.

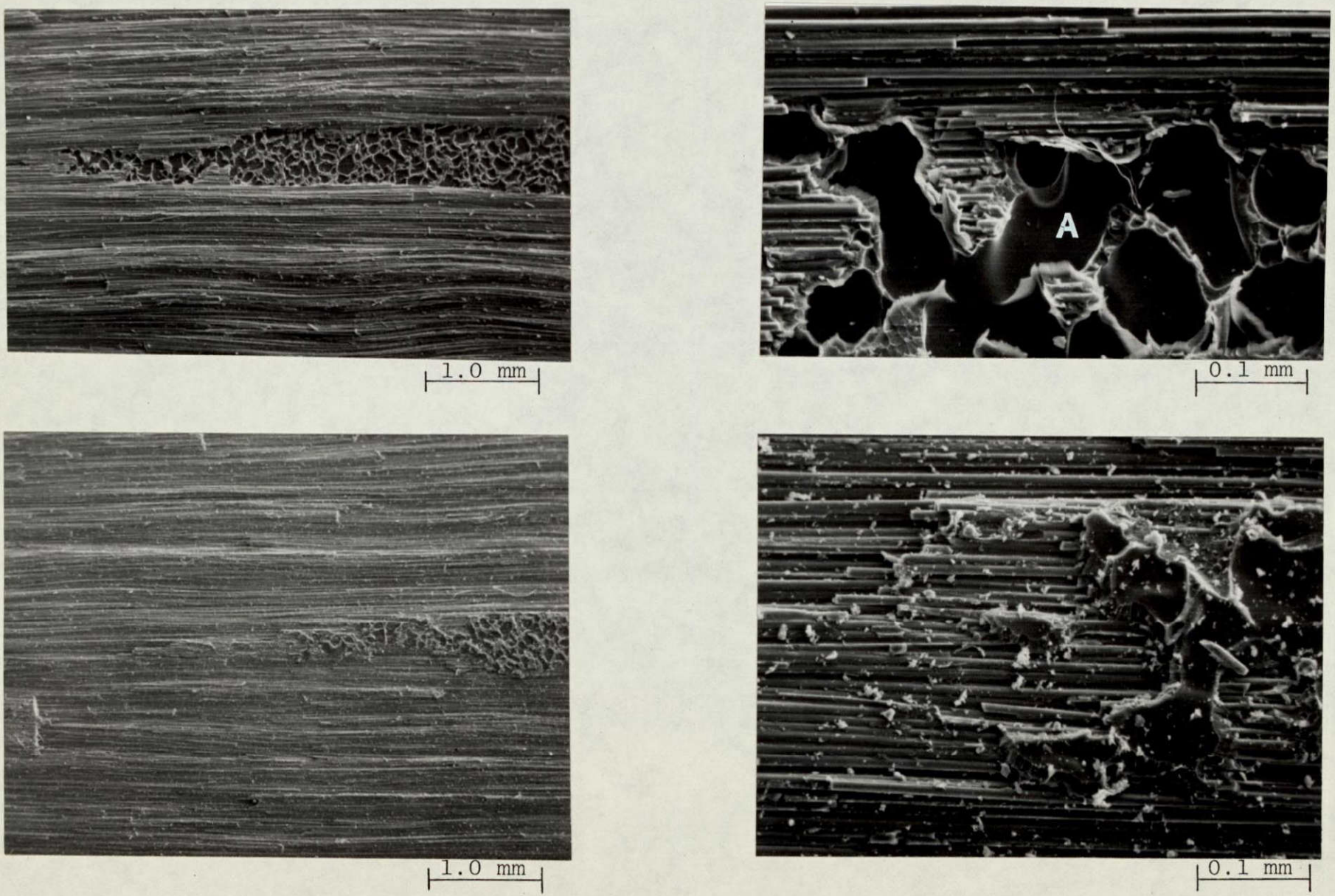

FIGURE 18. Two magnifications of opposite mating fracture surfaces from Sample #948D1; one adherend was titanium and the other was HT-S /P13N composite molded at 400 psi. Shear strength was 3750 psi and failure was mostly in the composite.

4. Aluminum Filler and Bonding Pressure

Progar and St.Clair found that the best balance of properties was obtained with the copolymer of 65/35 BTDA/PMDA+m,m'-DABP (6). Further improvement in high temperature strength was obtained by using aluminum powder as an adhesive filler and increasing bond pressure. These variables produce several changes in the appearance of fracture surfaces, as shown in Figures 19-24.

The aluminum filler is apparent as lumps about 1-10 μm in diameter, covered with at least a thin layer of polyimide. Fracture-surface features are much smaller than with unfilled adhesive. At high magnification it appears that the fracture initiates in a myriad of minute voids (or nucleation sites) existing in the walls of the larger void areas.

Figure 19 shows the increase in "lumpy" appearance caused by changing the filler content from 50% to 70% by weight. Also voids in the size range 10-50 μm seem to disappear.

Figure 20 shows a survey (20X) and fine detail (2000X) of the sample with 50% Al, bonded at 40 psi. At low magnification the balance of void and filigree areas is similar to many of the previous samples. The room temperature sample (#546D3) has good strength, and at high magnification the fracture surface is composed of very thin, plastically deformed microvoid-cell walls. This feature is unique to the filled adhesive. By contrast, the high temperature sample (#546D4, 1210 psi) appears melted and has no thin, drawn films. It looks as though the high temperature and stress softened the polymer and reduced its strength. No interfacial failure occurred, in contrast to the results at 250°C with

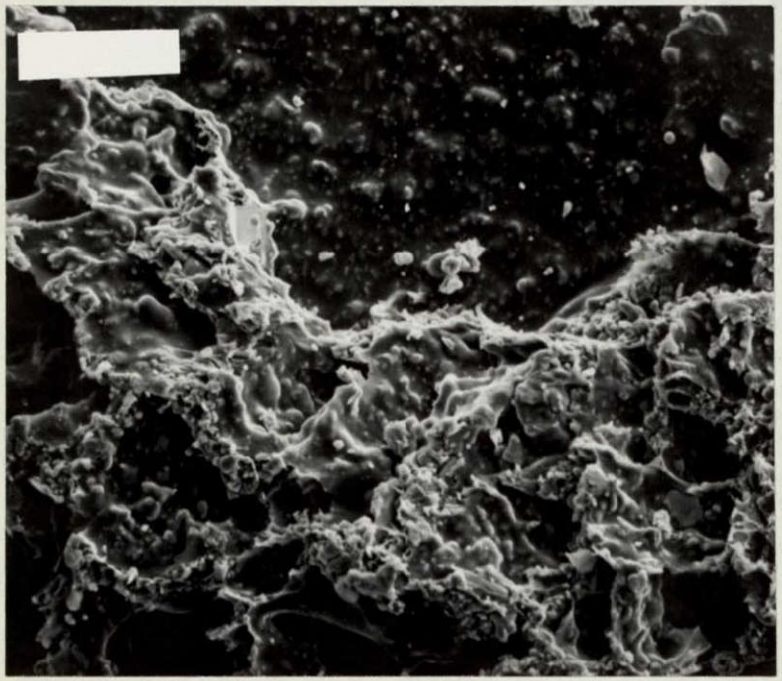

50% Al
#546D4

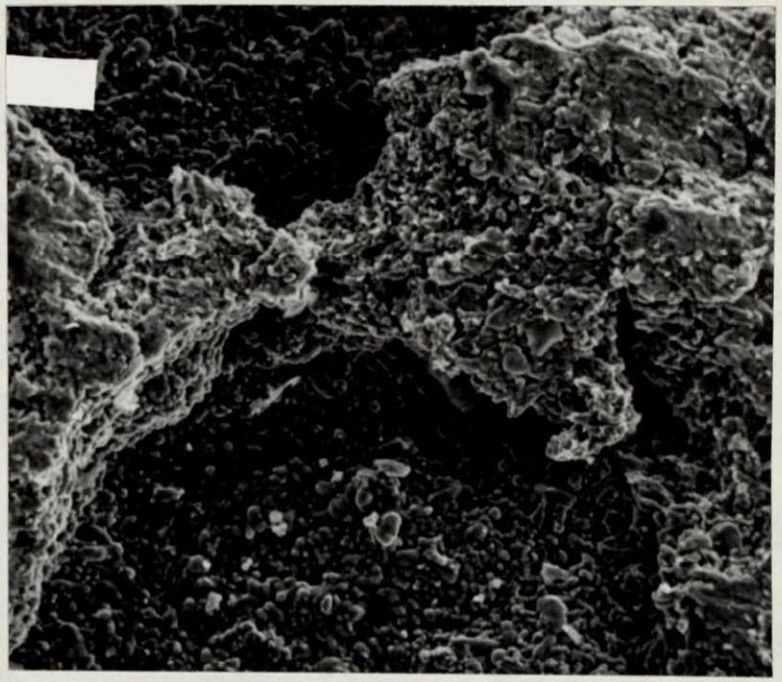

70% Al
#547D3

FIGURE 19. High magnification view of Sample #546D4 and #547D3, showing the effect of increasing filler content.

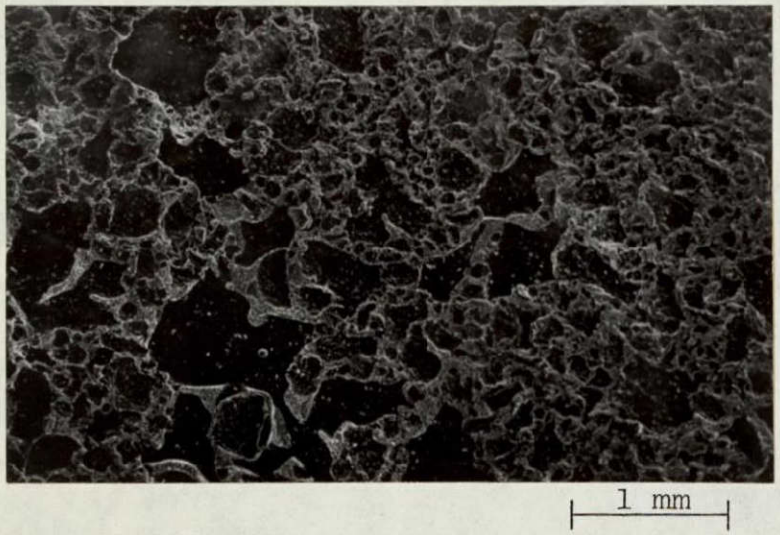

3775 psi
@ 25°C

#546D3

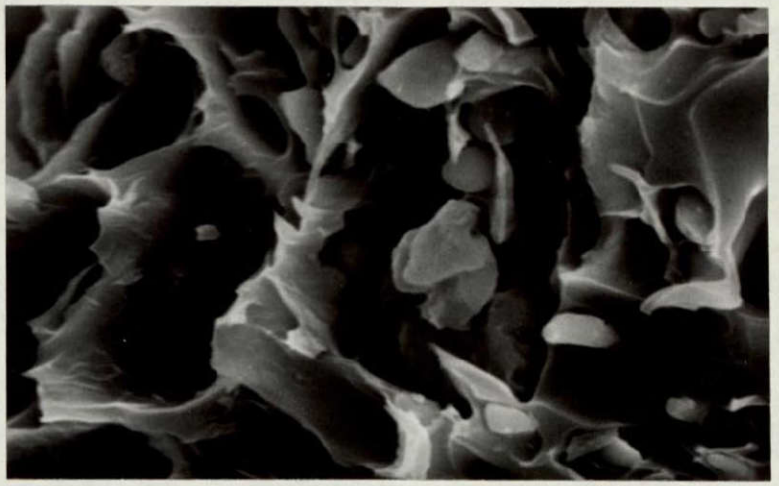

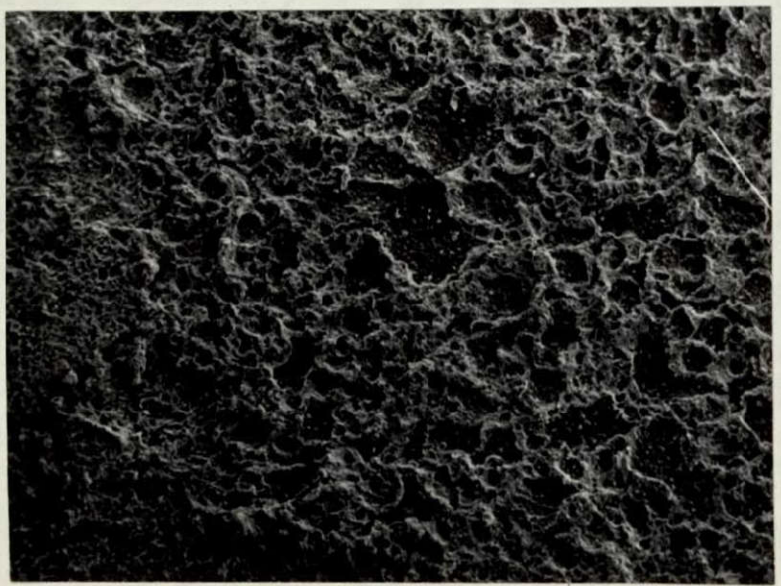

1210 psi
@ 250°C

#546D4

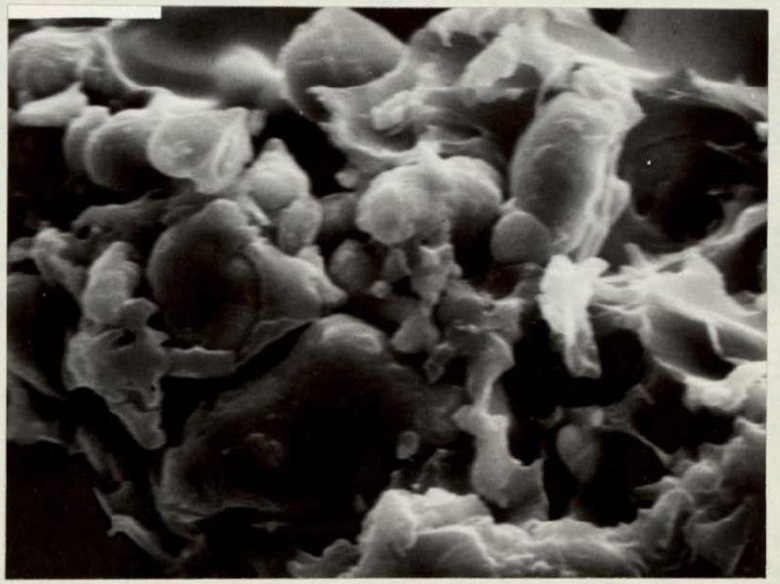

FIGURE 20. Two magnifications of sample #546D3 and #546D4, both with 50% Al, tested at 25° and 250°C, respectively. Shear strength dropped from 3775 psi to 1210 psi. "Melting" caused by high temperature and stress is visible in the lower right.

unfilled adhesive (see Figure 7). Perhaps the aluminum filler prevents interfacial failure at high temperature by adjusting relative thermal expansion.

One effect of higher (70%) filler content is to increase the amount of fracture-surface area by expanding the filigree pattern into a more continuous area shown at low magnification in Figure 21. The detailed view of the high temperature sample shows thin, plastic deformation indicative of high strength, and little indication of melting. Apparently the increased filler content retards the softening of the polymer, too.

Sample #547D3 was prepared at 40 psi with 70% filler and had only 3000 psi shear strength. Figure 22 indicates that the probable cause of the relatively low strength was an unusually large void area.

The new capability to obtain elemental analyses via the EDAX module was used extensively during the current grant period to help analyze the locus of failure. In several earlier examples, EDAX was always used to confirm cases that looked like interfacial failure. In the study of Al filler, EDAX was also provided information on the thickness of adhesive film remaining on the substrate after fracture. (The 25 kV electron beam should penetrate about 1 μm of organic polymer, a value comparable to the thickness predicted theoretically for δ, the thickness of the fracture zone.)

EDAX results from two magnifications of the room temperature samples are shown in Figure 23. (Al actually gave the largest peak in the original spectra, omitted here for clarity.) In line A (50% Al), all the adherend signal was found to be coming from small

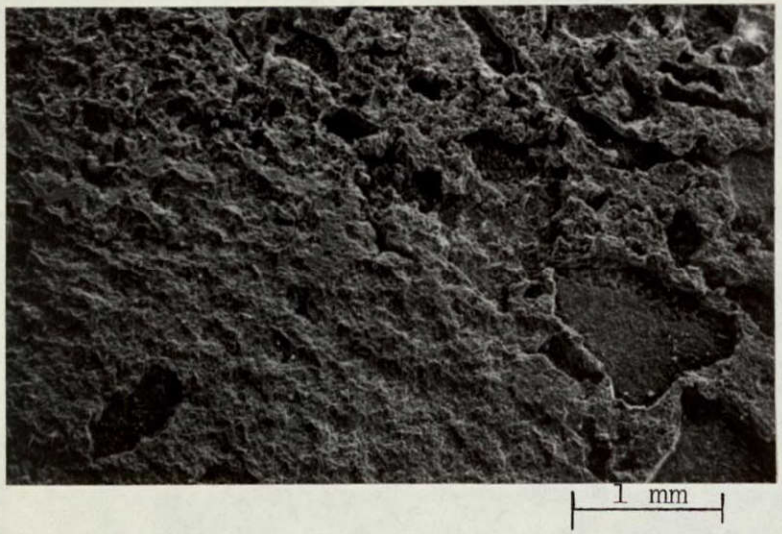

3715 psi
@ 25°C

#554D3

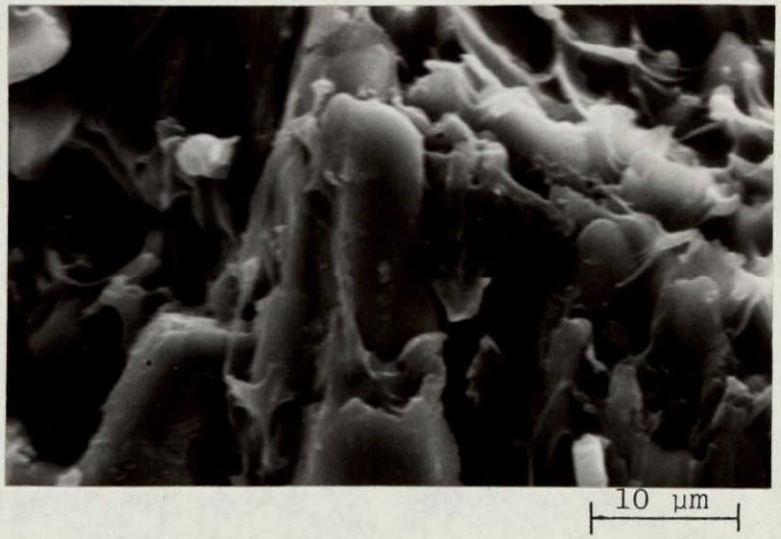

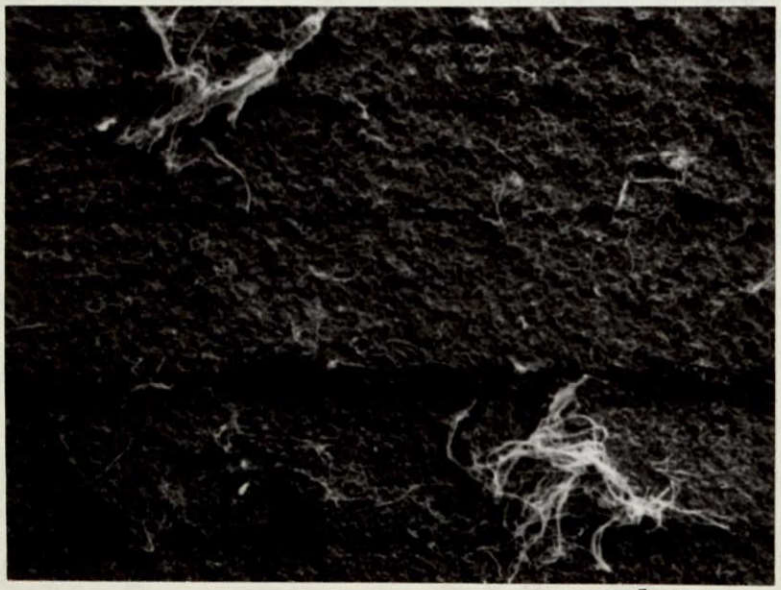

2335 psi
@ 250°C

#554D4

FIGURE 21. Two magnifications of Sample #554D3 and #554D4, both with 70% Al, tested at 25° and 250°C, respectively. Shear strength dropped from 3715 psi to 2335 psi. Higher filler content increases the fracture-surface area and prevents the "melting" at high temperature. Fibers are artifacts.

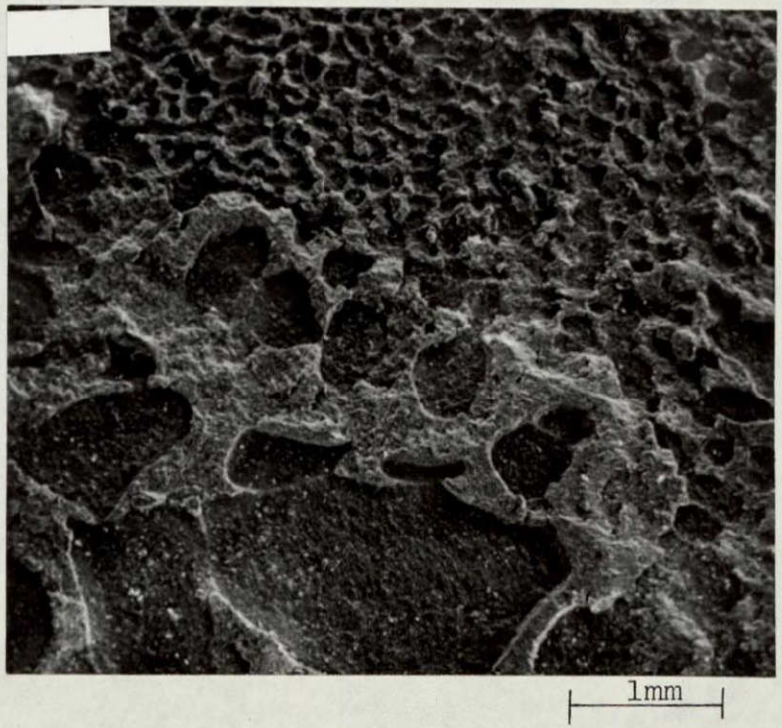

FIGURE 22. Sample #547D3, showing a relatively high ratio of void to fracture-surface area probably responsible for the relatively low 3000 psi shear strength.

holes, seen in Figure 24 (Sample #546D3). No Ti signal could be obtained at the bottom of voids. The opposite was true at 70% Al, line B. More Ti appears on the survey scan and it dominates the spectrum from void bottoms. Sample #554D3 in Figure 24 shows the area from which the last EDAX spectrum was taken. Clearly there is a layer of polymer there, but it seems to be so thin that titanium surface features show through. EDAX examination of both high temperature samples (#546D4 and #554D4) failed to uncover a Ti signal at any magnification. Thus it can be concluded that the room temperature fracture occasionally penetrates nearer to the adherend than the high temperature fracture, which never comes closer than 1μm.

The combination of SEM and EDAX provides most of the essential information on the locus and micromechanics of fracture. It is true that the SEM electron beam can penetrate several hundred Angstrom units of adhesive and give an EDAX signal from underlying adherend. However the combination between the EDAX spectra and the SEM photomicrographs usually leaves little doubt about the details of fracture, as illustrated in Figures 23 and 24. Moreover, by variation of the beam voltage and use of calibration samples of known thickness, it may be possible to make quantitative measurements of residual adhesive film thickness. A most important advantage of SEM/EDAX is the ability to focus the electron beam and analyze only very small, selected areas.

5. ESCA

This technique has the advantage of being sensitive to only a few Angstrom units of material at the surface, and therefore comple-

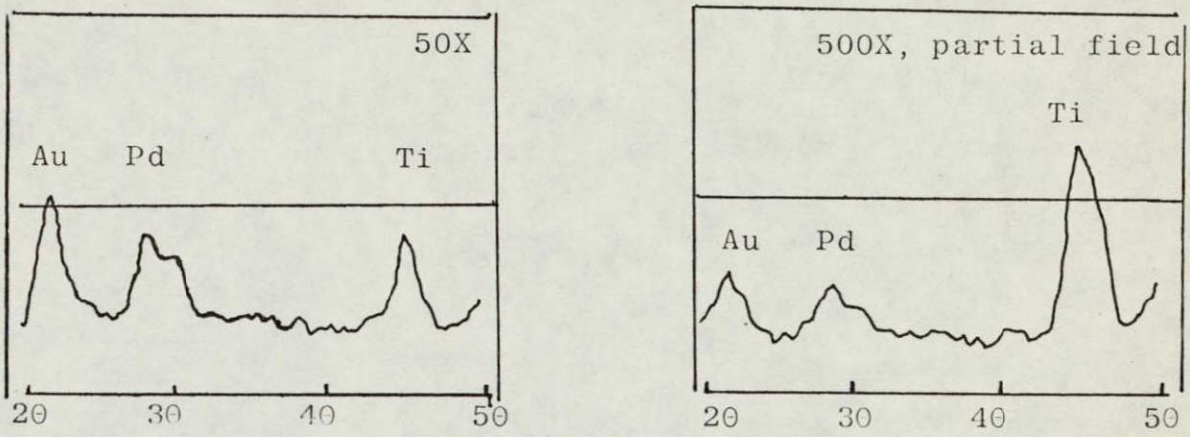

A. EDAX at two magnifications on sample #546D3. Some adherend shows through on the 50X "survey" on the left, and even more when the beam was focussed into the hole shown in Figure 24.

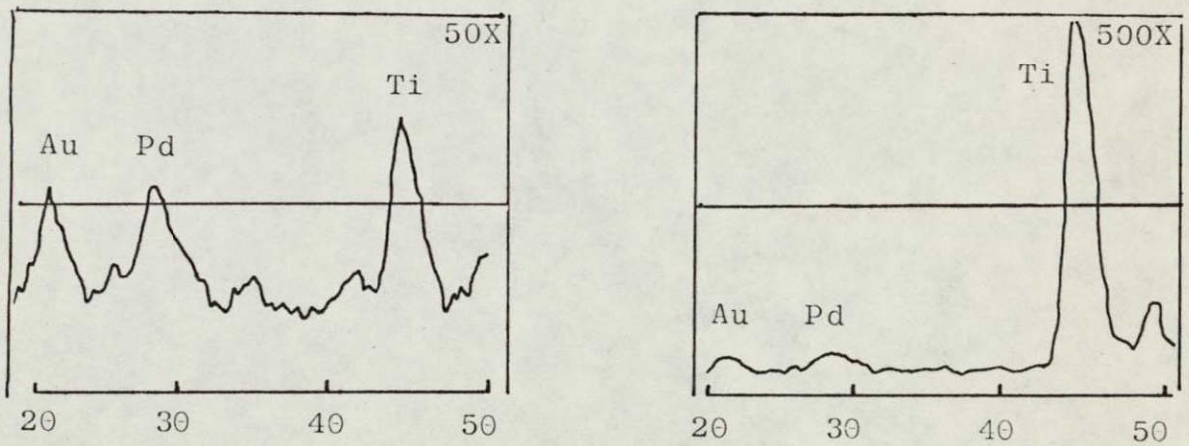

B. EDAX at two magnifications on sample #554D3. More adherend shows through at 50X, and dominates the spectrum when the beam was focussed into the bottom of the void shown in Figure 24.

FIGURE 23

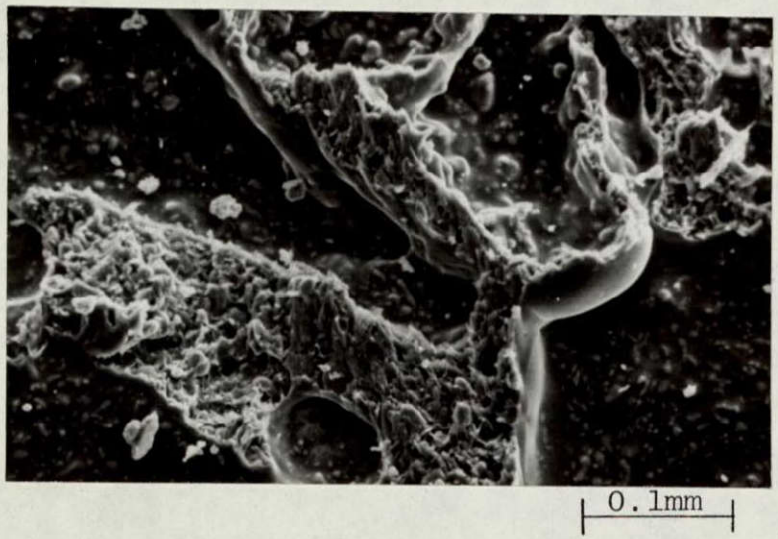

#554D3

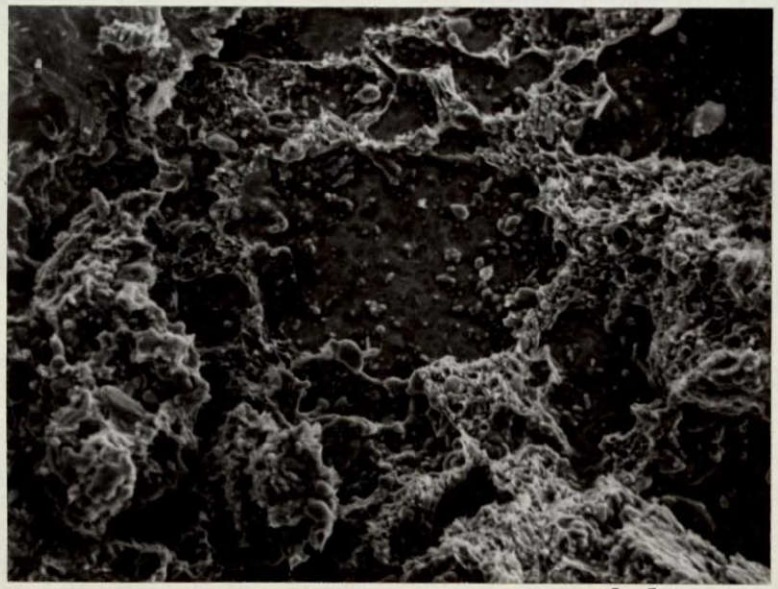

#546D3

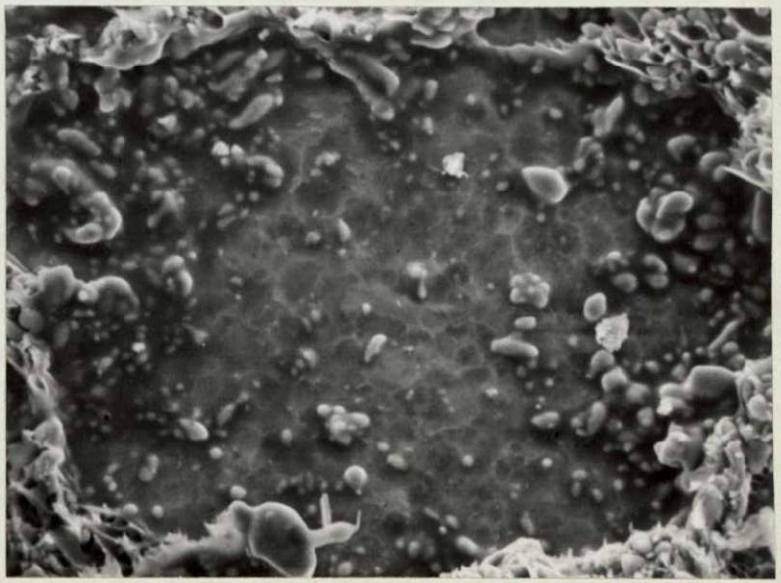

FIGURE 24. Two magnifications of sample #546D3 and #554D3, showing the areas from which the EDAX spectra of Figure 23 were collected.

ments the EDAX analysis. There are, however, two complications. Contamination from the laboratory atmosphere, sample handling, residual pump oil, etc. always gives an ESCA signal unless extraordinary precautions are taken, and these peaks are likely to arise at the same binding energies as the C, O and N of the adhesive. Secondly, the spectra are the average result obtained from the entire sample area of 0.1 x 0.5 cm, so if a small amount of interfacial failure is not covered with contamination it still may not give a significant enough signal.

Table II lists the binding energies of the fracture surfaces that were studied by ESCA. Charge correction was done by standardizing the carbon 1s electron at 284.0 eV and adjusting the other binding energies accordingly. The selection of samples includes the whole range of bond strengths, adhesive variables, and fracture micromechanics. Apparently none of these changes has any effect upon the basic chemical bonding of the polymer atoms, because the binding energy values are remarkably consistent. Judging from the SEM results, interfacial failure occurred in Samples #720D2, 731D1, 731D2 and 891D4, but the titanium substrate gives an ESCA signal in only one case. The problems mentioned above may be the reason for this. Special microscopic examination and selection of samples for ESCA study, in combination with <u>in situ</u> ion etching to remove contamination, may help to clarify some of these anomalies.

TABLE II

ESCA Binding Energies (ev) of Fracture Surfaces

#	Ti	N	O	C
720D2	X	399.	530.9	
720D4	X	399.	531.1	(284)
720D4	X	399.1	531.1	(284)
731D1	X	399.5	531.2	(284)
731D2	458.2	399.1	531.	(284)
878D3	X	399.6	531.2	(284)
880D3	X	399.5	531.	(284)
881D3	X	399.6	531.1	(284)
891D4	X	399.5	531.2	(284)

TABLE III

Fracture Surface Summary

Sample Identification	Lap Shear Strength(psi)	Surface Analysis	
		SEM Location*	Comments
Solvent Effect (BTDA+mm'-DABP)			
1. DG #219D2	5280	1-25,27,28,30; 3-6,9	∿50/50 filigree and void, almost no interfacial failure; thin plastic deformation, brittle fracture with louvers
2. DG #517D1	3860	2-2,3;3-10,11	Similar to line 1. at 100X and 500X.
3. DMAC #220D3	2510	1-26,29;3-7,8	Large void area and interfacial failure, no filigree; little deformation or brittle fracture surface.
4. DMF #848D2	3860	10	∿20/70/10 filigree/void/interfacial; little deformation but high area of brittle fracture with louvers
Anhydride Effect (m,m'-DABP/DG)			
5. BTDA	see line 1.		

* Reference No.-Figure No., except no Reference No. when the figure is in this report.

TABLE III (contd.)

Sample Identification	Lap Shear Strength(psi)	Surface Analysis SEM Location*	Surface Analysis Comments
6. PMDA #515D1	0	2-7,8;3-15,16	60/40 interfacial and void; small brittle fracture area
7. BTDA+PMDA #881D1 & #881D4	2640 5140	13	Little interfacial failure, strength proportional to filigree/void ratio; deformation & fracture like line 1.
8. ODPA #878D3	3250	11	High % filigree; short, thin deformation and brittle louvers
Amine Effect (BTDA/DG)			
9. m,m'-DABP	see line 1		
10. m,p'-DABP #516D4	2070	2-4,5,6;3-12, 13,14	50/50 void and interfacial; some hackled brittle fracture
11. p,p'-DABP #880D2	2310	12	Equal void, interfacial and filigree, thin deformation and some flat brittle fracture

* Reference No.-Figure No., except no Reference No. when the figure is in this report.

TABLE III (contd.)

	Sample Identification			Lap Shear Strength(psi)	Surface Analysis SEM Location*	Comments
	Temperature Effects (BDTA+m,m'-DABP)					
	Aging °C	Testing °C				
12.	232	25	#539D2	3700	2-9,10,11	Similar to line 1
13.	250	25	#539D3	3220	2-12	Similar to line 1
14.	300	25	#539D4	720	2-13,14,15	Large interfacial and void area; thick-wall deformation, brittle fracture with louvers
15.	295	25	#731D1	4320	5	Similar to line 1
16.	295	250	#721D1	2060	6	More interfacial and void area; thicker wall deformation, brittle fracture with louvers
17.	295	250	#721D2	1460	7	Similar to line 17, except more void and interfacial area
18.	295	270	#721D4	850	8,9	∿60/30/10 interfacial/ void/filigree; small plastic deformation and brittle fracture surface area

* Reference No.-Figure No., except no Reference No. when the figure is in this report.

TABLE III (contd.)

Sample Identification	Lap Shear Strength(psi)	Surface Analysis SEM Location*	Comments
Adherend Effect (BTDA:PMDA+m,m'-DABP/DG)			
19. Ti/Ti	See line 7		
20. Ti/Comp. #948D1 (400psi)	3750	18	Failure mostly in composite surface; Smaller voids than in line 19; Catastrophic brittle failure with much small debris
21. Comp./Comp. #946D1 (400 psi)	3360	15	Failure mostly in the tiny void cell walls in the adhesive layer; debris as in line 20.
22. Ti/Comp. #947D1 (1000psi)	3690	16	Similar to line 20,except failure 2/3 in composite
Al Powder Effect (BTDA:PMDA+m,m'-DABP/DG)			
23. 50% Al, 40 Bond. psi, 25 Test °C, #546D3	3780	20,24	∿60/40 void and filigree; much finer features at hi mag.-microvoids in walls; thin plastic deformation area large; lumps of Al seem covered with polymer. EDAX:Ti

* Reference No.-Figure No., except no Reference No. when the figure is in this report.

TABLE III (contd.)

	Sample Identification				Lap Shear Strength(psi)	Surface Analysis SEM Location*	Comments
	% Al	Bond. psi	Test °C				
24.	50	40	250	#546D4	1210	19,20	Similar to line 23 at 20X, but melting rather than drawing EDAX:No Ti
25.	70	40	25	#547D3	3000	19,22	Large void area
26.	70	100	25	#554D3	3720	21,24	Fracture area continuous instead of filigree, low void and no interfacial area; detail similar to line 23. EDAX:Ti
27.	70	100	250	#554D4	2340	21	Similar to line 26, except EDAX:no Ti
Imidized Flow Bonding							
28.	BTDA+EAH-13			#891D1	3500	14	100% interfacial; no voids, deformation, or brittle failure

6. Comparison With Previous Studies

The preceding five sections have presented numerous examples of the failure mechanisms discussed in the Introduction. The effects of several variables, such as solvent and polymer structure were discussed, but a wider range of these variables is encompassed in References (1) and (2). All the results to date can be interpreted in terms of the theory described in the Introduction; Table III summarizes the basic findings. The data are grouped by the effects of the parameters: solvent, anhydride, amine, temperature, adherend, Al powder adhesive filler, and imidized flow bonding.

Voids in the joints as made result from trapping of the water of imidization. This appears to be the major limitation on the strength of most joints studied. Variation in the strength of samples with identical parameters seems to be related to variable void distributions. Voids not only limit the area of polymer drawing and fracture, but also serve as nucleation sites for cracks. The effects of temperature, adherend and Al powder were described qualitatively in Sections 1., 3. and 4.; quantitative analysis of the photomicrographs is necessary to determine the relative amounts of the different failure mechanisms.

Different effects of solvent, anhydride and amine have been reported during each of the three years of study, as indicated in Table III. The solvent probably changes the nature of polymer-chain entanglement: DG and DMF allow good contact with the adherend, but DG results in plastic deformation while DMF results in high-area, brittle fracture; DMAC appears to give poor adherend

contact and little deformation or brittle fracture surface. Changes in the anhydride produce small effects (probable sample preparation errors in #515D1). Introducing para-structures in the amine decreases plastic deformation. Interfacial failure and low-area brittle failure increase.

B. SUBSTRATE SURFACES

Previous reports have described the characterization of titanium adherends as received and after various cleaning steps(1-3). During the current grant period we have used SEM and ESCA to characterize Ti and Al adherends after some different cleaning steps. Also we conducted some preliminary experiments on the acid/base nature of adherends.

1. SEM and ESCA

Figure 25 shows a high magnification view of the Ti 6-4 surface after the phosphate-fluoride and Turco cleaning processes. The phosphate-fluoride etch gives a similar SEM photomicrograph as reported for the Pasa-Jell process (3). However, the white β-phase particles are not as apparent in the panel cleaned by the Turco process.

An aluminum panel was cleaned in a sequence of steps: Alkaline rinse, wipe, acid rinse. High magnification photomicrographs after each step are shown in Figure 26. After the alkaline step, the surface appears like a structureless gel containing small white particles. Presumably these are various amorphous and crystalline forms of hydrous aluminum oxide-hydroxide gel. The wiping step removes the surface layer, leaving a solid surface covered with

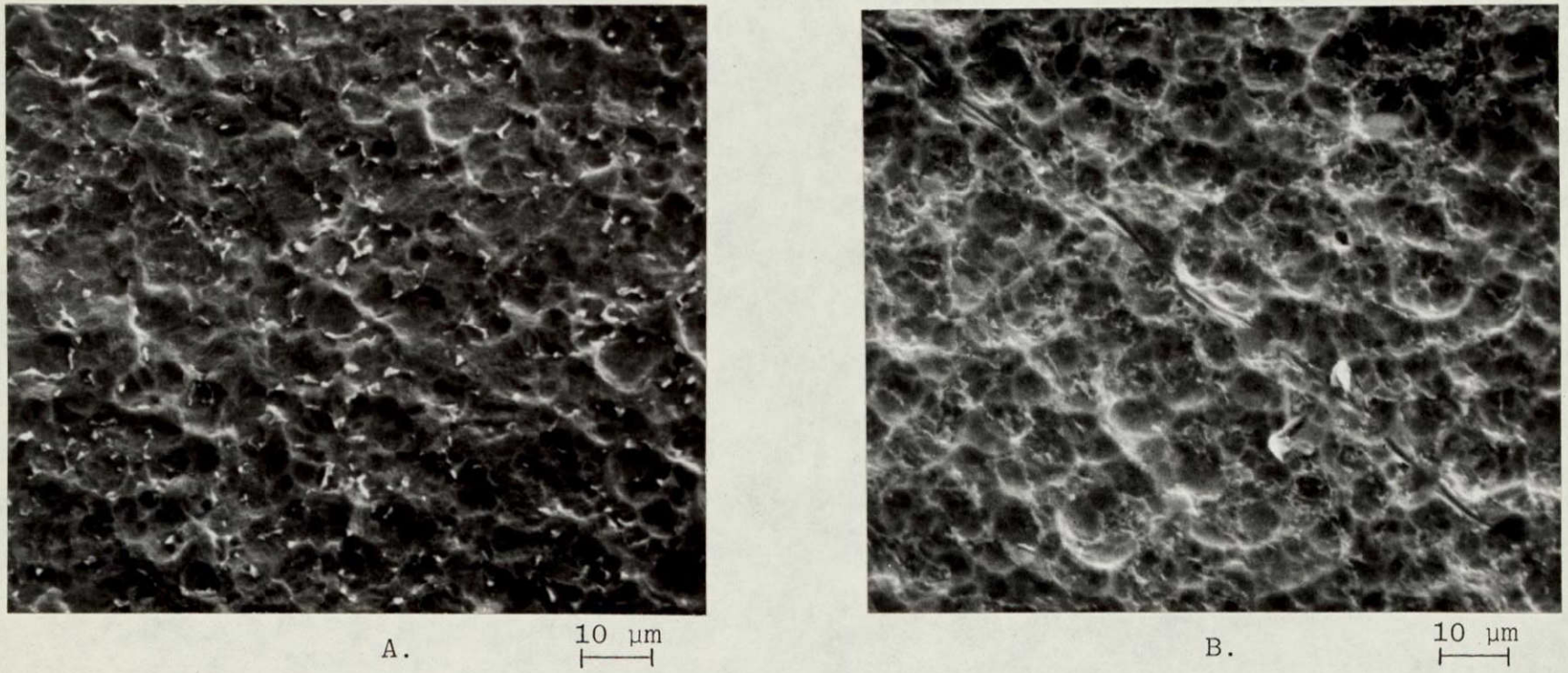

FIGURE 25. Titanium panels after two different cleaning processes: A. phosphate-fluoride. B. Turco.

FIGURE 26. Aluminum panels after fine sanding and sequential cleaning steps: A. alkaline clean. B. wipe. C. acid clean.

regular, sharply-defined pock-marks. The acid rinse appears to etch the whole surface lightly, rounding the edges of the depressions.

Table IV lists the ESCA binding energies observed for the five samples just discussed, as well as for Ti 6-4 after each step of the Pasa-Jell process. The binding energies of the Ti 6-4 surfaces after different cleaning processes were referenced to the Ti 3p electron at 457.7 ev except for the phosphate-fluoride etch where the N 1s electron at 399.2 ev was used. N is observed on Ti 6-4 surfaces with a very constant binding energy (399.0 $\pm$ 0.2). Cr(2p) was only observed after the fourth step of the Pasa-Jell process. F(1s) is observed on all Ti 6-4 surfaces again with a remarkably constant binding energy (687.4 $\pm$ 0.4). The appearance of one or two F peaks of varying intensity suggests bonding of F in two different surface states. P(2p) was observed after the phosphate-fluoride etch and after steps 3 and 4 of the Pasa-Jell process, with an average binding energy of 132.6 $\pm$ 0.1 ev. It is surprising that P would be present on the surface after steps 3 and 4 of the Pasa-Jell process. The doublet at 142.4 and 137.6 ev after steps 1 and 2 of the Pasa-Jell process are assigned to Pb (4f) electron. The presence of Pb is unexpected although the peaks match those reported for PbO previously (3). Si was noted in only one sample after step 2 of the Pasa-Jell process. The doublet at 102.7 $\pm$ 0.2 and 98.7 $\pm$ 0.3 after the phosphate-fluoride etch, steps 2, 3 and 4 of the Pasa-Jell process are assigned to Hg(4f). The presence of Hg is not surprising here since ESCA has the demonstrated capability to detect small quantities of Hg picked up from the lab environment.

TABLE IV

ESCA Binding Energies (ev) of Adherend Surfaces

Adherend	Ti	N	O	Pb	Cr	F	P	Si	Al	Hg
Ti: P-F etch	458.7	(399.2)			X	687. 683.7	132.5	102.5 98.6		
Ti: Turco	(457.7)	399.2			X	687.8 684.1	X	X		
Ti: P-J										
Step 1	(457.7)	399.2		142.4 137.7	X	687.3 684.0		X X		
Step 2	(457.7)	398.7		142.4 137.6	X	687.4		101.4		98.4
Step 3	(457.7)	398.9			X	687.4 683.7	132.5			103. 99.
Step 4	(457.7)	399.			576.6	687.1 684.0	132.7			102.8
Al-I			(531.1)						73.7	
-II			(531.1)						73.4 71.0	
-III			(531.1)						73.9	

A relatively thick (>25A) oxide layer is left on the aluminum surface after alkaline cleaning. However, wiping the surface results in a thin (<25A) oxide layer since Al in both the oxide and elemental state is observed in the ESCA spectra. The values for the two bonding states of Al(2p) agree well with the values reported by Barrie (14).

The presence of trace elements in the adherend surface may be partially responsible for the deleterious aging affects of adhesive joints via catalytic decomposition of the adhesive.

2. SRIRS

A study of the acid/base character of adherend surfaces was begun using SRIRS. Here, adherend samples are equilibrated with dilute solutions of lauric acid and undecyl amine in cyclohexane. The adherend samples are analyzed by SRIRS before and after equilibration with the solutions and after successive rinses with cyclohenane. The results are summarized in Table V. The fact that most of the adherend surfaces are acidic is reasonable since all the adherend surfaces consists of oxide layers. Subsequent hydrolysis of the oxide layer would lead to Bronsted acid surfaces sites.

TABLE V

Acid/Base Character of Metal

Adherend	Acidic	Basic
Al	X	
Cu	X	
Fe	X	
Ni	X	
Pb		X
Ti 6-4	X	
Sn	X	
Zn		X

IV. CONCLUSIONS

1. The unified theory of adhesive bonding indicates that the factors involved in joint strength are (a) voids or other inherent flaws initially present, (b) viscoelastic and plastic response of the materials, (c) brittle crazing and cracking and (d) interfacial failure.

2. The techniques available at VPI and SU, especially SEM/EDAX and ESCA are very useful to evaluate the extent of the different mechanisms by surface analysis of fractured joints.

3. The effects on the micro-mechanics of adhesive failure were determined when changes were made in amine, anhydride, solvent, adherend, Al powder adhesive filler, aging and testing temperature. The effects were interpreted in terms of the proportion of mechanisms 1.(a)-(d) operating.

4. Voids of trapped water of imidization appear to be the major factor to limit joint strength and reproducability of results.

5. Appreciable amounts of void or interfacial failure area correlates with low strength, except in the case of imidized flow bonding.

6. Addition of Al filler makes fracture features an order of magnitude smaller, eliminates interfacial failure at high temperature. At 70% loading it seems to decrease ductility.

7. Future studies should include:

a. Continued characterization of new NASA-LaRC fracture surfaces (especially composites) by the methods outlined above.

b. Quantitative analysis of photomicrographs.

c. Bulk viscoelastic and fracture properties of the polymeric adhesives.

d. Surface properties of cast polymer films.

e. Reduce the data for quantitative comparison with the theory.

V. REFERENCES

1. T. A. Bush, M. E. Counts, T. C. Ward and J. P. Wightman, NASA-LaRC Final Report NAS1-10646-14, Hampton, Va., November, 1973.

2. M. E. Counts and J. P. Wightman, NASA-LaRC Final Report NAS1-10646-25, Hampton, Va., November, 1974.

3. T. A. Bush, M. E. Counts, and J. P. Wightman, Polymer Preprints, 16(1), 770 (1975).

4. T. St.Clair and D. J. Progar, Polymer Preprints, 16(1), 538 (1975).

5. A. K. St.Clair and T. L. St.Clair, SAMPE Materials Rev., 7, 53 (1975).

6. D. J. Progar and T. St.Clair, Organic Coatings and Plastics Chemistry Preprints, 35(2), 185 (1975).

7. D. H. Kaelble, "Physical Chemistry of Adhesion," John Wiley & Sons, Inc., New York, New York, 1971.

8. R. J. Good, J. Adhesion, 1972 (4), 133 (1972).

9. E. H. Andrews and A. J. Kinloch, J. Polymer Sci.: Symp. No. 46, 1 (1974).

10. E. Orowan, J. Franklin Inst., 290(6), 493 (1970).

11. J. W. Obreimoff, Proc. R. Soc., A127, 290 (1930).

12. W. A. Zisman, in Contact Angle, Wettability and Adhesion, Adv. in Chem. No. 43, Amer. Chem. Soc., 1964, p.1.

13. O. C. Wells, Scanning Electron Microscopy, McGraw-Hill, 1974.

14. A. Barrie, Chem. Phys. Lett., 19, 109 (1971).

VI. APPENDIX

The Use of Scanning Electron Microscopy, Electron Spectroscopy for Chemical Analysis (ESCA) and Specular Reflectance Infrared Spectroscopy in the Analysis of Fracture Surfaces in Several Polyimide/Titanium 6-4 Systems.

Thurman A. Bush, Mary Ellen Counts and J. P. Wightman

(Reference 3)

THE USE OF SCANNING ELECTRON MICROSCOPY, ELECTRON SPECTROSCOPY FOR CHEMICAL ANALYSIS (ESCA) AND SPECULAR REFLECTANCE INFRARED SPECTROSCOPY IN THE ANALYSIS OF FRACTURE SURFACES IN SEVERAL POLYIMIDE/TITANIUM 6-4 SYSTEMS.

Thurman A. Bush, Mary Ellen Counts and J. P. Wightman

Virginia Polytechnic Institute and State University

Chemistry Department, Blacksburg, Virginia 24061

Scanning electron microscopy, electron spectroscopy for chemical analysis (ESCA) and specular reflectance infrared spectroscopy were employed to characterize titanium alloy (Ti-6Al-4V) surfaces before and after bonding with polyimide resins. Water contact angles on the titanium alloy surface were shown to correlate with surface contamination. Diglyme and DMAC contact angles correlated with fracture strength of the completed adhesive joints formed by the condensation polymerization of benzophenone tetracarboxylic acid dianhydride (BTDA) and m,m'-diaminobenzophenone (m,m' DABP). Octane/water interfacial contact angles were used to show the presence of polar forces at the adhesive/adherend interface. Variations in adhesive strength were noted for condensation polymers formed in diglyme solutions of (i) BTDA and m,m' DABP, (ii) BTDA and m,p' DABP and (iii) m,m' DABP and pyromellitic dianhydride (PMDA). Scanning electron microscopy was used to observe the titanium alloy surfaces after various pretreatments and the surfaces of fractured joints. ESCA spectra were obtained for the cleaned alloy surface and for fracture surfaces. The intensity of the titanium peak in the ESCA spectra was related to the presence of thin polyimide films. Specular reflectance infrared spectroscopy was also used in the analysis of the fracture surfaces.

I. INTRODUCTION

A number of organic polymer resins which were discovered in the 1960's have shown promise as candidates for formulation as thermally stable adhesives (1). However, the adaptation of such novel polymers as practical adhesives has been hampered by a lack of sufficient experimental and theoretical criteria for evaluating new resins and predicting their suitability for adhesive purposes.

The processes for forming adhesive bonds between materials have been developed empirically. Current theories of adhesion remain controversial (2-4). The development of a general theory of adhesion has been deterred in part due to the experimental inaccessibility of interfacial interactions between solids and the difficulty in establishing the nature of the interface (3).

The objective of this work was the utilization of some recently developed techniques that may be of value in the characterization of the adhesive process between a titanium alloy and a variety of polyimide resin systems. The techniques utilized were electron spectroscopy for chemical analysis (ESCA), specular reflectance infrared spectroscopy, and scanning electron microscopy. Contact angles of various liquids on the titanium alloy were also measured. Specifically, the question arises to what extent are any of these techniques of value in the characterization of the interface and in the determination of interactions for the titanium 6-4/polyimide resin systems. Dwight and Riggs (5) successfully used ESCA, soft X-ray spectroscopy, contact angle hysteresis and electron microscopy to examine fluoropolymer surfaces.

II. EXPERIMENTAL

A. Samples

Panels of Ti-6-4 alloy adherend were obtained from the NASA-Langley Research Center. The panels were either used in the as-received condition or cleaned by the Pasa-Jell 107 method, a commercial process (American Cyanamid) for cleaning titanium alloy surfaces. The primary steps in this cleaning process are, briefly: sample immersion in degreasing 1,2-dichloroethane; immersion in an alkaline cleaner, SPREX AN 9 solution; pickling in an HNO_3/HF solution; and treatment with Pasa-Jell 107 (a chromate based acid paste).

Two sets of fractured lap-joint samples were obtained from the

NASA-Langley Research Center. The characteristics of the samples in the two sets are given in Table I. The first set of samples were lap-joints of Pasa-Jell cleaned Ti-6-4 panels bonded with one polyimide resin adhesive. The resin adhesive was prepared from benzophenone tetracarboxylic acid dianhydride (BTDA) and m,m'-diaminobenzophenone (m,m'DABP). The structures of these compounds are given in Table II. The uncured adhesive was applied on the adherend in the polyamic acid stage from either diglyme or DMAC solution and then heat cured to the polyimide resin form. This condensation polymerization reaction is shown below.

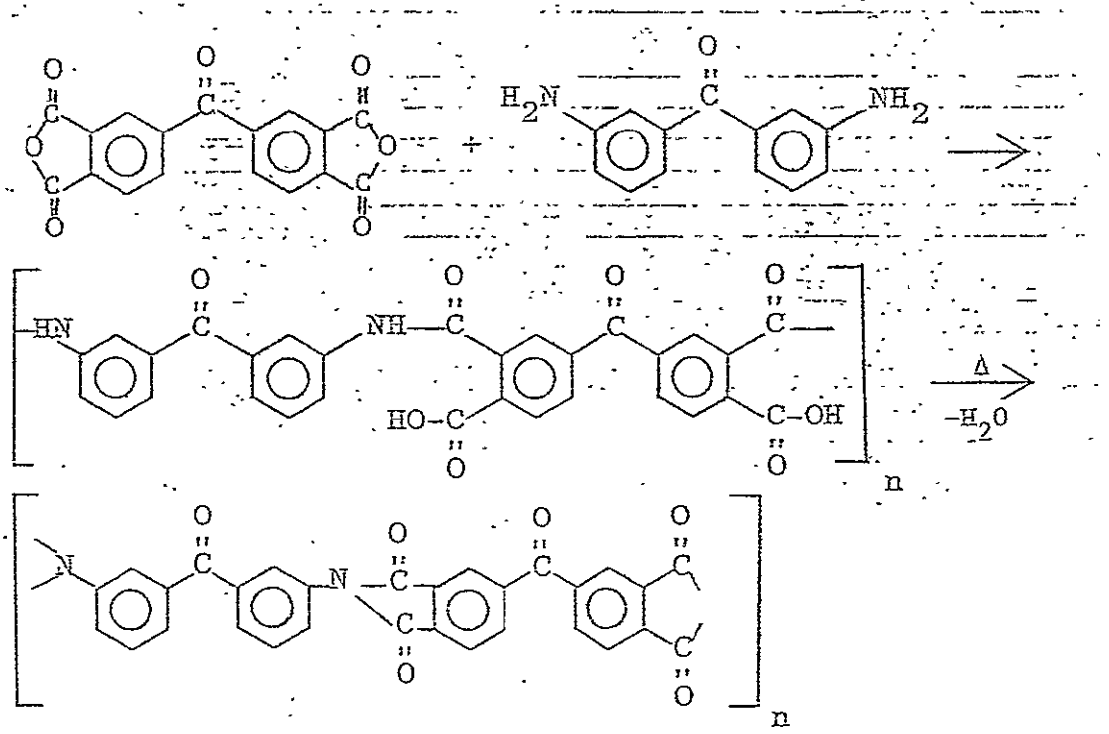

The second set of samples were lap-joints of Pasa-Jell cleaned Ti-6-4 panels bonded with various polyimide resin adhesives. The resin adhesives were prepared from BTDA or pyromellitic dianhydride (PMDA) and m,m'DAPB or m,p'-diaminobenzophenone (m,p'DABP). The structures of (PMDA) and (m,p'DABP) are also given in Table II. The uncured adhesive was applied on the adherend in the polyamic acid stage from the solvent diglyme and then heat-cured to the polyimide resin form. Tensile lap shear sandwich specimens were prepared by bonding 13 x 2.5 x 0.1 cm Ti-6-4 coupons with a 1.3 cm overlap. Typically, the coated coupons were air dried for 30 min at room temperature and then for 30 min at 60°C. Five successive coats were applied. The panels were overlapped at room temperature, placed under a constant pressure of 50 psi, and heated to 300°C at a rate of 5°C min^{-1}. The specimen was held at 300°C for

TABLE I

FRACTURE SAMPLE CHARACTERISTICS

Set	Code	Adhesive Sample	Solvent	Average Strength(psi)	T_G(°C)*
I	219D2	BTDA + m,m'DABP	diglyme	5280	
	220D3	BTDA + m,m'DABP	DMAC	2510	
II	1m2-517D(1,2,3,4)	BTDA + m,m'DABP	diglyme	3860	240-250
	1mp2-516D(1,2,3,4)	BTDA + m,p'DABP	diglyme	2073	260-270
	2m2-515D(1,2,3,4)	PMDA + m,m'DABP	diglyme	0	325-330

*maximum processing temperature ~ 300°C

TABLE II

STRUCTURES OF RESIN STARTING MATERIALS

BTDA = benzophenone tetracarboxylic acid dianhydride

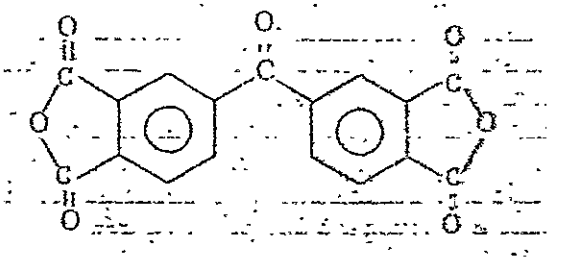

PMDA = pyromellitic dianhydride

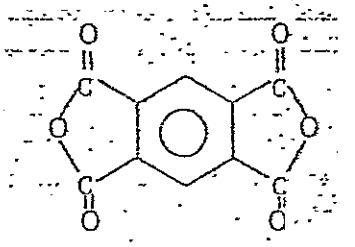

m,m'DABP = m,m'-diaminobenzophenone

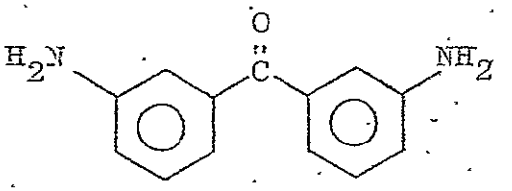

m,p'DABP = m,p'-diaminobenzophenone

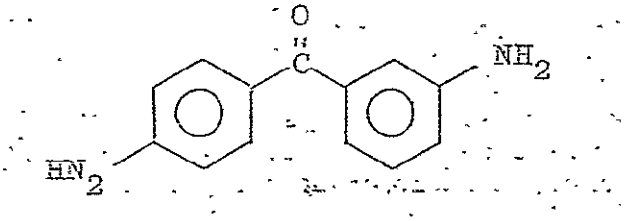

50 min. The lap-shear strength of each sample in both sets was determined at room temperature on a tensile tester (Cal-Tester Model TH-5).

B. Scanning Electron Microscopy

Representative samples were cut from both sets of the fractured lap-joint specimens. The samples were gold-coated and photomicrographs at various magnifications were obtained on an AMR scanning electron microscope (Advanced Metals Research Corporation: Model 900). Each sample surface was scanned totally to insure that the photographs were representative.

Five samples were cut from a bare Ti-6-4 panel. One sample, which served as a control, received no pretreatment and was placed into a vial. The Pasa-Jell cleaning process was applied to the four remaining samples. A sample after each step of the cleaning process was blown dry in a nitrogen stream and placed into a vial. Exposure time of the freshly cleaned material to the lab atmosphere was kept to a minimum. These five samples were examined in the scanning electron microscope.

C. Contact Angles

1. Materials. Distilled water was obtained from a Barnstead metal still. Mercury was obtained from the Glass Shop at the Virginia Polytechnic Institute and State University. Aldrich (99%) bis(2-methoxy ethyl) ether and octane were used. Dimethylacetamide (DMAC) was obtained from Burdick & Jackson (technical grade) and was distilled from calcium hydride. The degreaser used was 1,2-dichloroethane obtained from Fisher (ACS Certified). Metal coupons of the Ti-6-4 alloy (2.5 x 12 cm), and solutions of Pasa-Jell 107, HNO_3/HF, and SPREX AN 9 were furnished by the NASA-Langley Research Center. The polyamic acid (BTDA + m,m'DABP) was supplied by the NASA-Langley Research Center as a 20% solution of the polymer dissolved in diglyme [bis(2-methoxy ethyl) ether]. The solution was refrigerated to minimize degradation of the polymer.

2. Apparatus and Procedure. Contact angles of water, mercury, octane, DMAC, diglyme, and polymer resin were measured on prepared surfaces of Ti-6-4 samples with a Gartener Scientific microscope goniometer. Contact angle measurements were made on alloy surfaces cleaned by the Pasa-Jell method, and on the material as-received except for degreasing in 1,2-dichloroethane. Each liquid was introduced as drops delivered from a syringe inserted through the septum of a custom optical cell. Saturation of the vapor phase within the cell was insured by placing a small container of water within the

cell or, in the case of other liquids, placing several drops over the surface in addition to the one being measured. Equilibrium angles were recorded when the last two measurements separated by at least fifteen minutes agreed to within ± 1°. Octane/water and water/octane interfacial contact angles against the Ti-6-4 surface were measured in a custom optical cell. The temperature for all contact angle measurements was 25 ± 2°C.

D. Specular Reflectance Infrared Spectroscopy

A Unicam attachment was used with a Beckman IR-20A infrared spectrophotometer in the specular reflectance studies. The spectrophotometer was operated in both the single and double beam modes. IR reflectance spectra were obtained for the fractured samples of Set II. The samples were placed in the reflectance attachment so that the lapped portion of the panels covered the entire sample window. This method allowed spectra of the samples to be obtained in situ. Comparisons of intensities of individual peaks in the different sample spectra proved to be unsatisfactory in evaluating the amount of adhesive present on a panel. For this reason, reflectivity as measured by percent transmission in a non-absorbing region (2600 cm^{-1}) was considered as a possible characterization of the fracture surface. The percent transmission in this region was measured for each sample and also for a polished Ti-6-4 surface and a Pasa-Jell cleaned Ti-6-4 surface.

E. Electron Spectroscopy for Chemical Analysis (ESCA)

The ESCA studies of the fractured samples from Sets I and II were done with an AEI ES 100 photoelectron spectrometer using Al Kα radiation (1486.6 ev.). Data acquisition was accomplished using a AEI DS 100 Data System and a Digital PDP-8/e computer. Specific spectrometer conditions are noted on the spectra which follow. The cut samples were secured to the ESCA probe with double-sided tape. ESCA spectra also were obtained for Ti-6-4 samples in the as-received condition and cleaned by the Pasa-Jell method, and coated with the polymer resin. Two polymer coated samples were prepared by placing a 0.01 ml of 14% and 25% dilutions in diglyme of the stock resin solution of BTDA and m,m'DABP on cleaned Ti-6-4 panels. Each drop spread spontaneously over the entire sample surface. The samples were dried at room temperature for at least 24 hours prior to the ESCA and contact angle runs.

III. RESULTS AND DISCUSSION

A. Scanning Electron Microscopy (SEM)

1. Adherend Surfaces. The most striking feature in the scanning electron photomicrographs of the untreated metal surface is the amount of debris (large white particles) typically observed as shown in Figure 1. At 100 x the surface is noticeably fine

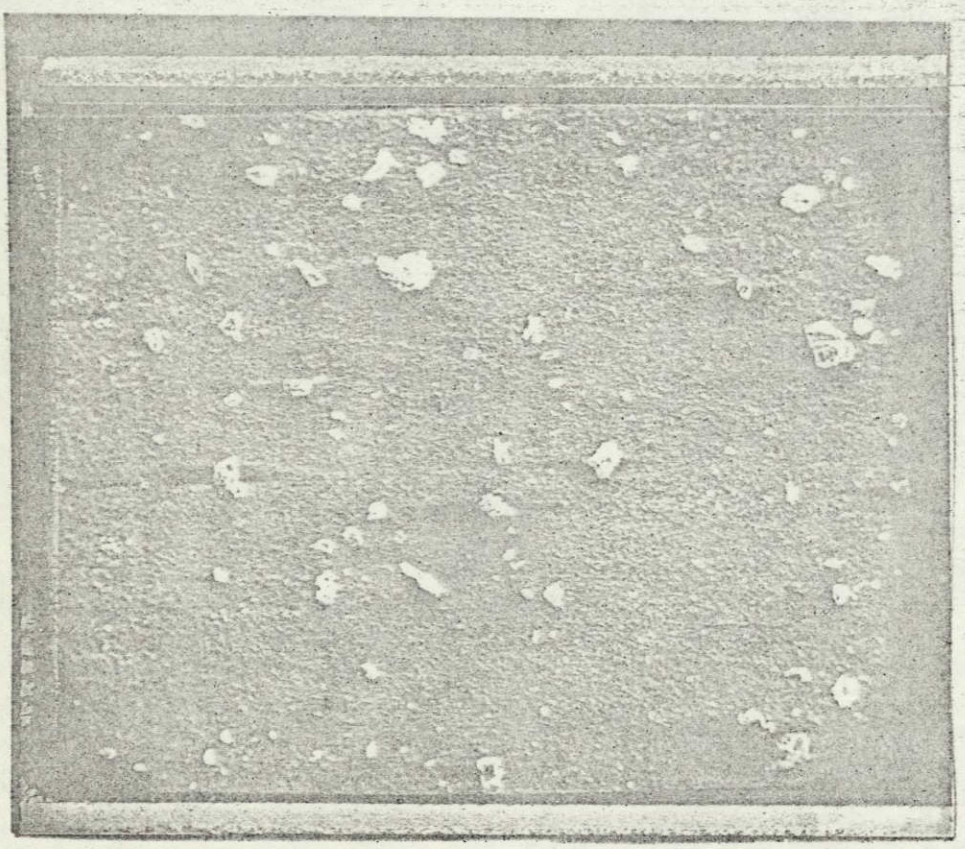

Fig. 1. Photomicrograph of Untreated Ti-6-4 Sample (100 X)

grained, whereas at the higher magnification (x1000) shown in Figure 2 the microscopic roughness readily becomes apparent. In addition, many smaller white presumably crystalline particles are contained in and projecting from a matrix of greyish material.

A photomicrograph (X1000) of the degreased sample in Figure 3 has the same surface features as the untreated sample except that the amount of debris is significantly reduced. The photomicrograph (X1000) in Figure 4 shows that the alkaline step of the cleaning

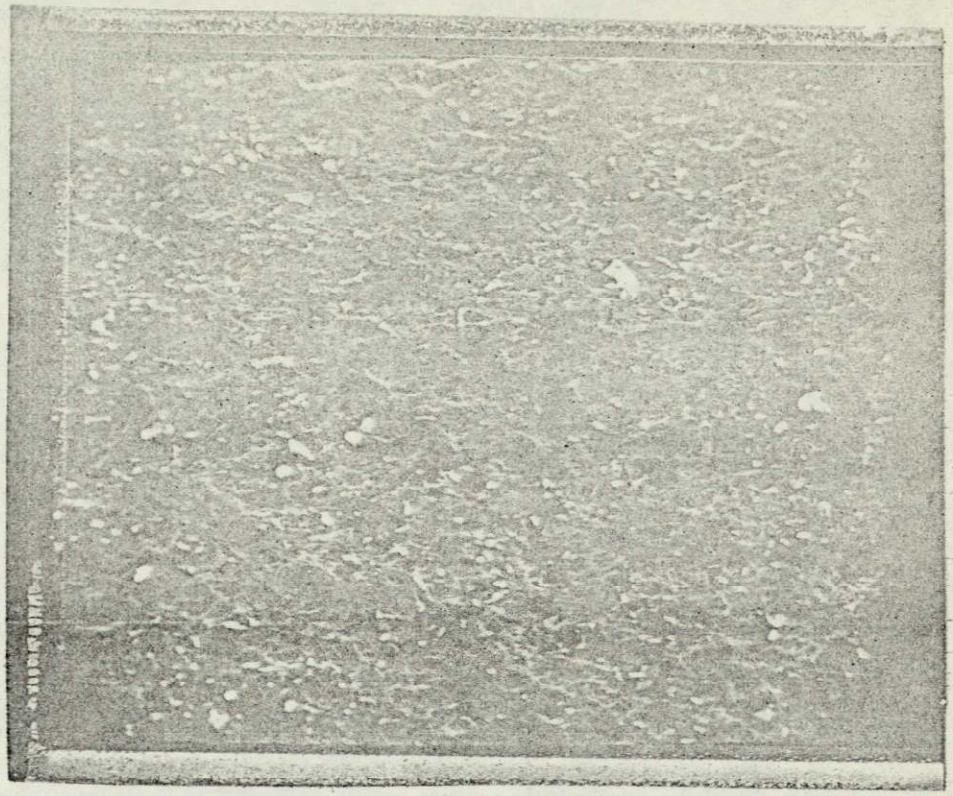

Fig. 2. Photomicrograph of Untreated Ti-6-4 Sample (1000 X)

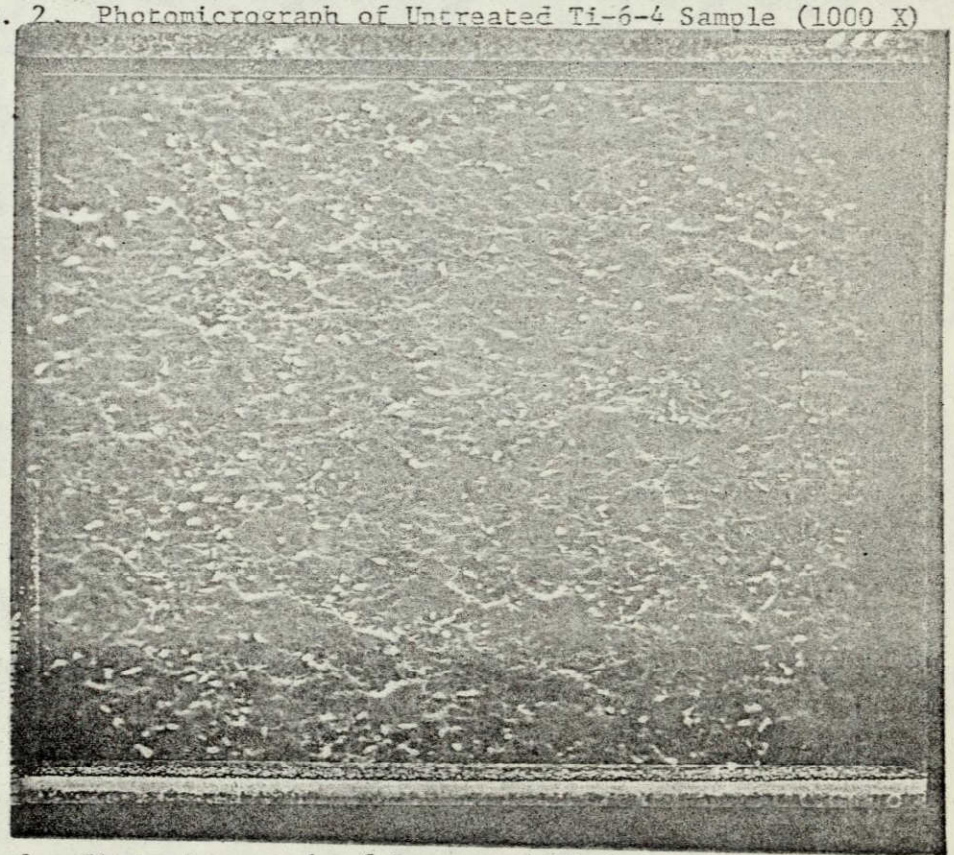

Fig. 3. Photomicrograph of Degreased Ti-6-4 Sample (1000 X)

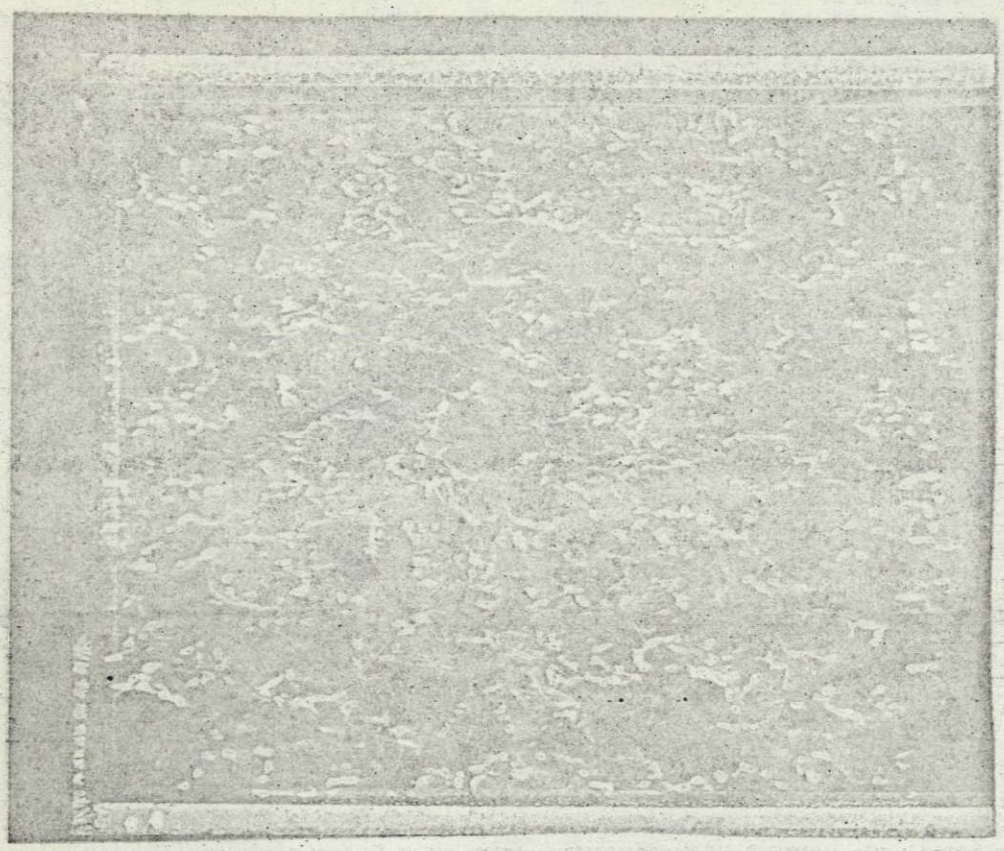

Fig. 4. Photomicrograph of Alkaline Cleaned Ti-6-4 Sample (1000 X)

process selectively etches the grey material, thus exposing more of the small white particles. Acid cleaning continues the selective etching of the grey material as indicated by the photomicrograph (X1000) in Figure 5. No discernibly different features were noted in the photomicrographs after the Pasa-Jell treatment. Thus, each step of the cleaning process produces distinct changes in surface features except the final Pasa-Jell treatment.

Ti-6-4 is an alpha-beta titanium alloy (6% Al, 4% V) readily available commercially (6,7). The alpha phase crystallizes in a hexagonally close packed array and the beta phase in a body centered cubic array. The beta phase is the high temperature form and exists in equilibrium with the alpha phase at room temperature. The photomicrographs in Figures 1 through 5 were compared with those of the ASM's Atlas of Microstructures of Industrial Alloys (6). On the basis of similarities in the photographs, the white particles in the photomicrographs are identified as the beta phase of the titanium alloy and the grey material as the alpha phase.

More of the beta phase particles of one to five microns in length are exposed in the cleaning process. The beta phase particles, occupying predominantly ridges and high points on the surface, would be expected to be the first points of contact for an adhesive

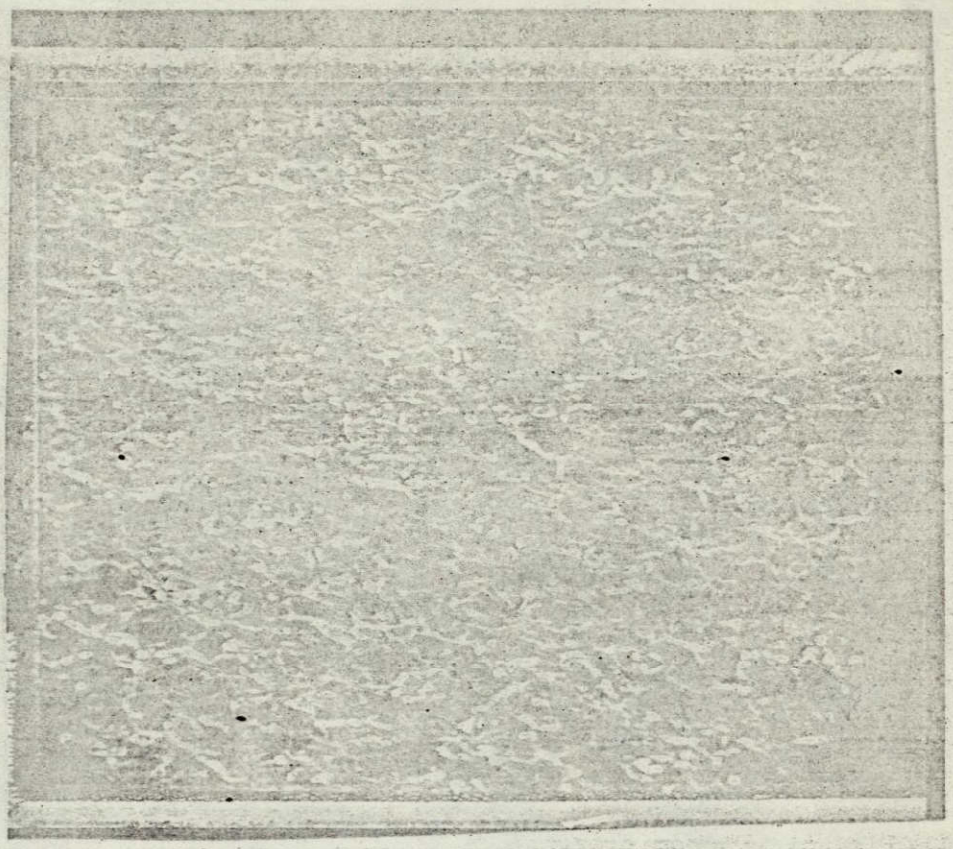

Fig. 5. Photomicrograph of Acid Cleaned Ti-6-4 (1000X)

material spread on the surface. Steps and ridges of the alpha phase become important features as etching takes place. Etching along planes of the crystal faces oriented oblique to the surface produces the steps and ridges as seen in Figure 5. Similar SEM results for Ti-6-4 have been reported by Hamilton (8).

Comparison of photomicrographs of three separate cleaned Ti-6-4 samples over a 12 month period shows the same details, thus indicating the reproducibility of the cleaning process in producing the surface effects noted.

2. Fracture Surfaces - Set I. Photomicrographs of the fractured samples from Sets I and II are shown in Figures 6 to 16. Diglyme was used as a solvent in Sample 219D2 whereas DMAC was used as a solvent in Sample 220D3 in Set I. The photomicrographs of Sample 219D2 in Figure 6 and of Sample 220D3 in Figure 7 indicate dramatically the difference in the extent of surface coverage of the adhesive in these two systems. Sample 219D2 (diglyme) exhibits an almost complete coverage of the metal surface by the adhesive with only small patches of metal exposed indicative of cohesive failure. On the other hand, the surface of sample 220D3 (DMAC) has large areas of metal exposed as seen in Figure 7 indica-

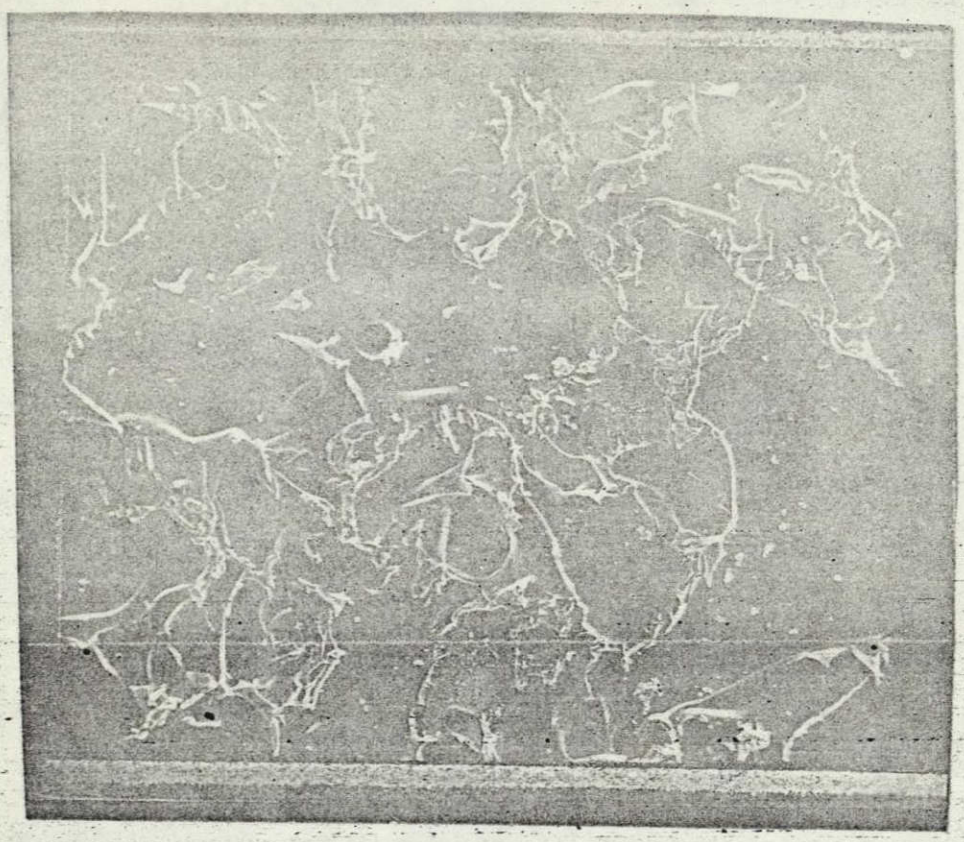

Fig. 6. Photomicrograph of Fracture Sample 219D2 (100 X)

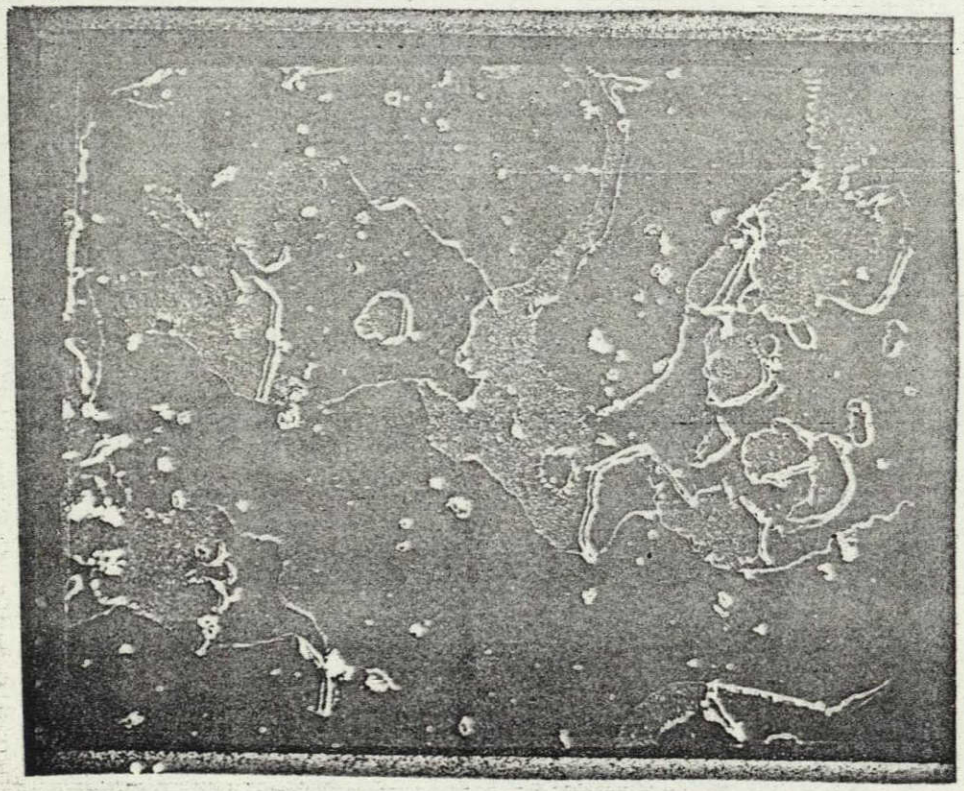

Fig. 7. Photomicrograph of Fracture Sample 220D3 (100 X)

tive of adhesive failure. The adhesive apparently did not wet the substrate in this system. Additional evidence for non-wetting of the substrate by the adhesive in the DMAC system compared to the diglyme system is seen on comparison of the photomicrographs in Figures 8 and 9. The adhesive/substrate interface in Figure 8 is

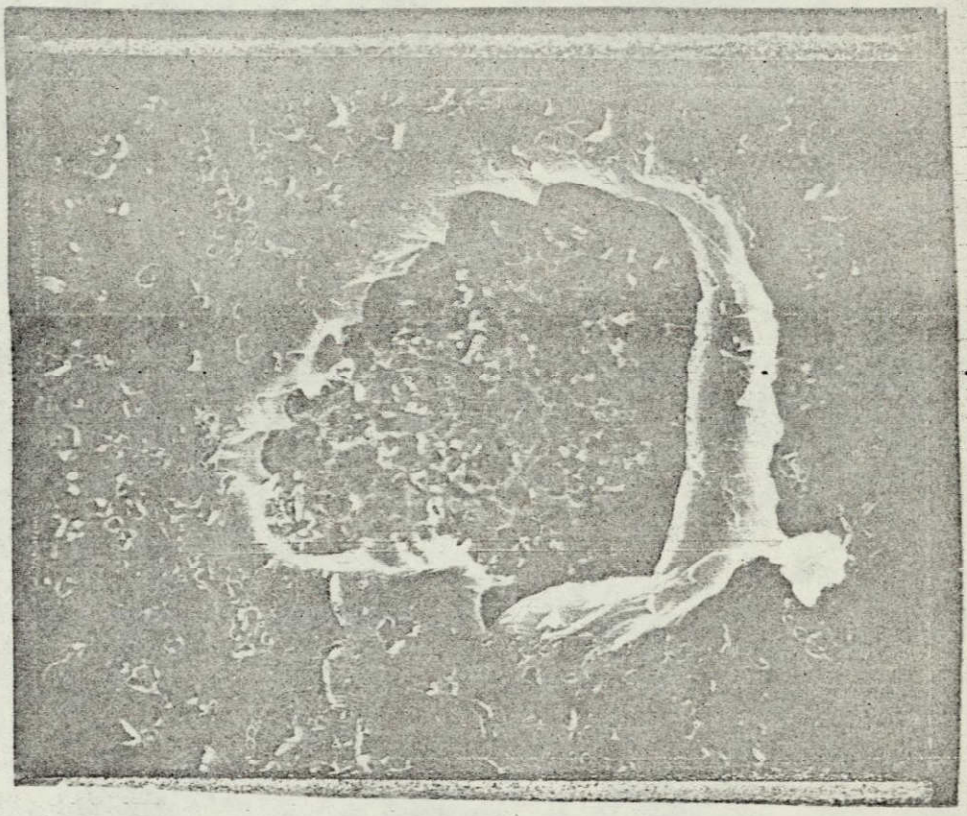

Fig. 8. Photomicrograph of Fracture Sample 220D3 (1000 X)

characterized by a sharp break whereas the same interface in Figure 9 is continuous. The better bonding in Figure 9 is obvious. The substrate surface of Sample 200D3 (Figure 8) appears to contain particles identified previously as the beta phase of the alloy whereas Sample 219D2 (Figure 9) shows less of this particular feature. Since the adhesive of Sample 219D2 has wet the surface, perhaps the fewer number of these particles observed is additional evidence for the presence of a film of adhesive on the surface.

The scanning electron microscope results described above correlate well with the breaking stress data of Table I. That is, the fracture strength of Samples 219D2 and 220D3 decreases as the extent of wetting or surface coverage decreases as seen in Figures 6 and 7.

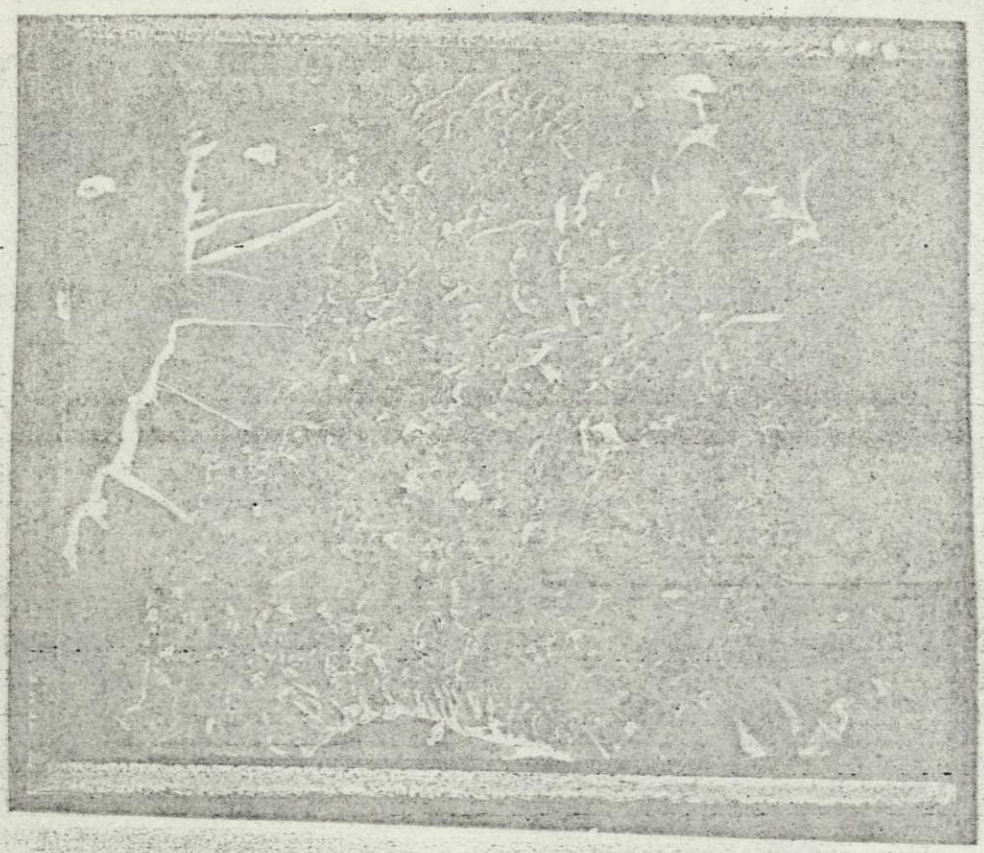

Fig. 9. Photomicrograph of Fracture Sample 219D2 (1000 X)

3. Fracture Surfaces - Set II. The samples in Set II were prepared twelve months after the samples in Set I. As noted in Table I, the average lap-shear strength of the samples in the 1m2-517 series (Set II) was 3860 psi. This series has the greatest lap-shear strength of the different series in Set II. The 1m2-517 series is the same adhesive-solvent system as the sample 219D2 in Set I. The difference in the absolute value of the lap-shear strength is not considered significant. In Figure 10 is seen a 100X photomicrograph of the sample 1m2-517D1. The features of this sample were representative of the other samples of this series. The significance of this photomicrograph was the apparent absence of the metal substrate structure. The excellent reproducibility of the SEM analysis of the fracture surface is demonstrated by the similarity of the features in Figure 10 and Figure 6 for Set I for the same BTDA + m,m'DABP/diglyme system. A closer examination of this sample at 500X can be seen in Figure 11. The smoothness of the pockets relative to the jagged areas is apparent. The jagged regions are believed to result from the fracture of contact areas between the two adhesive-coated panels when the samples were lap-shear tested. Adhesive strength might be substantially increased if more contact with the resin were possible. The pockets in Figure 11 represent non-bonding areas.

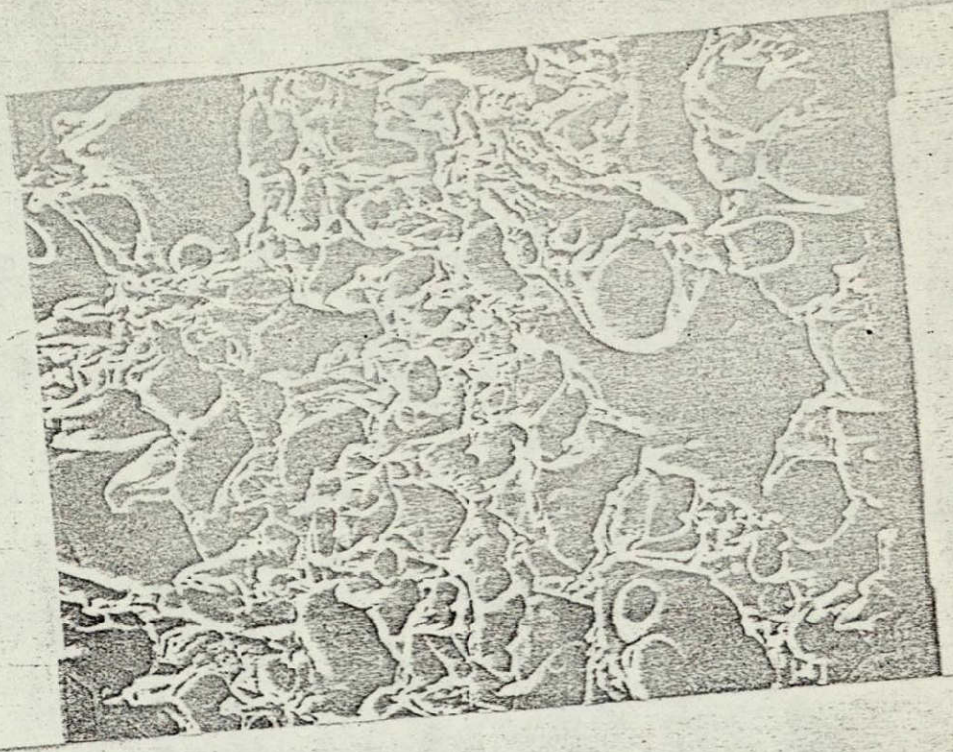

Fig. 10. Photomicrograph of Fracture Sample 1m2-517D1 (100 X)

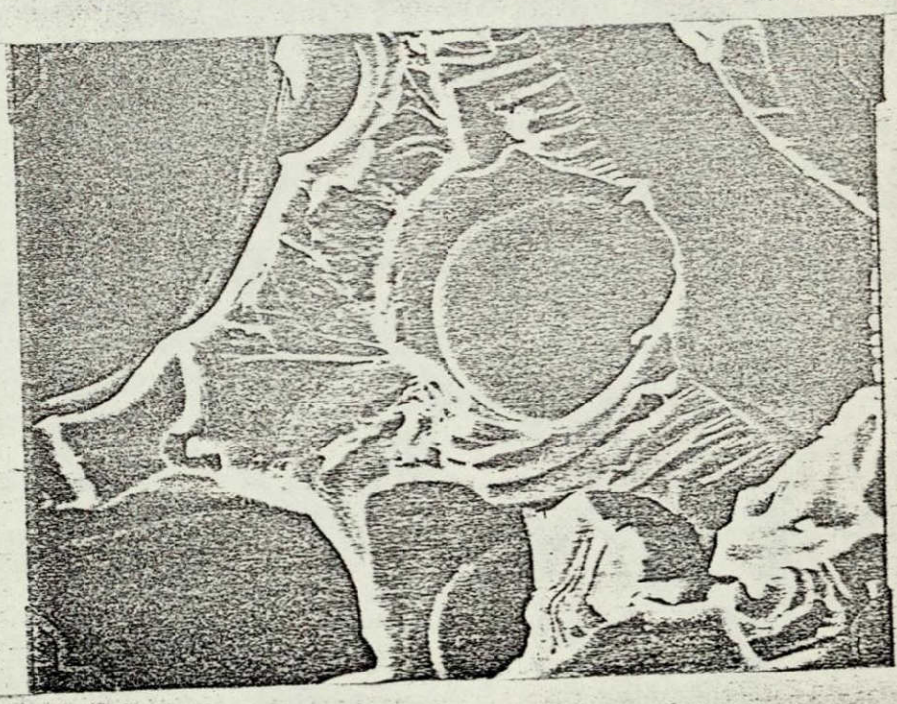

Fig. 11. Photomicrograph of Fracture Sample 1m2-517D1 (500 X)

The samples in the 1mp2-516 series had an intermediate average lap-shear strength of 2073 psi (Table I). A 20X photomicrograph, Figure 12, of the sample 1mp2-516D1 illustrates a structure very different from that observed for the 1m2-517 series of fracture samples. The dissimilarity of the 1m2-517 and the 1mp2-516 samples is more apparent in Figure 13 (500X) which is a photomicrograph of one of the lighter regions seen in Figure 12. Whereas in the 1m2-517 sample the adhesive appeared smooth, the adhesive in this photomicrograph appears porous and brittle-like. A closer examination of a darker region noted in Figure 12 is seen in Figure 14 (1000X). This region appears smooth with no evidence of metal substrate. The important feature to note in Figures 12-14 is again the lack of the metal substrate structure.

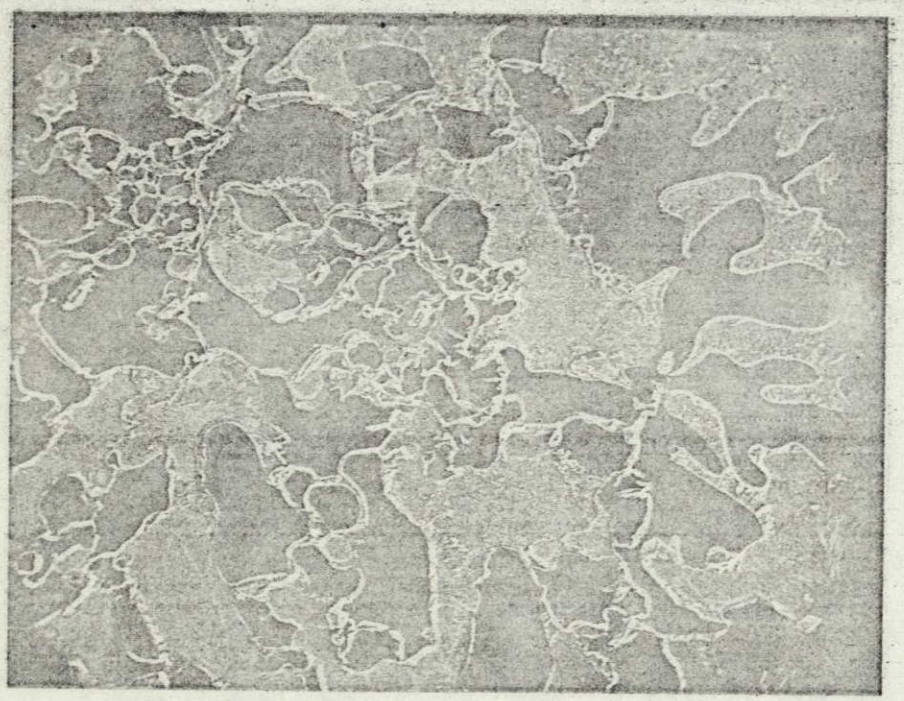

Fig. 12. Photomicrograph of Fracture Sample 1mp2-516D1 (20 X)

A 20X photomicrograph of sample 2m2-515D1, which is representative of the samples of zero strength, is seen in Figure 15. This sample has a jig-saw puzzle appearance in that the adhesive is cracked and broken. This feature is more clearly seen in Figure 16 (500X). The metal substrate structure is apparent and there appears to be little wetting between the adhesive and the

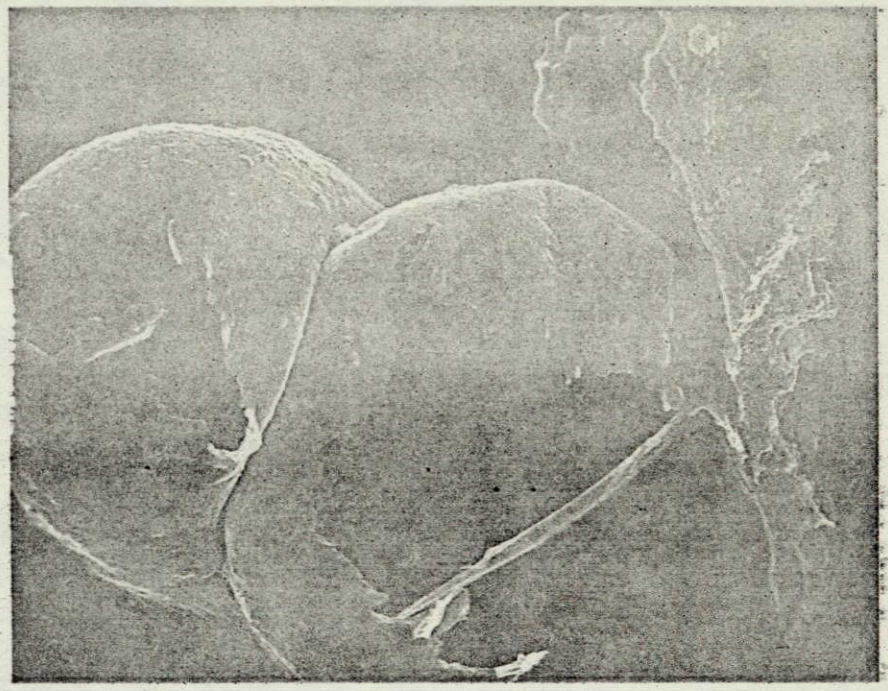

Fig. 13. Photomicrograph of Fracture Sample lmp2-516D1 (500 X)

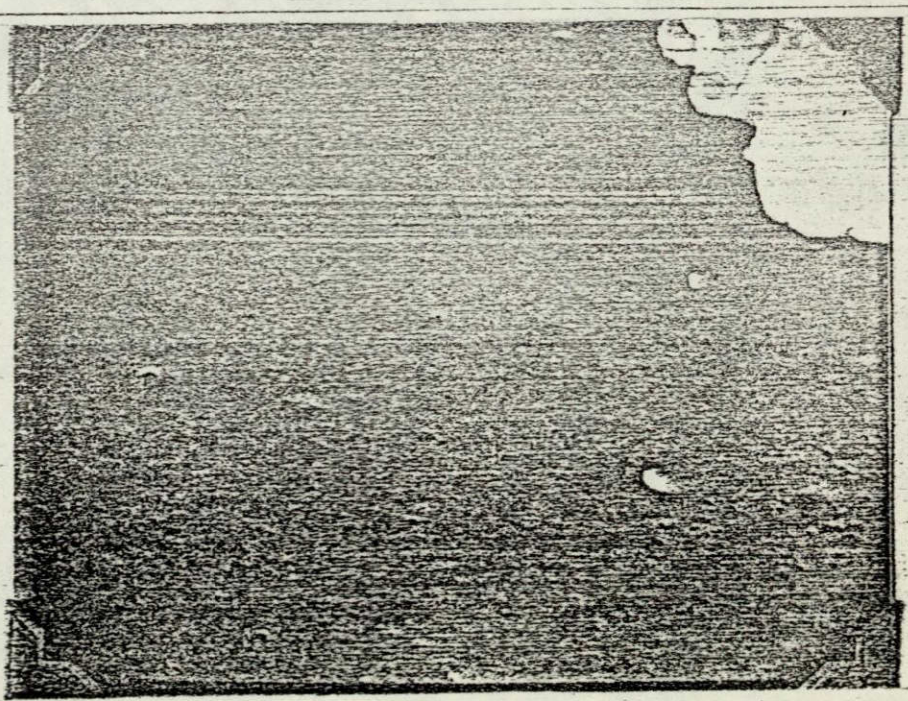

Fig. 14. Photomicrograph of Fracture Sample lmp2-516D1 (1000 X)

(20 X)

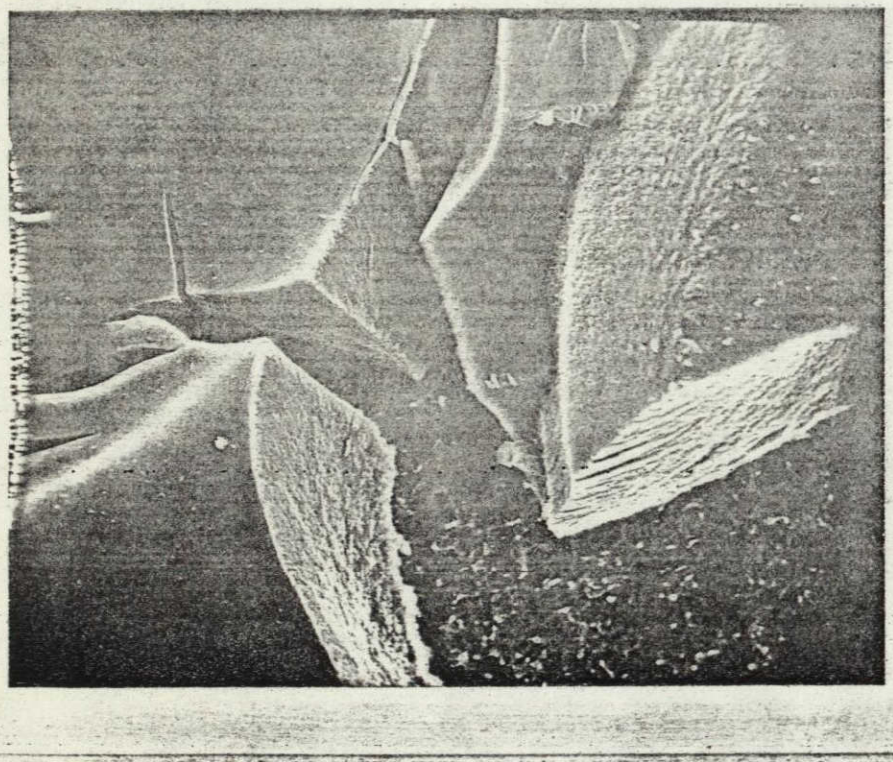

Fig. 16. Photomicrograph of Fracture Sample 2m2-515D1 (500 X)

adherend.

The SEM results suggest cohesive failure in the 1m2-517 and 1mp2-516 series because of the absence of metal substrate structure. The lower lap-shear strength of the 1mp2-516 series compared to the 1m2-517 series is attributed to a difference in the cohesive strength of the two polyimide resins. An adhesive failure mode is suggested for the 2m2-515 series of fracture samples from the appearance of metal substrate.

B. Contact Angles

1. Contact Angles for Various Liquids With Ti-6-4. The advancing contact angles are given in Table III for various liquids with the titanium alloy. Each value represents the average of at least three independent measurements. The use of distilled water in the Pasa-Jell process produced a surface that gave a water contact angle between 5 and 15°, whereas the use of deionized water gave an angle some ten degrees higher. It was further noted that if the drying was done in a nitrogen stream and the water drop introduced while the sample was still in the nitrogen atmosphere, the drop would spread as observed by Harkins and Grafton (9).

The effect of laboratory air present in the drying step of the alloy cleaning process was examined by measuring the water contact angle at various times of exposure to laboratory air for the alloy

TABLE III

CONTACT ANGLES OF VARIOUS LIQUIDS ON PREPARED SURFACES OF TI-6-Al-4-V SAMPLES AT 25°C

Liquid	Preparation	
	Cleaned	As-Received
Water	0–25°	54°
Mercury	Not Measured	160°
Octane	0°	0°
Diglyme	0°	5°
DMAC	8°	23°
Octane/Water	175°–180°	140°
Polyamic acid solution	12°	28°

surface after the nitrogen drying step of the Pasa-Jell method. Typical results are given in Figure 17. After each measurement, the drop was evaporated under a nitrogen stream followed by exposure to lab air for the indicated time and application of a new drop for measurement. The water contact angle (Figure 17)

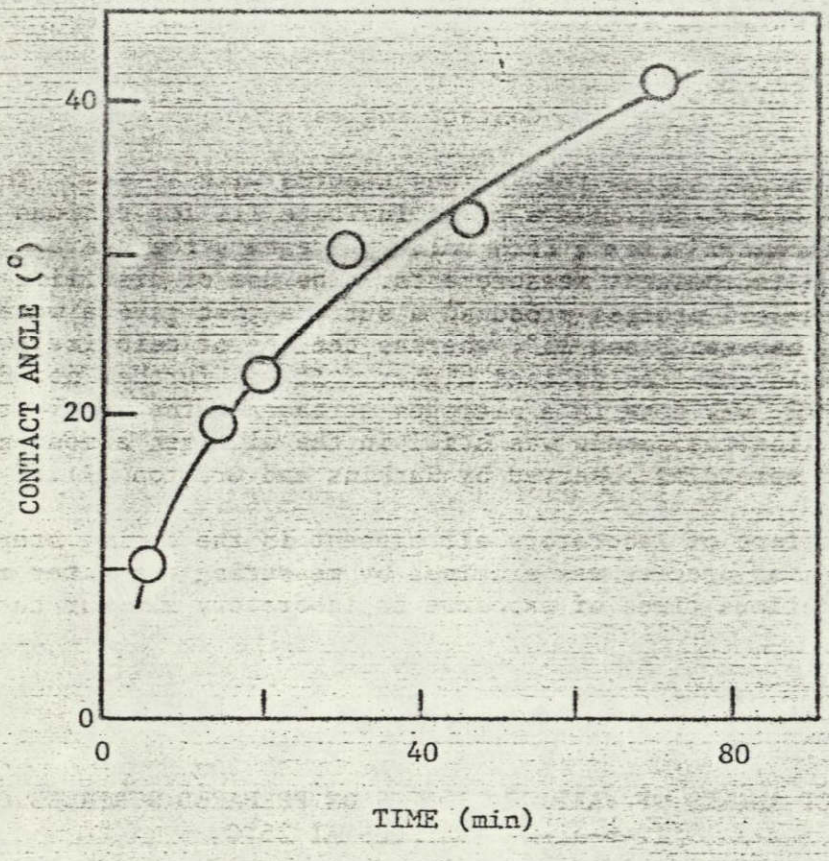

Fig. 17. Water Contact Angle Versus Lab Air Exposure Time for Cleaned Ti-6-4 Samples at 25°

after some four days of exposure to lab air was 60°. Koranyi and Acs (10) also reported an increase in the contact angle of water on glass from 4° to 23° within 4 hours after heating. The noted increase in contact angle (Figure 17) is taken to be indicative of contamination by adsorption of contaminants from laboratory air. This interpretation is in general agreement with the work of Bartell and Smith (11) for water contact angles on gold surfaces. They reported the following values for the conditions indicated: water vapor + pure air : 6°, water vapor + benzene vapor : 84°, and water vapor + lab air : 65°.

2. Octane/Water Interfacial Contact Angles. Measurement of the octane/water/titanium alloy interfacial contact angle verified the increasing contact angle noted in Figure 17. A freshly cleaned surface gave an interfacial contact angle of approximately 175° (Table III). Exposure to lab air for thirty minutes decreased the measured interfacial angle to 152°, close to the value observed for the untreated surface. Thus octane/water/solid contact angle decreased with increasing contamination of the Ti-6-4 surface.

The octane/water interfacial contact angle, according to Hamilton (12), indicates the hydrophilicity of the cleaned metal surface and provides an estimation of the polar forces (non-dispersion forces) acting across the interface. Hamilton's equation is

$$\text{Cos}\,\theta = (\gamma_w - \gamma_o - I_{sw})/48.3$$

where γ_w is the surface tension of water (72.0 dynes/cm), γ_o is the surface tension of octane (21.8 dynes/cm), and I_{sw} is the interfacial free energy contribution from hydrophilic (polar) interactions at the solid/water interface. The value of 48.3 is the experimentally determined water/octane interfacial energy (dynes/cm). According to Hamilton (12), solids capable of dispersion interactions only have a octane/water/solid contact angle of 50°. For surfaces with polar sites, the contact angle is $> 50°$ due to interaction of the polar sites with water. The smaller octane/water contact angles for the cleaned surface and the surface exposed to lab air shows the effect of contamination on contact angle.

Differences in the contact angles for diglyme and DMAC (Table III) on the titanium alloy make an interesting comparison in view of the scanning electron microscopy results. Diglyme wets the cleaned surface whereas DMAC has a finite contact angle. The as-received material which has a higher level of contamination still exhibits a smaller diglyme contact angle than does DMAC. The correlation between fracture strength and wetting as observed in the scanning electron microscope has been discussed above. The correlation is now further documented by the measured contact angles. The smaller contact angle for diglyme compared to DMAC may be indicative of the better wettability of diglyme for the titanium alloy.

Water and octane/water contact angles were measured on separate Ti-6-4 surfaces coated with 3% and 5% polyamic acid (BTDA + m,m' DABP) solutions in diglyme. The average values of the water and octane/water contact angles were 54 ± 1° and 114 ± 8°, respectively. The high and constant water contact angle indicates a compact partly hydrophobic surface film (13). The value of 114° for the octane/water contact angle is greater than the 50° contact angle for dispersion forces only and implies that the polyamic acid film is

capable of polar interaction.

Conflicting evidence on the role of contact angles in adhesion is found in the literature. Sharpe and Schonhorn (14) cite a zero degree contact angle for adhesive on substrate as a valid criterion for selection of a good adhesive. On the other hand, Muchnick (15) found a poor correlation between joint strengths and contact angles. At least for the titanium alloy/polyimide system, contact angles are significant as adhesion criteria for the following reasons: (1) in a qualitative way (ascertaining the wettability), contact angles of diglyme and DMAC correlated with the fracture strength of two samples as also shown by electron microscopy, (2) water contact angles were indicative of the level of contamination for the alloy surface, and (3) octane/water contact angles provided an insight into the nature of the forces capable of interacting at the alloy/adhesive interface.

C. Specular Reflectance Infrared Spectroscopy (SRIS)

The SRIS study was undertaken in an attempt to correlate the intensity of absorption peaks on the different samples to the amount of adhesive remaining on the panels. Reflectance spectra of the adhesive were obtained for all samples in Set II as expected because the scanning electron photomicrographs showed significant amounts of adhesive present on all samples. It should be emphasized that this is an in-situ method for the infrared analysis of fracture surfaces. The following assignments were made based on the major absorption peaks for sample lmp2-516: 700, 840, 920, 970, and 1080 cm^{-1} ($\delta\phi$), 1200 and 1370 cm^{-1} (ν C-N), 1270 and 1730 cm^{-1} (ν C=O).

It proved impossible to make any definite correlations between peak intensities and the quantity of adhesive present on a panel because of reflectivity differences of the samples. These differences prevented peak height comparisons from a common base line.

For this reason, reflectivity as measured by percent transmission was used to characterize the fracture surfaces. The percent transmission was measured at 2600 cm^{-1} where no absorption occurred. The percent transmission of a sample from each series in Set II and also for a polished Ti-6-4 panel and an as-received cleaned Ti-6-4 panel as determined in both single beam (SB) and double beam (DB) modes are listed in Table IV.

The percent transmission value obtained in the single beam mode for the fracture surfaces of Set II are plotted against the respective lap-shear strength in Figure 18. There appears to be a somewhat linear relationship between the percent transmission and the shear strength of the samples. This may be of no more than

TABLE IV

SRIS PERCENT TRANSMISSION OF FRACTURE SURFACES

Sample	Spectrum #		
	#18-SB	#19-DB	#24-SB
1m2-517	21 ± 2	19 ± 1	11
1mp2-516	39 ± 4	44 ± 4	19
2m2-515	56 ± 2	63 ± 3	29
Ti-6-4, cleaned			45
Ti-6-4, polished			97

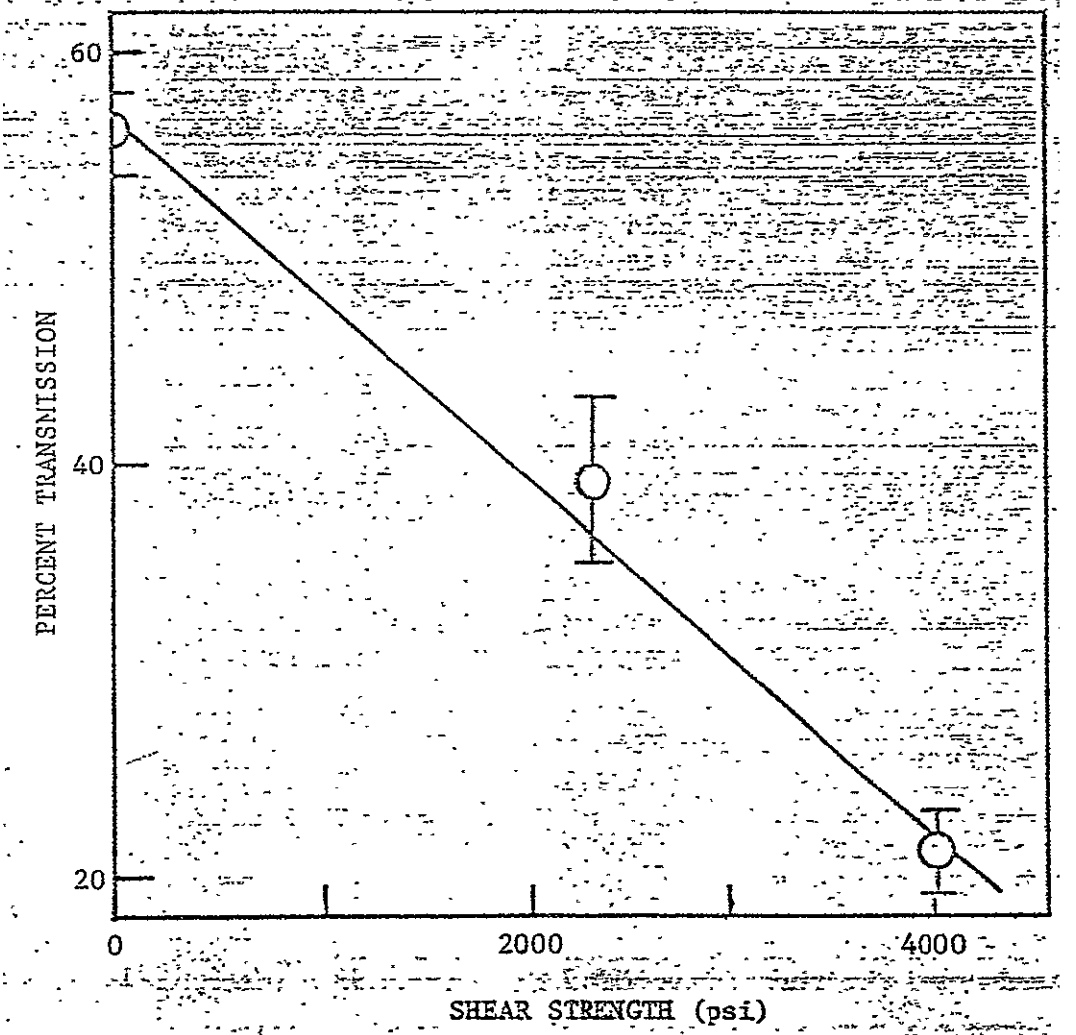

Fig. 18. Percent Transmission vs. Shear Strength for Set II Sample

qualitative significance but it is interesting to note that the samples of zero shear strength (series 2-2-315) in which bare metal was seen in the SEM micrographs have the highest reflectivity.

D. Electron Spectroscopy for Chemical Analysis (ESCA)

Figure 19 shows typical ESCA spectra for the titanium alloy selected from 23 separate ESCA runs on samples that were either in the as-received state or cleaned. Table V is a listing of the binding energies for titanium, oxygen, nitrogen, and carbon corrected for the work function of the spectrometer. The uncertainty in assignment of the cited binding energies is ± 0.3 ev at a 95% confidence level determined for five independent sample runs. The literature values and assignments in Table V are from Siegbahn (16). The binding energies for titanium and oxygen are in excellent agreement with the values of 457.9 and 529.6 ev reported by Hamilton (8) for Ti-6-4 samples. The observed shift in the binding energies of the titanium doublet from the literature values is taken to indicate the presence of an oxide film on the surface of the Ti-6-4 sample. The oxygen peak was typically broad as shown in Figure 19b with the main shoulder being of lower energy. The carbon peak in some spectra exhibited shoulders indicating different types of carbon contamination in contrast to the sharp peak exhibited in Figure 19c.

TABLE V

BINDING ENERGIES IN THE ESCA SPECTRA OF THE TI-6-AL-4-V SAMPLES

	Binding Energy(ev)			
Element	Cleaned	As-received	Lit. Values	Assignment
Ti	463.4	462.9	461	$2p_{1/2}$
	457.7	457.1	455	$2p_{3/2}$
O	529.3	528.9	532	$1s_{1/2}$
C	(284)	(284)	(284)	$1s_{1/2}$
N	ND	398.7	399	$1s_{1/2}$

ND - not determined

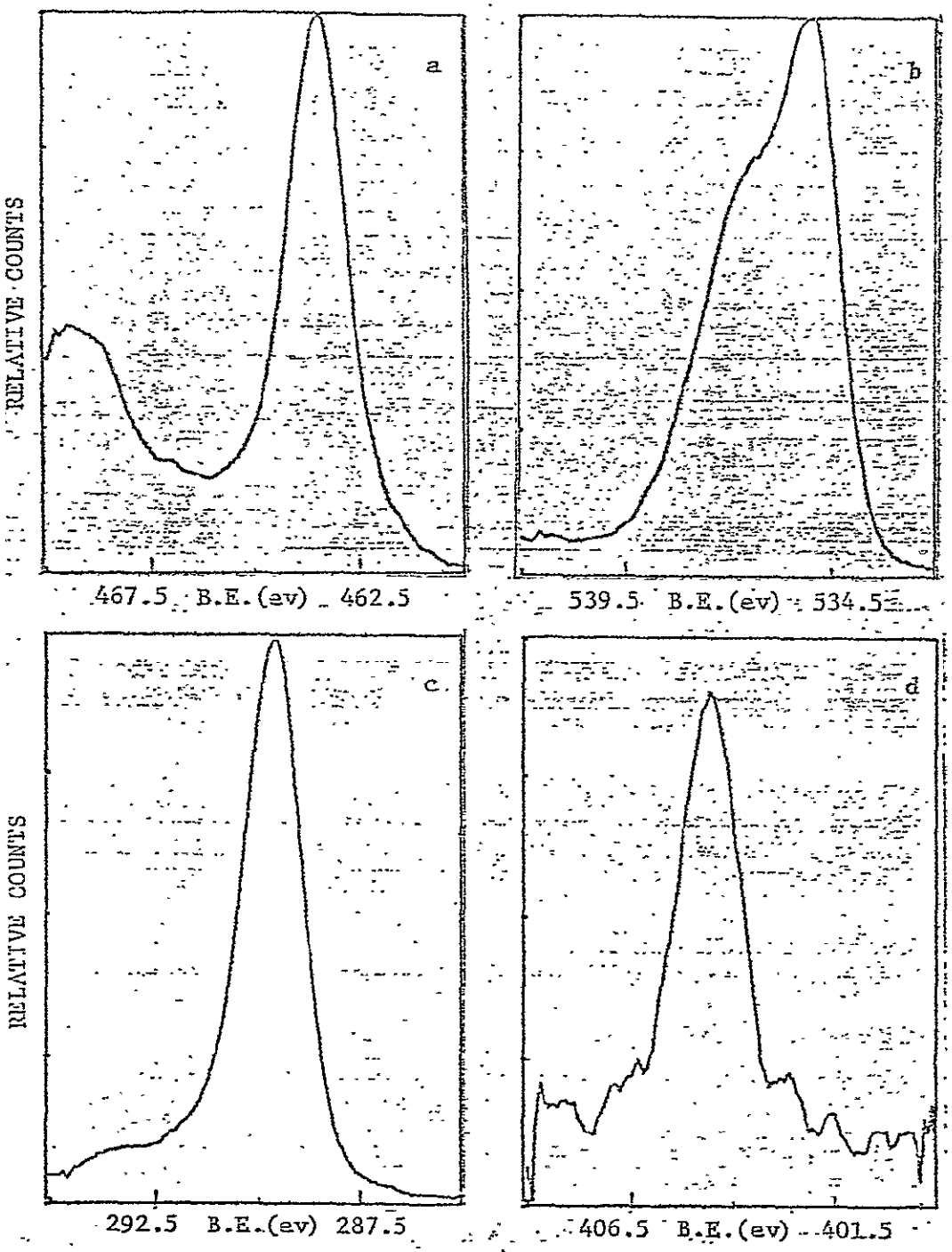

Fig. 19. a. Typical ESCA Spectrum of Titanium $2p_{1/2}$ and $2p_{3/2}$ Electron
b. Typical ESCA Spectrum of Oxygen $1s_{1/2}$ Electron
c. Typical ESCA Spectrum of Carbon $1s_{1/2}$ Electron
d. Typical ESCA Spectrum of Nitrogen $1s_{1/2}$ Electron

No Ti signal was observed in the ESCA spectra of separate Ti-6-4 surfaces coated with 3% and 5% polyamic acid (BTDA + m,m' DABP) solutions in diglyme. Since the escape depth of secondary electrons is 50-100 Å, the absence of a titanium signal is due to the presence of a uniform film thicker than 50-100 Å. The conclusion of a uniform film rather than a patch film is consistent with the measured contact angles.

ESCA studies proved to be of great value in assessing the failure mode of the lap joints. The escape depth of the photo ejected electrons from the Al Kα x-rays is 50 to 100 Å. It would be expected then that, if the samples were covered with a film thicker than 50-100 Å, the ESCA spectra of the elements of the adherend would not be observed. The lack of a Ti signal is seen in Figure 20b for sample 1m2-517D3 and a strong Ti signal is seen in Figure 20a for sample 2m2-515D4. The results of the ESCA studies on the samples in Set II are summarized in Table VI. Carbon, oxygen, and nitrogen were found on all fractured samples and on the as-received Pasa-Jell cleaned Ti-6-4 panel. The binding energies, BE_0, have been corrected for the work function of the spectrophotometer using the 2s electron of carbon at 284 ev. The intensity of the peak as measured by the ratio of the difference (Δ) between the maximum and the minimum counts peak width (ω) at half-height are also noted.

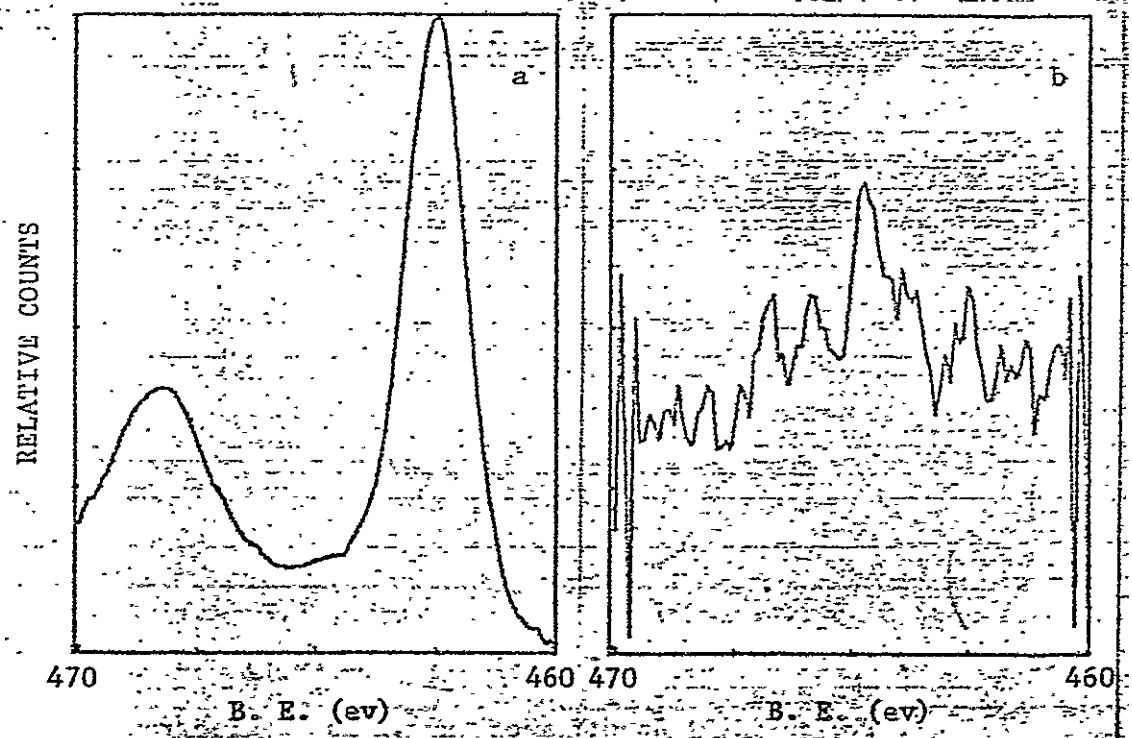

Fig. 20. a. ESCA Spectrum of Ti in Fracture Sample 2m2-515D4 Scanning: 100 channels, 3 sec/channel, 18 scans.
b. ESCA Spectrum of Ti in Fracture Sample 1m2-517D3 Scanning: 100 channels, 3 sec/channel, 18 scans.

TABLE VI

ESCA ANALYSIS OF FRACTURE SAMPLES

Sample Type		Ti-6-4 as rec'd		1m2-517D3	1mp2-516D4		2m2-515D4
Sample #		04230	05270	04180	05041		05043
Ti $2p_{3/2}$	BE_ϕ (ev)	457.0	458.0	NP*	NP		457.8
	Δ/MIN	5.70	4.70	0.14	0.14		2.82
	ω (ev)	1.8	2.0	NC*	NC		1.7
C $1s_{1/2}$	BE_ϕ (ev)	(284)	(284)	(284)	(284)		(284)
	Δ/MIN	6.87	6.75	24.7	34.0		10.6
	ω (ev)	1.6	1.7	2.1	1.7		2.2
O $1s_{1/2}$	BE_ϕ (ev)	529.3***	529.5***	531.0	532.4	531.2	531.8, 529.4
	Δ/MIN	2.33	2.07	3.22	2.00		2.19
	ω (ev)	NC	NC	NC	NC		NC
N $1s_{1/2}$	BE_ϕ (ev)	399.1	399.6	399.4	399.5		399.2
	Δ/MIN	0.41	0.41	0.89	0.39		0.87
	ω (ev)	2.1	2.5	2.0	2.1		2.3

*NP - no peak *NC - not calculable *** High energy shoulder

The most significant feature to note is that for the fracture samples (Table VI) no Ti signal was found for samples 1m2-517D3 or 1mp2-516D4 indicating the presence of a film at least as thick as 50-100 Å on the panels. This film is seen for the 1m2-517 and 1mp2-516 series in the SEM photomicrographs of Figures 10 and 12. The SEM results showed that bare metal was present on the 2m2-515 samples and the strong ESCA Ti signal for sample 2m2-515D4 clearly supports this finding. The ESCA results demonstrate the utility of the ESCA technique in establishing unambiguously adhesive or cohesive failure at the molecular level of 50-100 Å.

The present work demonstrates at least 3 factors contributing to adhesive strength. Differences in wettability were observed for the BTDA + m,m'DABP resin in diglyme compared to the same resin in DMAC (Set I). A higher adhesive strength was noted in the more wettable system. Alternately, relative solubility could be another factor to account for differences in adhesive strengths for BTDA + m,m'DABP and BTDA + m,m'DABP, BTDA + m,p'DABP and PMDA + m,m'DABP all in diglyme (Sets I and II). Decreasing adhesive strengths were noted with expected decreases in relative solubility. Finally the three resins (Sets I and II) have different glass transition temperatures. Again, the increasing adhesive strength parallels decreasing T_G values (see Table I). Work is in progress to delineate between these several factors.

IV. CONCLUSIONS

The techniques of (1) contact angle measurement, (2) electron spectroscopy for chemical analysis, (3) specular reflectance infrared spectroscopy, and (4) scanning electron microscopy are all of value in the characterization of the titanium alloy/polyimide resin adhesive system. The titanium alloy was identified as being composed of an α and a β-phase based on scanning electron microscopy. Scanning electron photomicrographs revealed definite changes in surface topography of the titanium alloy after the alkaline-cleaning and the acid pickling steps of the cleaning process. A correlation of wettability to fracture strength for the DMAC and diglyme solvent systems was made by use of the scanning electron microscope. Failures in both the adhesive and cohesive mode were noted in the scanning electron photomicrographs for fracture surfaces. The DMAC and diglyme contact angles on the titanium alloy correlated with fracture strength. Octane/water-titanium alloy interfacial contact angles indicated that both the polyamic acid film and the alloy surface can interact by non-dispersion forces. Atmospheric contamination reduces the octane/water/solid contact angle. The infrared spectrum of fracture surface can be obtained in situ by specular

reflectance infrared spectroscopy. The reflectivity of fracture surfaces is directly related to fracture strengths. Analysis of ESCA spectra based on binding energies and peak intensities can be used to detect the presence of ultra-thin adhesive surface layers.

Further, the techniques of Scanning Electron Microscopy (SEM), Specular Reflectance Infrared Spectroscopy (SRIS), and Electron Spectroscopy for Chemical Analysis (ESCA) have proved complementary in this investigation of the relationships between adherend surfaces and adhesive properties. As SRIS results have shown the presence of adhesive on all fracture samples, ESCA and SEM results further clarified the nature of the fracture surface through the presence or absence of a Ti ESCA spectrum and the observation or lack of observation of the substrate structure in the SEM photomicrographs. It is concluded from the results of the three techniques that for the Set I samples, cohesive failure was noted for 219D2 whereas adhesive failure was noted for 220D3. Cohesive failure was noted for samples 1m2-517 and 1mp2-516 and adhesive failure was noted for 2m2-515 in Set II.

V. ACKNOWLEDGEMENT

Financial support for this work under NASA Contracts NAS1-10646-14 and NAS1-10646-25 including graduate research assistantships for two of us (TAB, MEC) is acknowledged gratefully. The very capable experimental assistence of Dr. James S. Jen, Frank Mitsianis, Charles Potter, and Dr. T. L. St. Clair is acknowledged.

VI. REFERENCES

1. T. L. St. Clair and D. J. Progar, presented in part at the ACS Macromolecular Secretariat Symposium on Science and Technology of Adhesion, Philadelphia, PA., April, 1975.

2. J. J. Bikerman, The Science of Adhesive Joints, 2nd ed., Academic Press, New York, 1968.

3. J. R. Huntsberger in Treatise on Adhesion and Adhesives, R. L. Patrick, Ed., Marcel Dekker, Inc., New York, New York, 1967, Chapter 4.

4. S. Wu, J. Phys. Chem., 74, 632 (1970).

5. D. W. Dwight and W. M. Riggs, J. Colloid Interface Sci., 47, 650 (1974).

6. L. Taylor, Ed., Metals Handbook, Atlas of Microstructure of Industrial Alloys, Vol. 7, American Society for Metals, Metals Park, Ohio.

7. ASTM Spec. Tech Pub. No. 204, Symp. on Titanium, American Society for Testing Materials, Philadelphia, Pa.

8. W. C. Hamilton, Applied Polymer Symp., #19, 105 (1972).

9. W. D. Harkins and E. H. Grafton, J. Amer. Chem. Soc., 44, 2665 (1922).

10. G. Koranyi and M. Acs, Acta Chem. Hung., 24, 333 (1960).

11. F. E. Bartell and J. T. Smith, J. Phys. Chem., 57, 165 (1953).

12. W. C. Hamilton, J. Colloid Interface Sci., 40, 219 (1972).

13. L. S. Bartell and R. J. Ruch, J. Phys. Chem., 63, 1045 (1959).

14. L. H. Sharpe and H. Schonhorn, Adv. Chem. Ser., 43, 189 (1964)

15. S. N. Muchnick, WADC Tech. Rept. 55-87 Part II, Feb. 1958.

16. K. Siegbahn et. al., ESCA-Atomic, Molecular and Solid State Structure Studied by Means of Electron Spectroscopy, Almquist and Wiksells, Uppsala, 1967.